ASTRONOMY & ASTROPHYSICS
SUPPLEMENT SERIES

NOVEMBER I **1994**, PAGE 563

Astron. Astrophys. Suppl. Ser. **107**, 563-647 (1994)

A large-scale survey of OH in the galactic centre

P.J. Boyce[1] and R.J. Cohen[2]

[1] Department of Physics and Astronomy, University of Wales College of Cardiff, 5 The Parade, PO Box 913, Cardiff CF2 3YB, U.K.
[2] University of Manchester, Nuffield Radio Astronomy Laboratories, Jodrell Bank, Macclesfield, Cheshire SK11 9DL, U.K.

Received October 22, 1993; accepted May 17, 1994

Abstract. — Results are presented from an absorption line survey of the galactic centre region in the OH main lines (frequencies 1667.359 MHz and 1665.402 MHz). The survey was made using the 250ft Lovell Telescope at Jodrell Bank which has a beamwidth of 10 arcmin at these frequencies. Spectra were taken on a grid with 0°.2 spacing. The entire region between $354° \leq l \leq 8°.6$ and $-1°.0 \leq b \leq +1°.0$ was surveyed with extensions out to $b = -2°.0$ and $b = +1°.6$ at some longitudes. The spectra were taken using an autocorrelation spectrometer with spectral bandwidth 5 MHz, a velocity range of 900 km s^{-1} and a resolution of 3.1 km s^{-1}. The rms noise level achieved was typically 80–90 mK. The data are presented as a series of longitude–velocity (l–V), latitude–velocity (b–V) and longitude–latitude (l–b) contour maps of line temperature and apparent opacity. The survey reveals that the molecular gas in the galactic centre is much more extensive than previously thought. The molecular nuclear disk can be traced over the entire region $354° < l < 6°$, a projected size of ~ 1.8 kpc. The disk appears to be warped, lying preferentially to positive latitudes at negative longitudes and negative latitudes at positive longitudes. The gas reaches latitudes of $\pm 1°.6$, corresponding to z–distances of ± 240 pc out of the galactic plane. The new features are described in detail. There are 7 broadline "clumps"; concentrations of molecular gas with angular sizes typically 0°.6 and large velocity extents of typically 200 km s^{-1}. The clumps have positive gradients of velocity with galactic longitude. Some of the clumps appear to be connected by narrow filaments which have velocity widths of typically 30 km s^{-1}. There are also a number of molecular spur features which extend outwards from the nucleus to latitudes of $\pm 1°.0$. These appear to be associated with radio continuum features, including the galactic centre lobe.

Key words: surveys — ISM: molecules — Galaxy: center — Galaxy: structure — radio lines: ISM

1. Introduction

The galactic centre is the scene of many remarkable phenomena on scales from several kiloparsecs down to less than 1 parsec. Across the whole electromagnetic spectrum there are types of activity seen nowhere else in the Galaxy. The most energetic phenomena may be driven by a massive black hole at the centre, massive star clusters, or a central stellar bar. Detailed reviews of the complex observational picture and the possible interpretations are given by Oort (1977), Brown & Liszt (1984), Genzel & Townes (1987), Townes (1989) and Blitz et al. (1993).

The galactic centre contains the largest concentration of molecular gas in the Galaxy. The galactic centre molecular clouds are characterised by large turbulent linewidths and large non–circular motions. Previous large–scale surveys of the region have been carried out in OH (Robinson & McGee 1970; Cohen & Few 1976), H_2CO (Whiteoak & Gardener 1979; Cohen & Few 1981), CO (Bania 1977; Dame et al. 1987; Bally et al. 1987, 1988) and CS (Bally et al. 1987, 1988). The groundstate lines of OH at 18 cm wavelength have particular advantages for such a survey. The OH lines are seen in absorption against the radio continuum emission and so are sensitive to very small molecular column densities. Furthermore the absorption lines give information about the relative positions of the molecular clouds and the radio continuum sources, particularly when used in conjunction with emission lines from other molecules such as CO. Finally it is possible to cover large areas of sky in a reasonable time, albeit at modest angular resolution.

This paper presents the observational results from an extensive survey of the OH mainlines at 1665 and 1667 MHz . The survey covers the inner 14°of the Galaxy with an angular resolution of 0°.2. This was the first survey to reveal the full extent of the molecular nucleus. Some preliminary results have already been published by Cohen (1982), Cohen & Dent (1983), Boyce & Cohen (1989). The observational data are now presented in their entirety for the first time, as complete sets of l–V, b–V and l–b maps

(Sect. 4, Figs. 2–9), and the many new features found in the survey are described in detail (Sect. 5). An astrophysical analysis of the results will be presented elsewhere.

2. Equipment and observing technique

The observations were made at Jodrell Bank in 1981 April-July using the 76 m Lovell telescope which was illuminated so as to have a halfpower beamwidth of 10 arcmin at the OH mainline frequencies. The telescope was equipped with a dual–channel receiver which received signals of left and right–hand circular polarisation. The first stages of amplification were provided by room temperature parametric amplifiers and the resulting system noise temperature was 90 K on blank sky, and typically 20–30 K higher near the galactic centre.

Observations were made between longitudes 354°and 8°.6 and between latitudes −2°and +1°.6, sampling every 0°.2 in longitude and latitude. The coverage was not complete above latitude +1°.0 and below −1°.0. Figure 1 shows the positions observed.

Spectra were taken using a 1024–channel autocorrelation spectrometer (Pointon 1977) which was configured as two banks of 512 channels. The spectral bandwidth was 5 MHz, which corresponds to a velocity range of 900 km s^{-1}and a channel spacing of 1.8 km s^{-1}. This gave a velocity resolution of 3.1 km s^{-1}after triangular weighting of the autocorrelation function, which was done online. The spectral band covered the two OH lines at 1665 and 1667 MHz. Because the lines are very broad near the galactic centre and because of differential galactic rotation it was necessary to adjust the first local oscillator to keep all the absorption features in the band. The band centre was set at a velocity of +240 km s^{-1}in the 1665 MHz line for positions at positive longitude and at a velocity of +140 km s^{-1}for positions at negative longitude. Positions close to zero longitude were observed twice, once at each setting. The 100 km s^{-1}velocity shift corresponds to 57 spectral channels. Spectra were taken in the frequency–switching mode, switching the first local oscillator by 4.6 MHz. This large frequency switch introduced a slope across the difference spectra which was calibrated by observations of reference regions which are believed to be free of OH absorption. The reference positions used were G0°.0–5°.0, G10°.0–5°.0, G0°.0+10°.0 and G7°.0+2°.0.

Each survey point was observed for at least ten minutes. Longer integrations were made, to improve the signal–to–noise, on positions close to the galactic centre where the continuum level added appreciably to the receiver noise. The rms noise on the final spectra was always less than 100 mK and was typically 80–90 mK.

The radio continuum emission from the survey region at 1660 MHz was measured separately in July 1981 using total power scans. The scans were made between longitudes 354°and 9°, spaced every 0°.2 in longitude. Scans covered a latitude range of ±5°, except for longitudes 354°to 355°, where the range was −4°to +5°. Calibration was done by firing the noise diode at the beginning and end of each scan. Scans were made at the rate of 1°per minute, with an integration time of 6 s. In the offline processing the data were interpolated onto a uniform 0°.1 grid in galactic latitude. Baselines were determined by subtracting second order polynomials from the scans. From comparisons with published surveys we estimate that the continuum temperatures derived from our scans are accurate to 0.5–1.0 K.

3. Data reduction

The reduction of the data from the raw spectra from the spectrometer to the final maps consisted of two main parts. Firstly, the individual spectra were processed using the Spectral Line Analysis Package (SLAP) (Staveley–Smith 1985). The spectra were then read into a datacube using the IRAF software package within which the image production and analysis was performed.

A reference baseline for each days observations was constructed by averaging together each of the reference integrations for that day and smoothing the result by a Gaussian of 10 channels full width to half maximum (FWHM). After subtraction of this baseline from a spectrum, any remaining baseline error was removed by fitting a Chebychev polynomial to those parts of the spectrum believed to be free of absorption. In most cases a second order fit was adequate, and the baseline error was $\leq$0.1 K. However, in a few cases a third or higher order fit was necessary. In positions where the absorption was spread over most the band, a comparison with previously published OH spectra for these positions was made in order to determine a reasonable baseline fit. A few such spectra near l =0°, b =0° have baseline errors of 0.3–1.0 K.

Each spectrum was corrected for atmospheric attenuation using a gain–elevation correction determined empirically by observations of maser point sources made during the session. After this the spectra of right and left hand polarisation were added to give the unpolarised spectra used to produce the maps. Since the system noise in both polarisation channels was similar (to within 10%) the two channels were given equal weighting. The datacube had a total velocity range of 1000 km s^{-1}corresponding to 569 channels. The 57 channels not observed at any given position were set to zero in the datacube. Channels affected by narrow–band interference were also set to zero in some of the spectra. The spectra were then read into an IRAF datacube. Within this cube slices could be made through any dimension of the cube. The maps presented below were produced in this way.

A second datacube of OH apparent opacity (τ_a) was also formed using the spectral line data and also the data from the 18 cm continuum survey of the region. Apparent

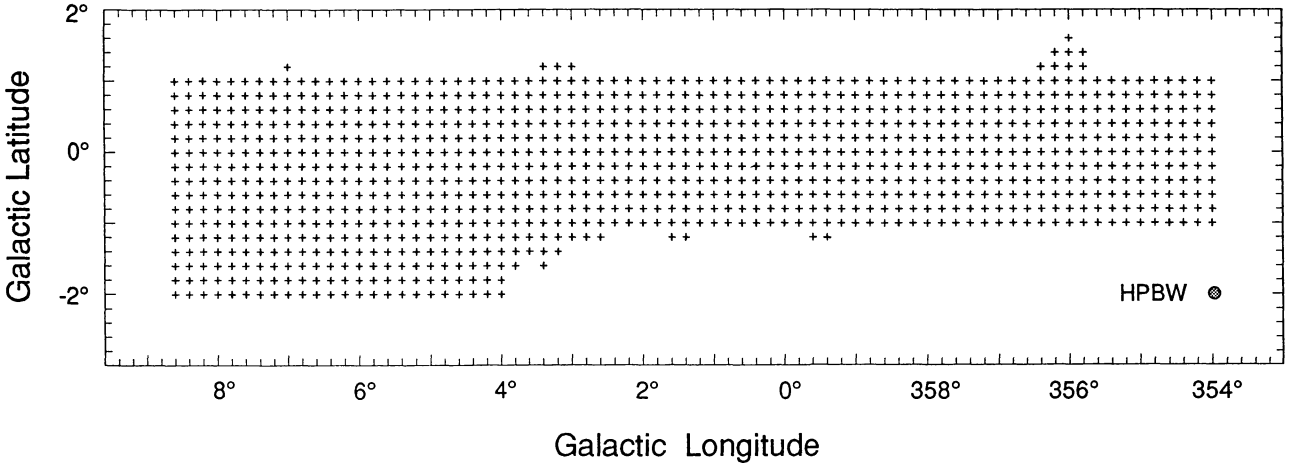

Fig. 1. Positions at which spectra in survey were observed

opacity is defined by

$$\tau_a = -\frac{T_L}{T_c}$$

and is a useful way of partially correcting for the effect which the uneven distribution of the continuum on the sky has on the observed absorption lines. The data from the continuum survey were used to form a 2–D datacube of the same spatial dimensions as the line temperature cube (see Boyce 1990 for a detailed description of this process). The apparent opacity datacube was then formed by dividing the line temperature datacube by the continuum temperature datacube.

4. The results

The full results of the OH survey are presented in Figs. 2–9 as sets of l–V, b–V and l–b maps taken from the IRAF datacubes. These maps can be found at the end of this paper. The line temperature maps are in units of antenna temperature T_A. A correction into units of brightness temperature T_B can be made by multiplying the levels by 1.50±0.08. This correction factor was determined during the survey by observations of the moon.

Figure 2 presents a full set of l–V maps for each of the galactic latitudes observed in the survey. The resolution of the maps is 3.1 km s^{-1} × 12 arcmin. The maps show the absorption resulting from both the 1667 MHz line and the 1665 MHz line. The 1667 MHz absorption is seen on the left of these maps and the velocity ranges associated with the two lines are separately labelled. It can be seen that the gas distribution traced by the two lines is practically identical. The major obvious difference between them is that the 1665 MHz line is generally weaker than the 1667 MHz line. For an optically thin cloud in local thermodynamic equilibrium the lines would have a ratio of 5:9. In practice line ratios nearer unity are observed for the deepest absorption features and there is line broadening due to saturation (Cohen & Few 1976). The 1665 MHz line generally has a lower optical depth than the 1667 MHz line, and in some situations the 1665 MHz line traces the individual structures in velocity space more clearly than the 1667 MHz line because of this. It should be noted that in several places near to l =0°.0 the high positive velocity absorption from the 1667 MHz line overlaps with the high negative velocity absorption from the 1665 MHz line. For example, absorption from gas having V =+150 km s^{-1} seen in the 1667 MHz line has the same frequency as absorption from the 1665 MHz line at V = –202 km s^{-1}. In the cases where this overlap occurs the 1667 MHz line can be used to trace the negative–velocity features and the 1665 MHz line used to trace the high positive–velocity features.

Figure 3 presents a full set of l–V contour maps taken from the apparent opacity datacube. As mentioned above the use of apparent opacity τ_a eliminates some of the problems caused by the uneven continuum distribution in the survey region. The τ_a maps show a similar distribution to the line temperature maps but the relative strengths of some features are very different. In addition, the signal–to–noise ratio within the apparent opacity datacube varies considerably with position depending on the strength of the continuum. In areas of low continuum temperature there is a much lower signal–to–noise ratio than in high continuum areas. For this reason two separate contour level regimes have been used in these maps. Between latitudes ±0°.8 a 0.02 contour is shown. At higher latitudes the continuum temperature is generally <7 K (antenna temperature) and the noise level is generally 0.02 or greater. The weaker features in these maps should be checked against the line temperature maps to determine whether they are real or not.

Figure 4 shows a full set of b–V maps from the line temperature datacube. The contours are plotted at the same intervals as for the longitude–velocity maps in order to make the two sets comparable. The comments made above concerning the merging of the lines at high veloci-

ties near the centre also, of course, apply to these maps. Figure 5 presents the equivalent set of apparent opacity b–V maps. Large negative and positive longitudes suffer from a similar problem with noise as the high latitude maps in the l–V plots. The contours are set at the same values as in the l–V apparent opacity maps. The 0.02 contour is shown at longitudes $|l|$ <4°and omitted for higher longitudes.

Figures 6 and 7 present sets of l–b maps for the 1667 MHz line and the 1665 MHz line respectively. Each of these maps shows the spatial distribution of the line temperature integrated over a velocity interval of 20 km s^{-1}. The maps cover the velocity range –300 km s^{-1}to +300 km s^{-1}for each line. It should be noted that at velocities above +100 km s^{-1}in the 1667 MHz line maps various negative velocity 1665 MHz features are also seen. Similarly at 1665 MHz velocities less than –80 km s^{-1} some high velocity 1667 MHz gas is seen. To avoid misinterpreting these maps, a comparison between the two sets is necessary (e.g. to ascertain which of the gas at +200 km s^{-1}in the 1667 MHz maps is high velocity 1667 MHz gas comparison should be made with the +200 km s^{-1}1665 MHz and the –150 km s^{-1}1667 MHz maps). Figures 8 and 9 present similar sets of l–b maps for the two lines, this time showing the apparent opacity averaged over 20 km s^{-1}intervals. The comments above relating to the line temperature l–b maps also, of course, apply to these maps.

5. Overview of main results

Galactic centre features dominate the maps compared to gas along the line of sight. Weak narrow lines at 0, –30, –50 km s^{-1}due to gas outside the galactic centre contribute little to the total OH observed and will not be discussed further in this paper. We concentrate here on the dense molecular nucleus. Our major results concern the asymmetric distribution of molecular gas about zero longitude and the warp of the molecular layer (Sect. 5.1), the detection of numerous broadline "clumps" and of "filaments" connecting them (Sects. 5.2 and 5.3), and the detection of molecular spurs pointing out of the galactic plane (Sect. 5.4).

OH column densities for some features have been calculated using the formula $\frac{N_{OH}}{T_{ex}} = 2.25\ 10^{14} \int \tau_{1667}\, dV$ cm $^{-2}$K^{-1} where T_{ex} is the excitation temperature in K, τ_{1667} is the apparent opacity in the 1667 MHz line, and V is the radial velocity in km s^{-1}. The combined error due to continuum baseline uncertainties and spectral baseline errors is <5% near the galactic plane and rises to $\sim$ 10% at higher latitudes. The OH column densities have in turn been used to estimate the mass of OH in the molecular features, assuming T_{ex}=10 K.

5.1. *Projected molecular distribution*

Figure 10 presents the spatial distribution of molecular gas as seen by the OH survey compared to two earlier surveys. These are the OH survey by McGee et al. (1970) and the CO survey by Dame et al. (1987). The McGee et al. (1970) map shows the envelope of OH detected by them with average radial velocities marked at certain positions. The map from the present survey was found by integrating over both lines over all velocities except –10 km s^{-1}< V <+10 km s^{-1} (to exclude local gas). The greater coverage of the present survey is clearly seen. The full extent of the molecular nuclear disk as seen in OH covers the region 354°< l <6°, corresponding to a projected size of ~1.8 kpc at the distance of the galactic centre. Most previous molecular line surveys of the galactic centre have covered only a fraction of this molecular nuclear disc. Only the CO survey by Dame et al. (1987) covered the whole disc, and this was at a resolution of 0°.5. Their results are shown for comparison in Fig. 10.

The most striking aspect of the OH distribution is the apparent asymmetry of the gas to positive longitudes. Because OH is seen in absorption throughout the galactic centre the observed distribution depends to a large extent on the relative distribution of the OH and the radio continuum. The apparent opacity maps help to overcome the effect of an uneven distribution of continuum with position on the sky. However, the position of the continuum along the line–of–sight relative to the molecular gas is still not known. The asymmetry is also seen in the ^{12}CO surveys of Dame et al. (1987) and the ^{13}CO surveys of Bally et al. (1988). Since CO is seen in emission, this implies that the asymmetry seen in OH is not simply a result of an uneven continuum distribution, but reflects a true asymmetry in the distribution of molecular gas.

The second striking feature of Fig. 10 is the apparent displacement of gas at large positive longitudes to negative latitudes and the similar displacement of gas at large negative longitudes to positive latitudes. This gives the molecular disk a warped appearance. The maximum extensions of the warp are to latitudes ±1°.6 (240 pc at the distance of the galactic centre). A similar warp has previously been detected in both HI data (Cohen & Davies 1976) and CO data (e.g. Bally et al. 1988). The most widely quoted model to explain the HI warp is that of an inclined nuclear disk undergoing both rotation and expansion (Burton & Liszt 1978; Liszt & Burton 1980). However, this model does not fit either our data or Dame et al. 's CO data in some important ways.

a) Large parts of the model tilted disc are not observed in molecular lines, in particular the extensions to latitudes 2°to 4°.

b) The projected molecular distribution is not seen to be tilted within 3°of the nucleus (see Fig. 10). At $|l|$ >3° the molecular gas does warp away from the galactic plane. This suggests that there is not a constant tilt angle, and

for this reason we prefer to describe the molecular disc as warped.

A third result from the survey is that many of the out–of–plane features appear to be relatively compact spatially but cover a very large velocity range. These are examples of the molecular "clump" features which are discussed in Sect. 5.2. The clumps are sometimes connected to other clumps by narrow filaments, as discussed in Sect. 5.3.

Figure 10 illustrates another major result of the survey. This is the detection of several spur–like features which appear to stretch from the molecular disk to higher latitudes. The most prominent of these can be seen at $l \sim 359.^{\circ}4$ and $0.^{\circ}0$ stretching to positive latitudes and at $l \sim 358.^{\circ}8$, $359.^{\circ}6$ and $0.^{\circ}2$ stretching to negative latitudes. A more detailed description of these spurs is given in Sect. 5.4.

5.2. *Broadline clumps*

The most interesting and puzzling result of the survey is the detection of a large number of broadline regions. These are molecular cloud complexes which are typically half a degree in angular width (FWHM) but which cover an enormous velocity range of 100–200 km s^{-1}. Bania (1977) coined the name "clumps" to describe these features and we will retain this term here. However, the term wide–line clouds (WLCs) has also been used in the literature (Stacy et al. 1989). Table 1 lists the observed properties of seven of the major clumps detected in the present survey. Errors in the M_{OH} values are typically 10–15% after allowing for a baseline error in the spectra and in the continuum scans. Bania's (1977) nomenclature for Clumps 1 and 2 has been retained, and the other features are labelled Clump 3 to Clump 7 in order of decreasing galactic longitude. We have not attempted to identify clumps in the central region $|l| < 1.^{\circ}4$, but it should be noted that there are broadline features in this region which have been ascribed to the rotating nuclear disc and the expanding molecular ring.

Figure 11 presents l–b maps of six of the clumps, with contours of the OH line integral and representative velocities marked. A striking result is that the clumps display systematic shifts of velocity with position. The velocity gradients are typically 2 km s^{-1}arcmin^{-1}, which corresponds to 0.8 km s^{-1}pc^{-1} at the distance of the galactic centre. In each case the component of the velocity gradient along the galactic plane, dV/dl, is positive, following the sense of galactic rotation. A short description of each clump follows.

Clump 1: This clump was first identified by Bania (1977). It is best seen in our data in the l–V plots (Figs. 2 and 3) at $b = +0.^{\circ}4$, at longitude $l = 354.^{\circ}8$, between velocities +55 and +120 km s^{-1}. It has a very large non-circular velocity. In our data it appears to be an isolated feature, although it is close in l–V space to Clump 7. A detailed CO study of Clump 1 was made by Bania et. al. (1986), who found considerable fragmentation in the cloud structure, with discrete components of sizes ~ 5 arcmin (15 pc) and masses $\sim 10^4$–10^5 $M_{\odot}$. There is an associated HII region G354.67+0.25 with a velocity of +100 km s^{-1}(Caswell & Haynes 1982).

Clump 2: This was first detected in OH by McGee et al. (1970), and it has been studied in CO and CS by Stark & Bania (1986) and in H_2CO by Zylka et al. (1992). It is best seen in our data in the l–V plots at $b = +0.^{\circ}4$, at longitude $3.^{\circ}2$ and velocities between −45 and +245 km s^{-1}. It appears to be connected to Clump 4 by Filament B at latitude $b = -0.^{\circ}6$ and velocity +40→+70 km s^{-1}(see Figs. 6,

Table 1. Properties of broadline molecular clumps

Feature	l range	b range	V range	N_{OH}/T_{ex}	M_{OH}
	deg	deg	km s^{-1}	$\times 10^{14}$ cm^{-2} K^{-1}	$M_{\odot}$
Clump 1	354.4→355.2	0.0→+0.6	+55→+120	2.6±0.7	1.0±0.1
Clump 2	2.8→3.8	−0.4→+0.8	−45→+245	16.0±2.3	21.6±2.4
Clump 3	5.2→6.0	−0.8→+0.2	−30→+210	6.7±2.3	6.0±0.7
Clump 4	4.4→4.8	−1.2→−0.4	+15→+195	6.7±2.3	2.4±0.3
Clump 5	1.0→2.0	−0.6→+0.4	−45→+220	18.4±2.3	18.4±2.1
Clump 6	355.8→356.4	+0.2→+1.2	−120→+30	3.4±1.1	2.1±0.7
Clump 7	355.4→355.6	+0.4→+0.6	+15→+95	2.4±0.9	0.30±0.05

Table 2. Properties of filaments

Feature	l range	b range	V range	$\Delta V_{1/2}$	N_{OH}/T_{ex}	M_{OH}	Associated
	deg	deg	km s^{-1}	km s^{-1}	cm^{-2}K^{-1}	$M_{\odot}$	Clumps
Filament A	4.6→5.0	−0.4→0.0	+20→+50	30	1.5×10^{14}	0.4	3, 4
Filament B	3.4→4.2	−1.0→−0.4	+40→+70	18	3.7×10^{14}	1.7	2, 4
Filament C	5.0→5.4	−0.8→−0.6	+170→+220	19	1.4×10^{14}	0.3	3, 4
Filament D	4.8→5.4	−1.6→−1.2	+185→+220	20	1.7×10^{14}	0.4	4
Filament E	1.8→3.0	−0.2→+0.4	−40→+50	35	1.2×10^{14}	9.6	2, 5
Filament F	1.8→2.6	−0.4→−0.2	+115→+160	16	3.3×10^{14}	0.9	2, 5

Table 3. Properties of molecular spurs

Spur	l	$\lvert b\rvert_{max}$	V range	N_{OH}/T_{ex}	M_{OH}	Comment
	deg	deg	km s^{-1}	cm^{-2}K^{-1}	$M_{\odot}$	
Spur I	0.0	+1.0	−180→−85	7.0×10^{14}	0.1	Associated with GCL (Sofue & Handa 1984)
			∼0→+95			
Spur II	359.4	+0.8	−155→−85	4.4×10^{14}	0.1	
			∼0→+90			
Spur III	0.2	−1.0	−150→−55	6.5×10^{14}	0.2	
			∼0→+70			
Spur IV	359.6	−1.2	−160→−85	8.3×10^{14}	0.4	Associated with G359.1–0.5 (Uchida et al 1992)
			∼0→+70			
Spur V	358.8	−1.0	−155→−110	5.2×10^{14}	0.1	
			∼0→+70			

Table 4. Masers

Source	OH main line	V (km s^{-1})	T_a (K)
G358.16+0.50	1665	−15, +28	0.3, 0.5
G359.37–1.25	1665	−227, −208	0.4, 0.5
G1.33+1.01	1667	−28, +3	1.2, 1.3

7, 8 and 9). It also appears to be connected to Clump 5 by low–velocity gas (Filament E) at +20→+40 km s^{-1} and latitude b =+0°.2.

Clump 3: This new Clump was reported by Boyce, Cohen & Dent (1989) and Stacy et al. (1989). It is best seen in the l–V plots at b =–0°.4 at longitude l =5°.4 and velocities between –30 and +210 km s^{-1}. It is connected to Clump 4 by two filaments, a high velocity Filament C at +180→+200 km s^{-1}, and a low velocity Filament A at +20→+40 km s^{-1}, as discussed below. The H_2CO study by Boyce et al. (1989) resolved the clump into 11 molecular cloud components with typical sizes $\sim$ 15 pc and implied masses of $\sim 10^5\ M_\odot$.

Clump 4: This new feature is a companion to Clump 3. It is seen most clearly in the l–V plots at b = –0°.8, at longitude l = +4°.8. The absorption is strongest near velocities of +80 and +170 km s^{-1}. Clump 4 seems to be connected to Clump 3 by a low– and a high–velocity filament of molecular gas as discussed below (Filaments A and C respectively). Two other molecular Filaments (B and D) also emanate from Clump 4.

Clump 5: This is related to the l = +1°.5 complex identified in CO by Bally et al. (1988). Our OH data trace the feature above the plane to b = +0°.6. The feature is most clearly seen in the l–V plots at b =+0°.4 at l =+1°.4. The velocity extent at this point is much greater than seen in CO. At lower latitudes the feature becomes very difficult to separate from other molecular complexes near the galactic plane. For this reason we have not attempted to plot the column density of Clump 5 in the composite Fig. 11.

Clump 6: This new feature is the only clump at negative velocity. It can be seen clearly in the l–V maps at b = +0°.8 at longitude l = 356°.2. The absorption is strongest at velocities near 0, –70 and –100 km s^{-1}. The feature is unusual in having a large gradient of velocity with galactic latitude. The feature extends to latitude b = +1°.2. Its large displacement above the plane and the approximate symmetry with Clump 4 on the opposite side of the galactic centre below the plane contribute in no small measure to the warped appearance of the molecular layer.

Clump 7: This feature is a companion to Clump 1. It is seen in the l–V maps at b = +0°.6 at longitudes l = 355°.4. Like Clump 1 it has a large forbidden (positive) velocity. The edge of this feature seems to have been detected in CO by Bania et al. (1986). The feature can be seen clearly in the CO data of Bally et al. (1987), their Fig. 4, b = +0°.6. As it is well separated spatially from Clump 1 we prefer to treat it separately. However, Bally et al. (1988) have loosely referred to the whole positive velocity complex from l = 354°.3 to l = 357° as Clump 1.

In Fig. 12 the clumps are identified on an integrated l–b plot. Their positions in l–V space are marked on a schematic l–V plot in Fig. 13.

To summarise, the broadline clumps are typically 100 pc in projected size and 200 km s^{-1} in velocity width. Their total mass is typically $10^7\ M_\odot$, as estimated from various molecular lines (CO, H_2CO). One new property to emerge from the present observations is that the clumps show positive gradients of velocity with galactic longitude (i.e. following the sense of galactic rotation). When observed at higher resolution Clumps 1, 2, and 3 have been found to be made up of cloud components typically 15 pc in size and with velocity extent 20 km s^{-1} and estimated masses $\sim 3\ 10^5\ M_\odot$.

5.3. *Filaments*

A second major result presented here is the detection of filaments which appear to be connecting several of the broadline clumps. These new structures can be traced in Fig. 10. They are identified in l–b space in Fig. 12. The l–V loci of these features are included in Fig. 13. The full l–b–V ranges for these features are presented in Table 2 together with other parameters. The error in $\frac{N_{OH}}{T_{ex}}$ is 0.3 10^{14} cm^{-2} K^{-1} for each filament, and the error in M_{OH} is typically 13%, allowing for baseline errors. The filaments are typically 1° long and have $\Delta V \sim 30$ km s^{-1}. Typically they have a velocity gradient of 30 km s^{-1} per degree. Apart from Filament D (see below) they appear to form connections between the clumps but do not extend beyond the clumps.

Filament A: This is best seen in the l–b plots (Figs. 6, 7, 8 and 9) at velocities +20→+40 km s^{-1} at b = –0°.2 and l = 4°.8→5°.2. It appears to connect the low velocity ends of Clumps 3 and 4. Its velocity is close to the mean velocity of Clump 3 at the position where the two features appear to meet (see Fig. 11).

Filament B: This is best seen in the l–b plots at velocities +60→+80 km s^{-1} at b = –0°.6 between longitudes l = 3°.4→4°.6. It appears to connect Clump 4 to Clump 2. It shows a systematic increase in average velocity from $V \sim$ +40 km s^{-1} near Clump 4 to $V \sim$ +100 km s^{-1} near Clump 2. Its velocity at the position where it appears to join Clump 2 is close to that of the clump (see Fig. 11).

Filament C: This is best seen in the l–b plots at velocities +180→+200 km s^{-1} at longitude l = 5°.0 and latitude b = –0°.8. It appears to connect the high velocity ends of Clumps 3 and 4.

Filament D: This filament is best seen in the l–b plots at velocities +200→+220 km s^{-1} at longitude l = 5°.2 and latitude b = –1°.6. It appears to be connected to the high velocity end of Clump 4 and to stretch from this clump down to b = –1°.6.

Filament E: This filament can be best seen in the l–b plots at velocity +20→+40 km s^{-1} between longitudes l = 2°.0→3°.0 at latitude b = +0°.2. It appears to form a

connection between the low velocity end of Clump 2 and Clump 5.

Filament F: The l–V plots (Figs. 2 and 3) at $b = -0.^\circ4$, $-0.^\circ2$ and $0.^\circ0$ show this filament clearly, stretching between $l \sim 1.^\circ6$, $V \sim 160$ km s^{-1}and $l \sim 3.^\circ2$, $V \sim 100$ km s^{-1}. It connects Clumps 5 and 2. It also connects smoothly in l–V space with Filament B.

5.4. *Molecular spurs*

The third major result of the survey is the detection of several spur–like features extending outwards from the nucleus to latitudes of $\pm1°$. The most prominent molecular spurs seen in the survey are shown in Figs. 12 and 14 and are labelled I to V. The full l–b–Vranges of these features are presented in Table 3 along with other parameters. The error in $\frac{N_{OH}}{T_{ex}}$ is typically 10^{14} cm^{-2} K^{-1} and the error in M_{OH} is typically 20%. All the spurs show a double peaked velocity structure with absorption in similar velocity ranges ($V \sim -150 \rightarrow -90$ km s^{-1} and $V \sim 0 \rightarrow +80$ km s^{-1}). Our b–V maps of the region close to the nucleus show that the OH absorption at high latitudes is very strongly concentrated into the observed spurs. Integrating the $\tau_a$profiles over all $\mid b \mid \geq 0.^\circ8$ in the region $358.^\circ8 \leq l \leq 0.^\circ4$ suggests that about three–quarters of the gas in this region lies within the spurs. The spurs are associated with radio continuum features, as we now describe.

Spurs I and II: These two features at longitudes $0.^\circ0$ and $359.^\circ4$ appear to be associated with the galactic centre lobe (GCL), a well–known radio continuum structure described by Sofue & Handa (1984). The OH absorption features can be followed from latitude $+0.^\circ4$, where they first emerge from the molecular concentration near the nucleus, to latitude $+1.^\circ0$. For each spur the OH profiles show broad absorption at two velocities, typically -130 km s^{-1}and $+50$ km s^{-1}. The features can be seen in individual l–b maps (Figs. 6–9). They are better shown in the l–b maps of Figs. 12 and 14 where the OH absorption has been integrated over large velocity ranges. A possible weak bridge of absorption connecting these spurs is also seen at latitude $+0.^\circ8$ and velocity -120 km s^{-1}. The positional agreement of the spurs and bridge with the galactic centre lobe is shown in Fig. 14. Parts of Spurs I and II appear to have been detected in CO by Sofue (1985) (part of Spur I at $+90$ km s^{-1}), and by Uchida et al. (1990) (part of Spur II at $+50 \rightarrow +150$ km s^{-1}). However, the CO measurements did not reveal the double velocity structure of the spurs, or the molecular bridge between them.

Spur III: This new feature appears at longitude $0.^\circ2$ and extends to latitude $-1.^\circ0$. It has the same twin velocity structure as Spurs I and II. Spur III is approximately symmetric about the galactic centre with Spur I. It appears to be associated with the radio continuum spur known as the southern galactic centre lobe (Seiradakis et al. 1989).

Spurs IV and V: These two features are associated with the non–thermal galactic centre radio shell G359.1–0.5 (Uchida et al. 1992). Spur IV at longitude $359.^\circ6$ can be traced in our OH data to latitude $-1.^\circ2$, and Spur V at longitude $358.^\circ8$ can be traced to latitude $-1.^\circ0$. Spur IV has the twin velocity structure characteristic of the other galactic centre molecular spurs, with broad weak absorption features at approximately -120 km s^{-1}and $+40$ km s^{-1}. Spur V is clearly detected at negative velocities, with a broad weak absorption feature at approximately -130 km s^{-1}. It is much weaker at positive velocities and cannot be seen in the individual l–b plots in Figs. 6–9, although it is clearly seen in the integrated l–b plot in Fig. 14. The two features are most clearly seen in the l–b maps of the 1667 MHz line (Figs. 6 and 8) between -160 and -60 km s^{-1}. They are also shown in Fig. 14, where the integrated OH absorption is compared with the radio continuum features in the region. The low latitude parts of Spurs IV and V were detected in CO at negative velocities by Uchida et al. (1992), who noted that they encircle the radio continuum shell source G359.1–0.5. The OH spurs extend to more negative latitudes than this to the limits of our survey, and there is no clear evidence for a bridge between then as seen in the CO measurements. Spur IV may also be associated with the radio continuum sources G359.23–0.82 and G359.0–0.9.

Finally we note that our OH survey has some drawbacks when studying these molecular spurs as it has modest angular resolution, is undersampled, and relies on a continuum background against which absorption can be detected. These factors all make it difficult to test for a true physical association with radio continuum features. It is therefore important to extend the surveys in the CO and other emission lines at higher angular resolution.

5.5. *Previously known features*

The region between longitudes 358°and 3°and latitudes $\pm0.^\circ5$ contains many strong features which are well known, and which will not be discussed in detail here. The schematic l–V plot Fig. 13 shows the strongest of them. The expanding molecular ring feature is the dominant negative–velocity feature between $\pm1.^\circ4$ (e.g. Figs. 2 and 3, $b = -0.^\circ4$, $-0.^\circ2$). There is no symmetric counterpart at positive velocities; instead there is a string of strong absorption features at lower velocities (Scoville's ring 2), and a weak feature XVI at higher velocities. The nuclear disc feature can be traced at negative velocities from $l = 358.^\circ4$, $V = -200$ km s^{-1}to $l = 359.^\circ8$, $V = -40$ km s^{-1} (e.g. Figs. 2 and 3, $b = 0.^\circ2$, $+0.^\circ2$). The positive–velocity counterpart is weaker and is confused with other features.

Further details on these features, and references to earlier work, can be found in the survey papers by Cohen & Few (1976) in OH, Whiteoak & Gardener (1979) and Co-

hen & Few (1981) in H_2CO, and Bally et al. (1987, 1988) in CO.

5.6. *Maser emission*

The OH survey also detected a number of OH maser sources in emission. Nine previously known OH–HII region sources were detected. All can be found in catalogues by Caswell & Haynes (1983a,b). Several previously known OH–IR sources were also detected in mainline emission for the first time. These new detections are listed in Table 4 where we give the antenna temperatures and velocities of the detected features. Antenna temperature may be converted to Janskys by multiplying by 1.2.

6. Concluding remarks

The OH survey has revealed for the first time the large–scale structure of the molecular gas in the galactic centre region. The molecular nuclear disk can be traced over the entire region $354° < l < 6°$, corresponding to a projected diameter of ~ 1.8 kpc. The structure is warped, lying preferentially below the galactic plane at positive longitudes, and above the plane at negative longitudes. The warp extends to at least $\pm 1\overset{\circ}{.}6$ in latitude, corresponding to z–distances of ± 240 pc. The warp is in the same sense as the warp seen on a larger scale in the HI distribution (Cohen & Davies 1976).

It is possible that the OH survey has not traced the full z–extent of the molecular distribution. There are a few positions where OH absorption was detected at the outermost latitudes of the grid, for example at the lower extremities of Spurs IV and V. Furthermore the detection of OH absorption relies on a continuum background. In the present survey OH absorption was detected only at positions where the radio continuum was at least 5 K of antenna temperature (corresponding to 7.5 K of brightness temperature). Therefore it is possible that molecular gas could have been present far from the galactic plane in regions of low radio continuum emission, and not have been detected in the OH survey. The CO emission line observations by Dame et al. (1987) show that there is no large concentration of molecular gas far from the plane ($|b| < 8°$), but those observations would not have been sensitive to narrow filamentary structures such as the molecular spurs reported here.

The OH survey has revealed three new phenomena. Perhaps the most striking are the broadline clump features, of which there are at least 7. The large number of these clumps, and the fact that they show positive gradients of velocity with longitude, put strong constraints on their possible origin. At positive longitudes the clumps appear to be connected by filaments which have typical widths of 30 $\mathrm{km\,s^{-1}}$, much narrower than those of the clumps. Together the clumps and filaments appear to form an organized structure which accounts for most of the molecular gas at $l > 2°$. The clumps at negative longitudes have lower apparent opacities, and it is possible that filaments connecting them would have been below our detection limit. The third new phenomenon is the existence of molecular spurs near $l = 0°$which point out of the galactic plane and extend to latitudes of at least $\pm 1°$. The spurs all appear to be associated with radio continuum features. Spurs I and II follow the galactic centre lobe (Sofue & Handa 1984), Spur III follows the southern galactic centre lobe (Seiradakis et al. 1989), and Spurs IV and V are associated with the shell source G359.1–0.5 (Uchida et al. 1992). CO observations of these spurs would be desirable to trace their full extents and to study at higher angular resolution their association with the radio continuum features.

Acknowledgements. PJB acknowledges financial support from the SERC during the period which this work was carried out.

References

Bally J., Stark A.A., Wilson R.W., Henkel C. 1987, ApJS 65, 13
Bally J., Stark A.A., Wilson R.W., Henkel C. 1988, ApJ 324, 223
Bania T.M. 1977, ApJ 216, 381
Bania T.M., Stark A.A., Heiligman G.M. 1986, ApJ 307, 350
Blitz L., Binney J., Lo K.Y., Bally J., Ho P.T.P. 1993, Nat 361, 417
Boyce P.J. 1990, PhD thesis, University of Manchester
Boyce P.J., Cohen R.J. 1989, ed. M. Morris, The Centre of our Galaxy, I.A.U. Symp. No. 136 (Kluwer Academic Publishers, Dordrecht) 141
Boyce P.J., Cohen R.J., Dent W.R.F. 1989, MNRAS 239, 1013
Brown R.L., Liszt H.S. 1984, ARA$A 22, 223
Burton W.B., Liszt H.S. 1978, ApJ 225, 815
Caswell J.L., Haynes R.F. 1982, ApJ 254, L31
Caswell J.L., Haynes R.F. 1983a, Aust. J. Phys 36, 361
Caswell J.L., Haynes R.F. 1983b, Aust. J. Phys 36, 417
Cohen R.J. 1982, eds. J.E. Beckman, J.P. Phillips, Submillimetre Wave Astronomy (Cambridge University Press) 185
Cohen R.J., Davies R.D. 1976, MNRAS 175, 1
Cohen R.J., Dent W.R.F. 1983, eds. W.B. Burton, F.P. Israel, Surveys of the Southern Galaxy (Reidel, Dordrecht) 159
Cohen R.J., Few R.W. 1976, MNRAS 176, 495
Cohen R.J., Few R.W. 1981, MNRAS 194, 711
Dame T.M., Ungerechts H., Cohen R.S. et al. 1987, ApJ 322, 706
Genzel R., Townes C.H. 1987, ARA&A 25, 377
Liszt H.S., Burton W.B. 1980, ApJ 236, 779

McGee R.X., Brooks J.W., Sinclair M.W., Batchelor R.A. 1970, Aust. J. Phys 23, 777
Oort J.H. 1977, ARA&A 15, 295
Pointon L. 1977, J. Phys. E 10, 883
Robinson B.J., McGee R.X. 1970, Aust. J. Phys 23, 405
Seiradakis J.H., Reich W., Sofue Y. 1989, ed. M. Morris, The Centre of our Galaxy, I.A.U. Symp. No. 136 (Kluwer Academic Publishers, Dordrecht) 237
Sofue Y. 1985, PASJ 37, 697
Sofue Y. & Handa T. 1984, Nature 310, 568
Stacy J.G., Bitran M.E., Dame T.M., Thaddeus P. 1989, ed. M. Morris, The Centre of the Galaxy, I.A.U. Symp. No. 136 (Kluwer Academic Publishers, Dordrecht) 157
Stark A.A., Bania T.M. 1986, ApJ 306, L17
Staveley–Smith L.G. 1985, PhD Thesis, University of Manchester
Townes C. 1989, ed. M. Morris, The Centre of our Galaxy, I.A.U. Symp. No. 136 (Kluwer Academic Publishers, Dordrecht) 1
Uchida K.I., Morris M., Serabyn E. 1990, ApJ 351, 443
Uchida K.I., Morris M., Bally J., Pound M., Yusef–Zadeh F. 1992, ApJ 398, 128
Whiteoak J.B., Gardener F.F. 1979, MNRAS 188, 445
Zylka R., Gusten R., Henkel C., Batrla W. 1992, A&AS 96, 525

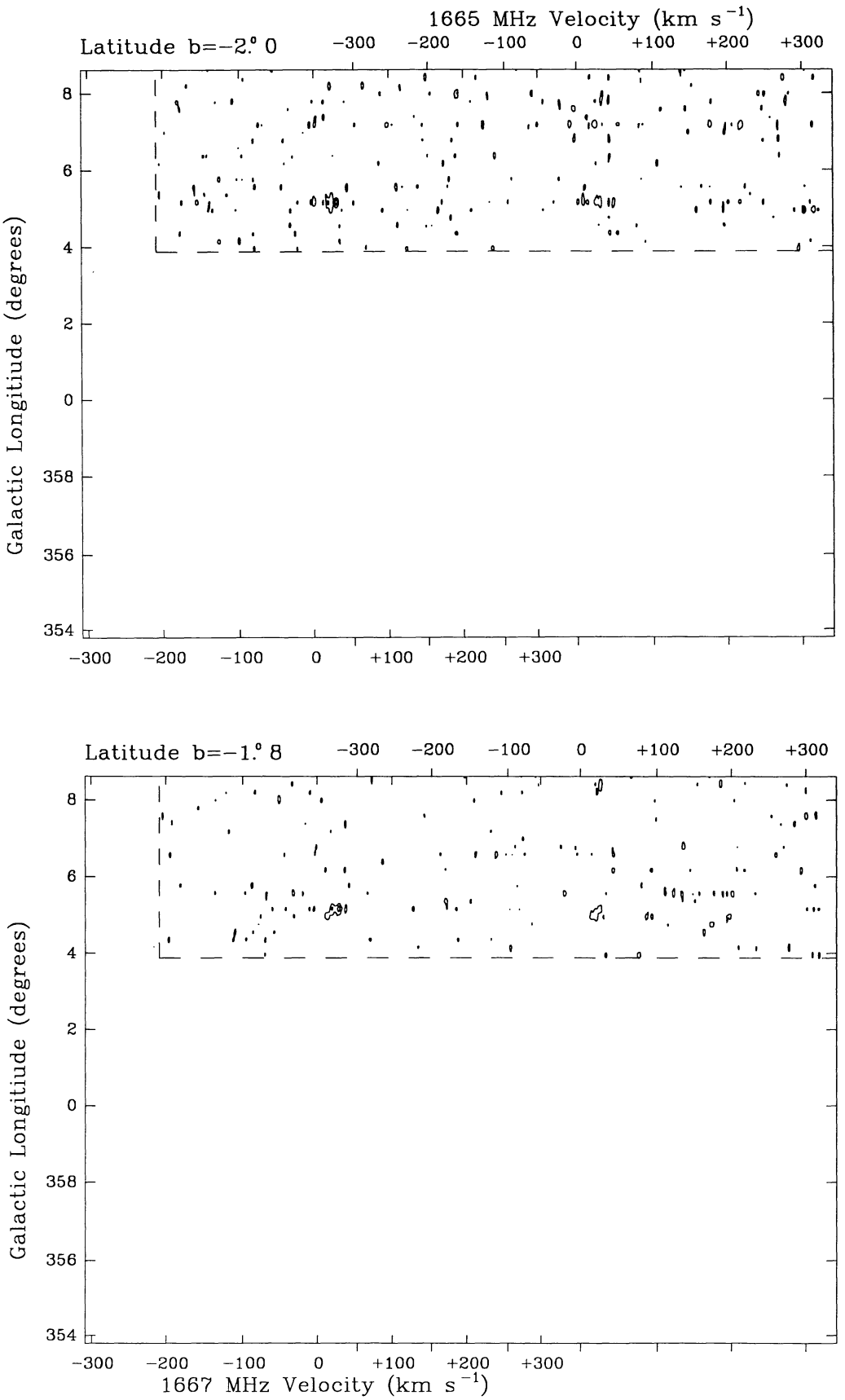

Fig. 2. Longitude-velocity maps of the OH absorption. Contour levels are in units of antenna temperature and set at intervals of −0.16, −0.32, −0.64, −1.28, −2.56, −5.12, −10.24, −20.48 and −40.96 K. The resolution is 3.1 km s^{-1} × 12′

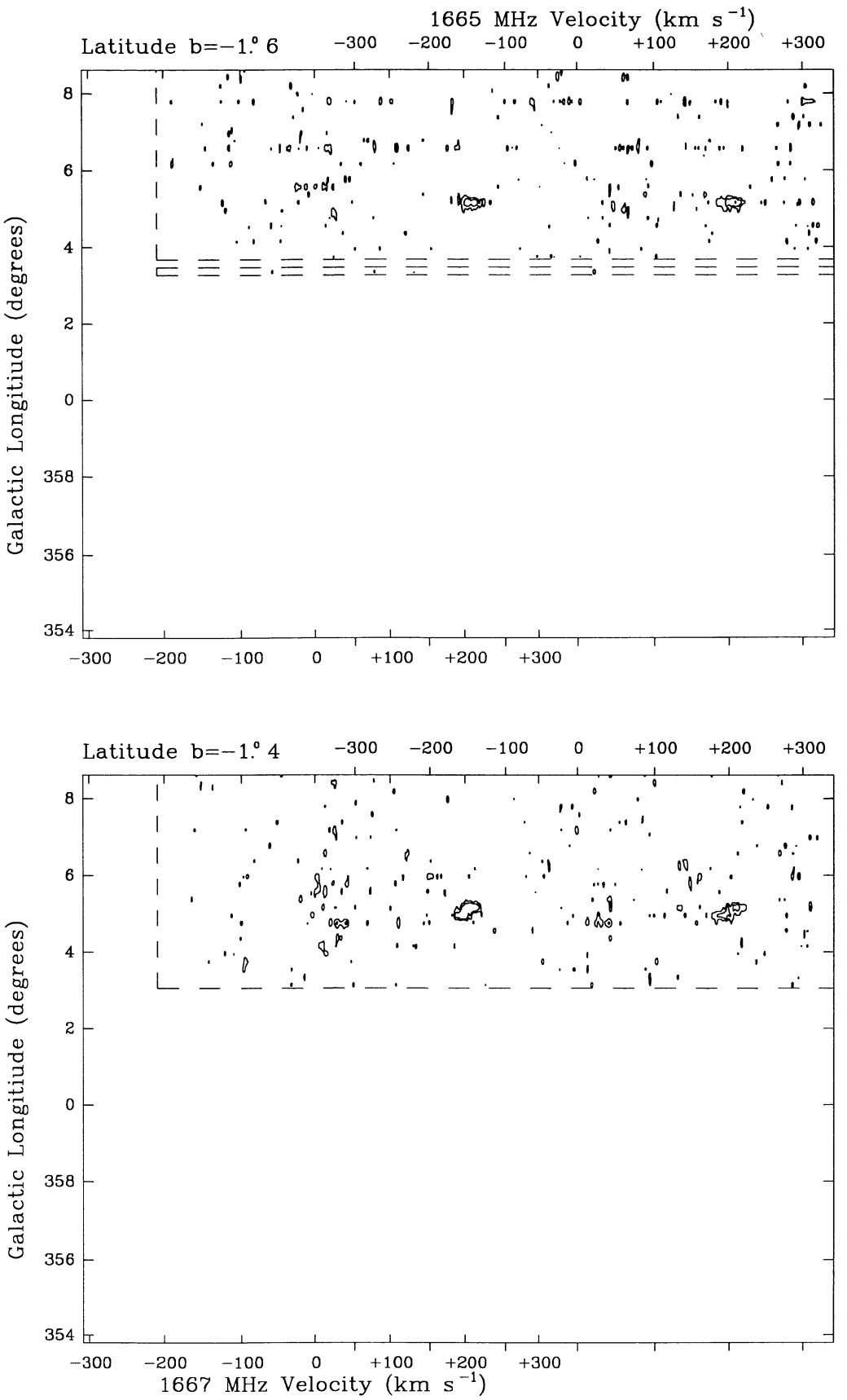

Fig. 2. continued

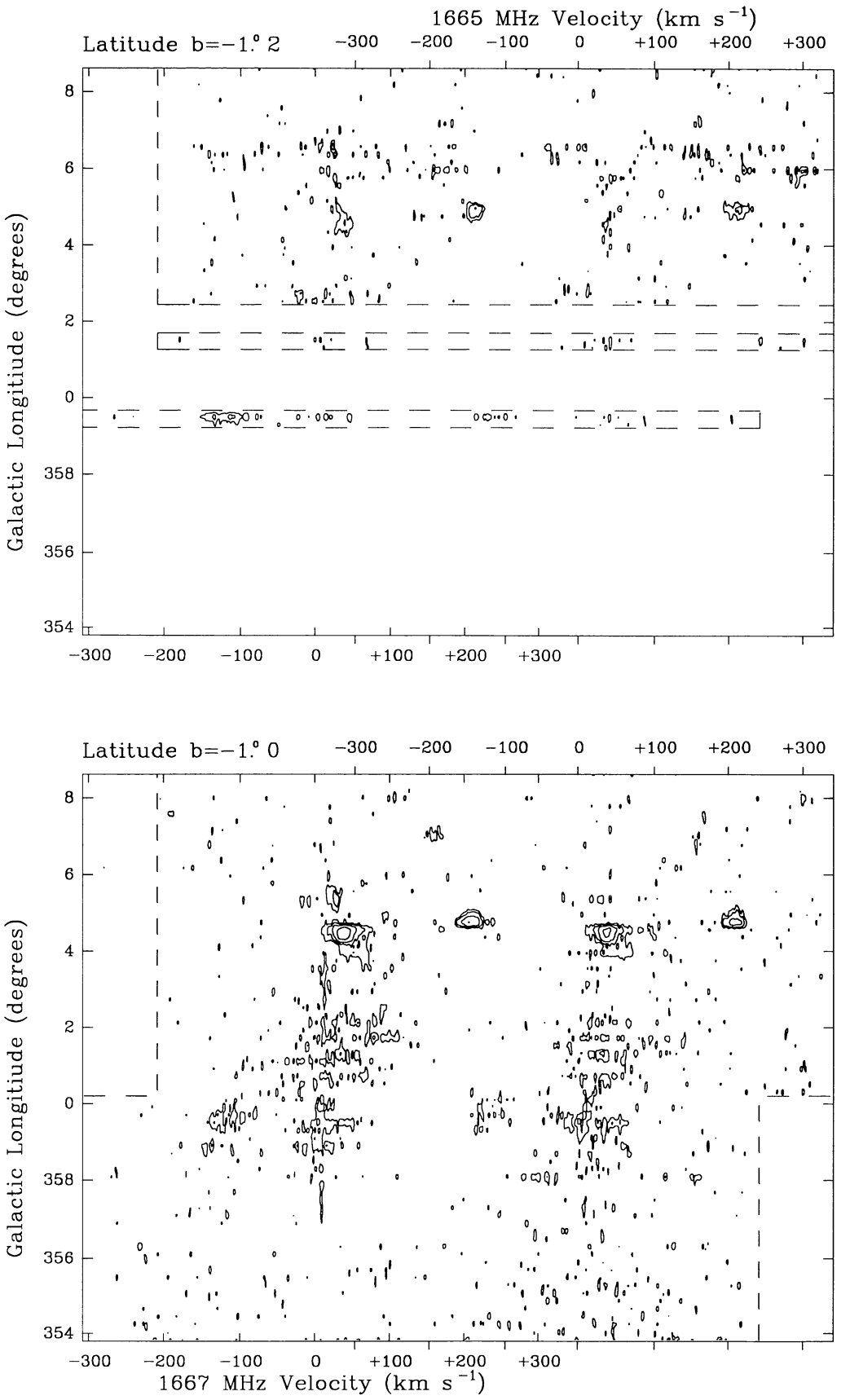

Fig. 2. continued

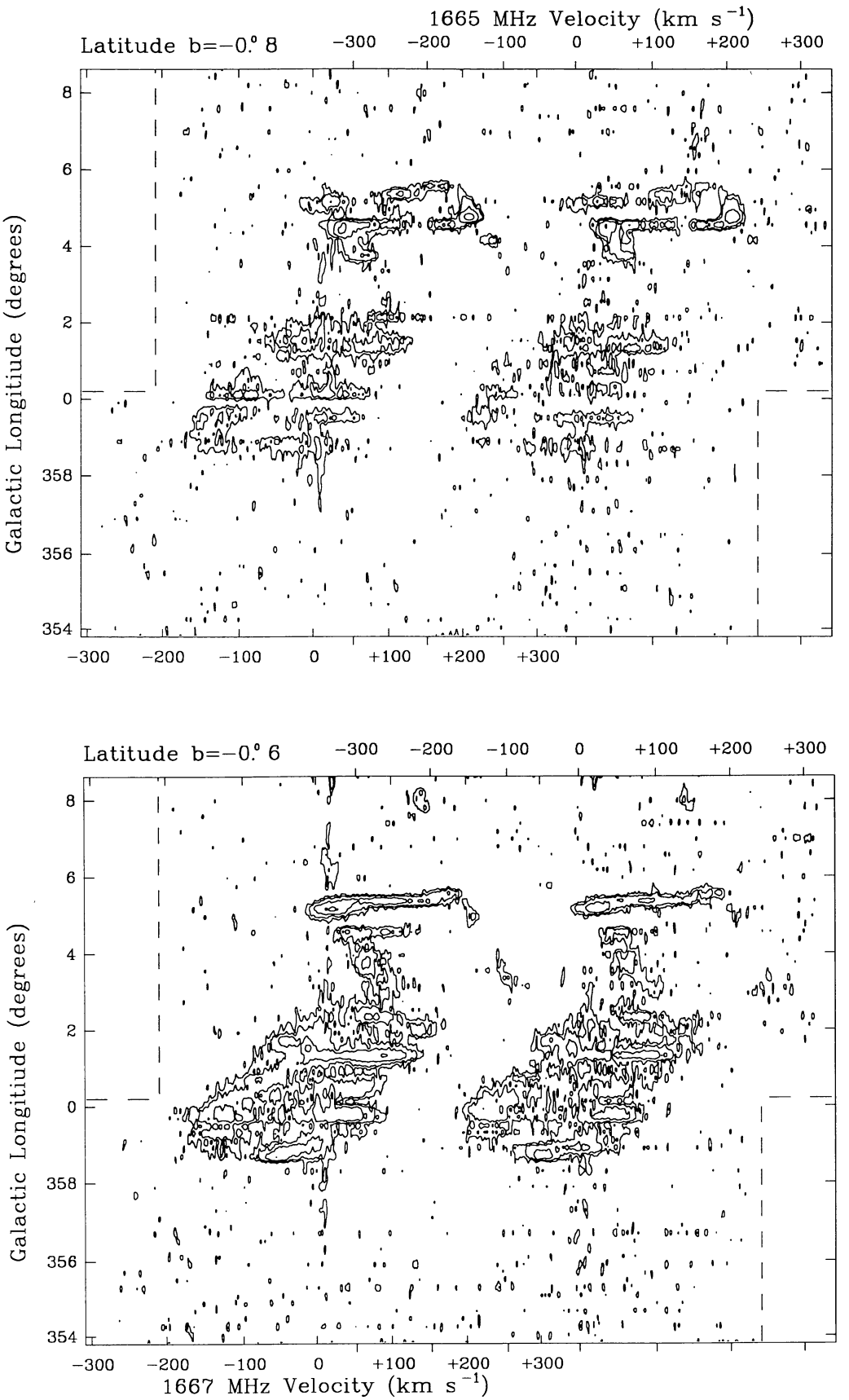

Fig. 2. continued

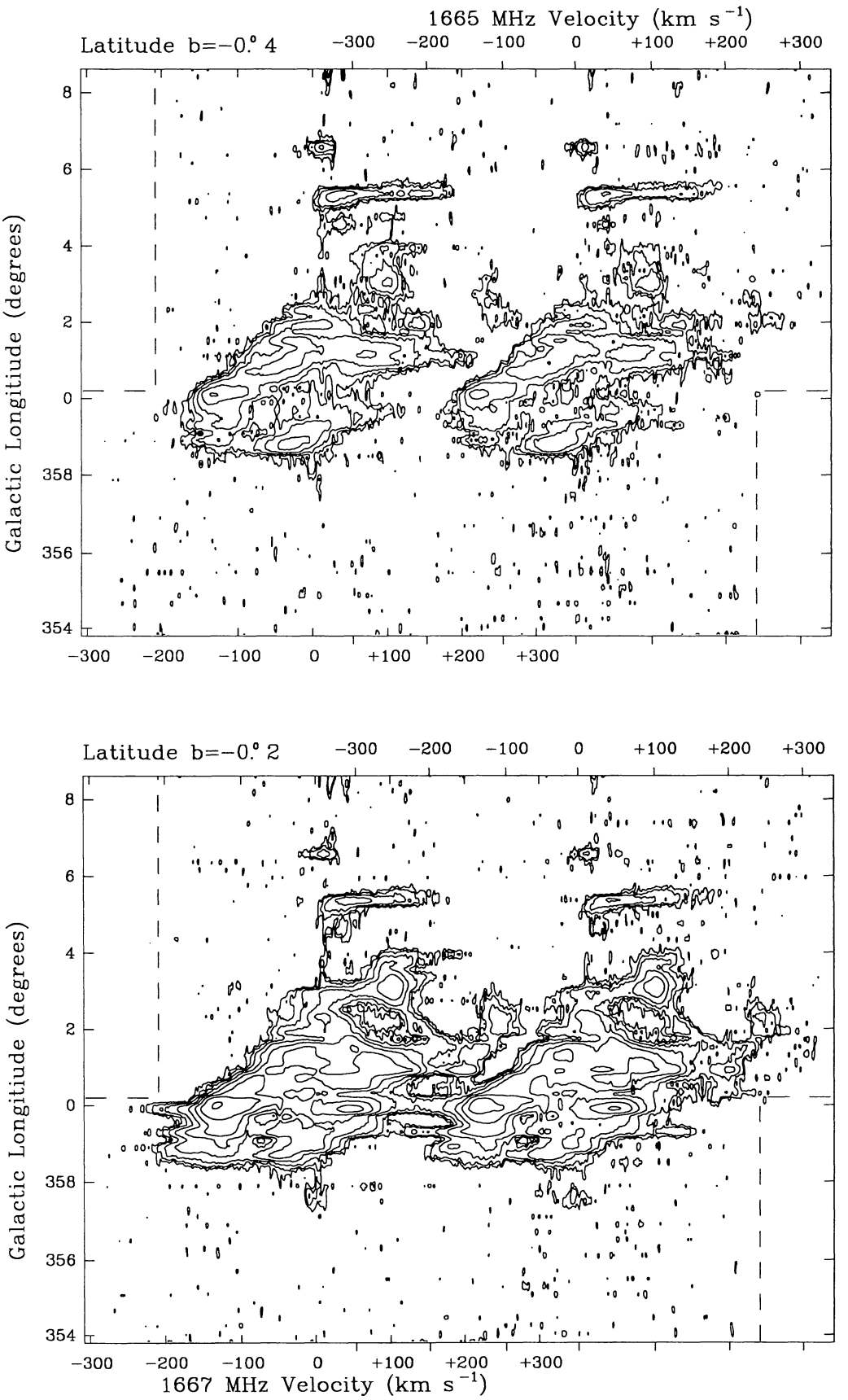

Fig. 2. continued

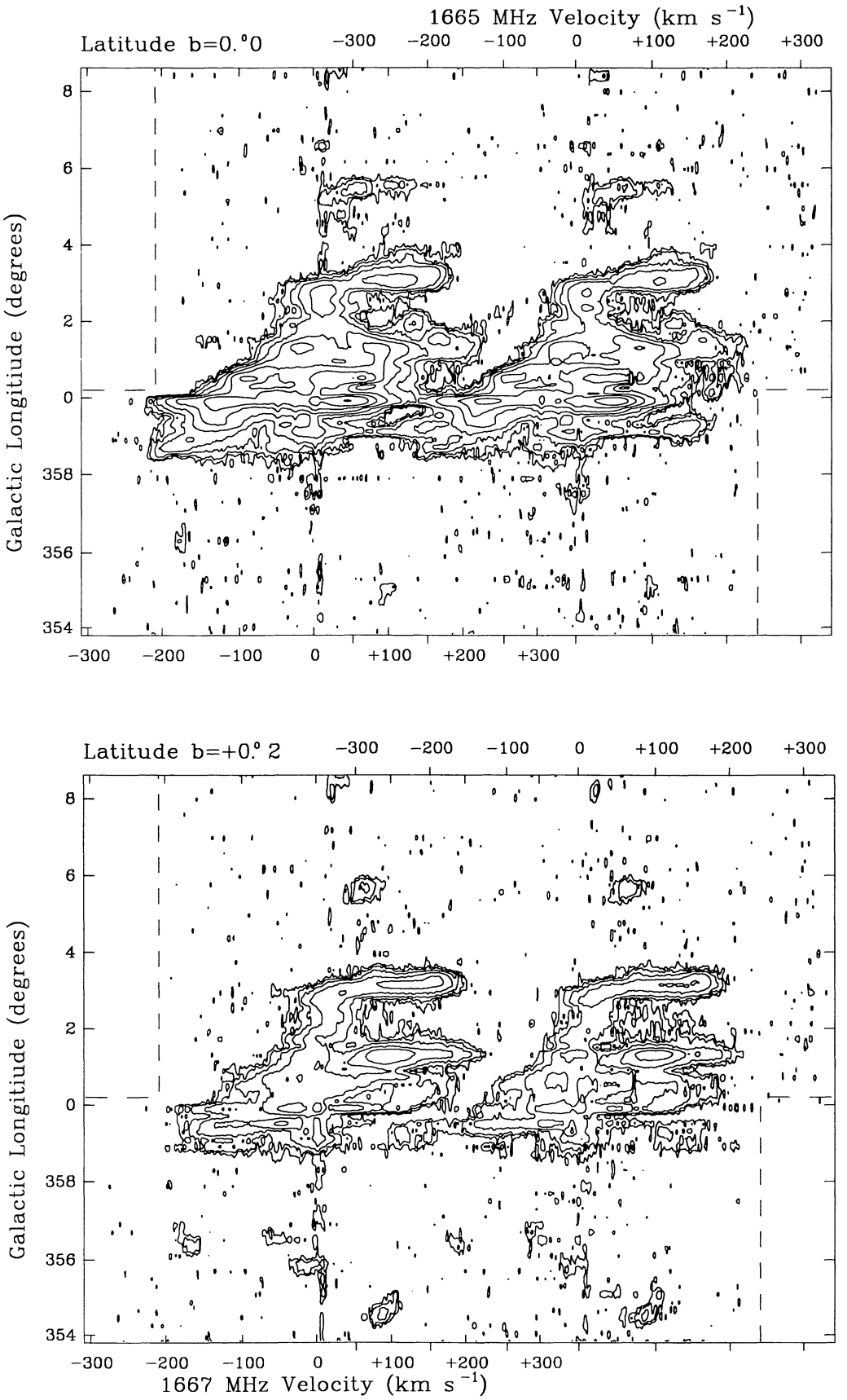

Fig. 2. continued

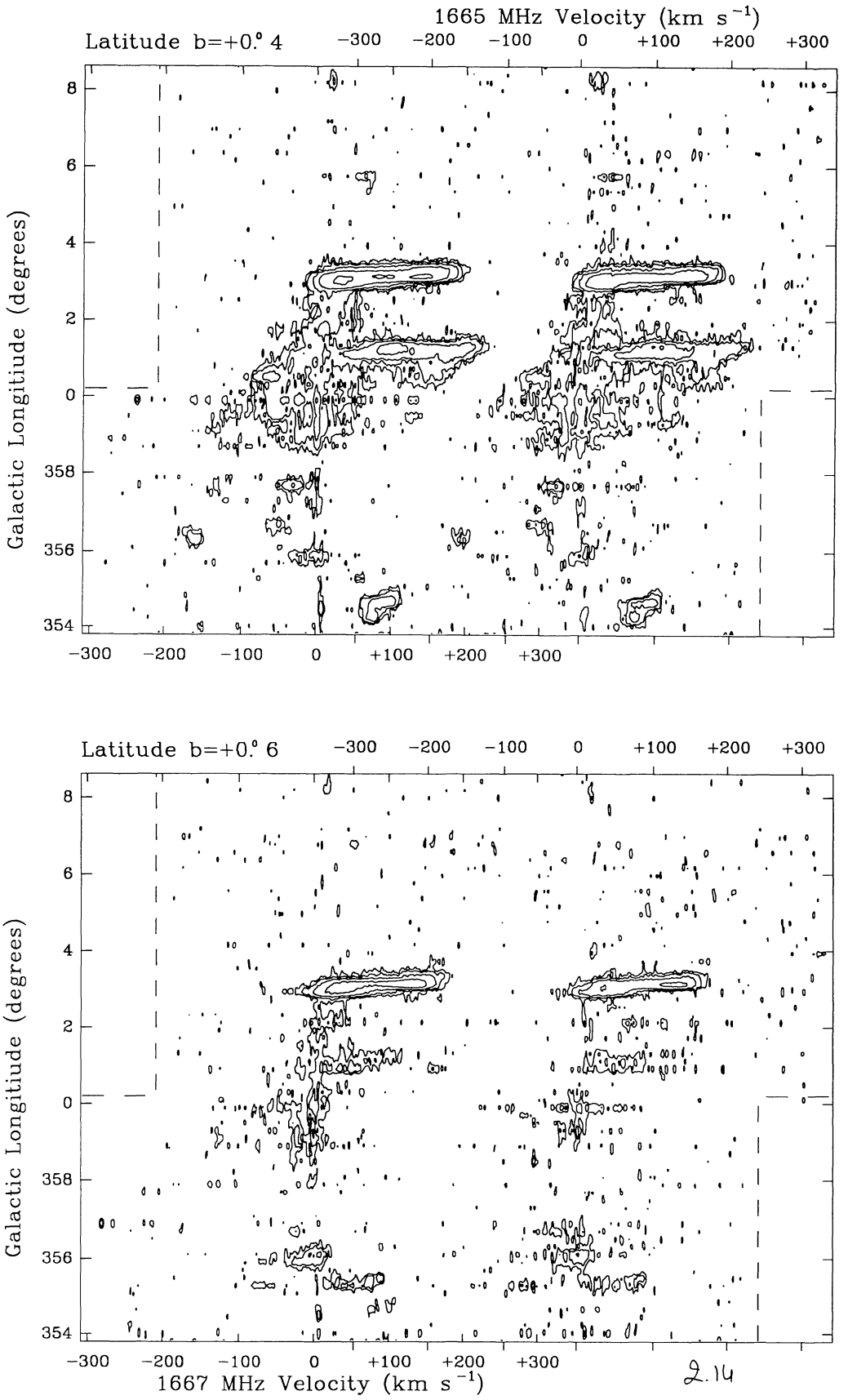

Fig. 2. continued

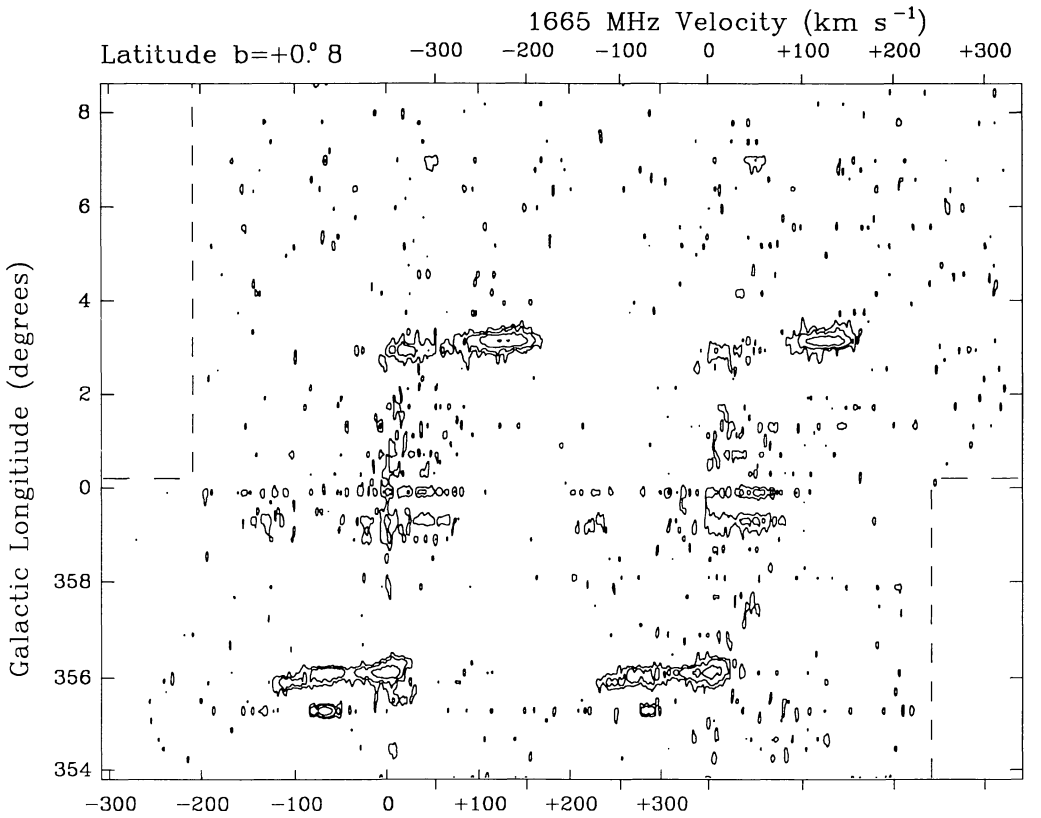

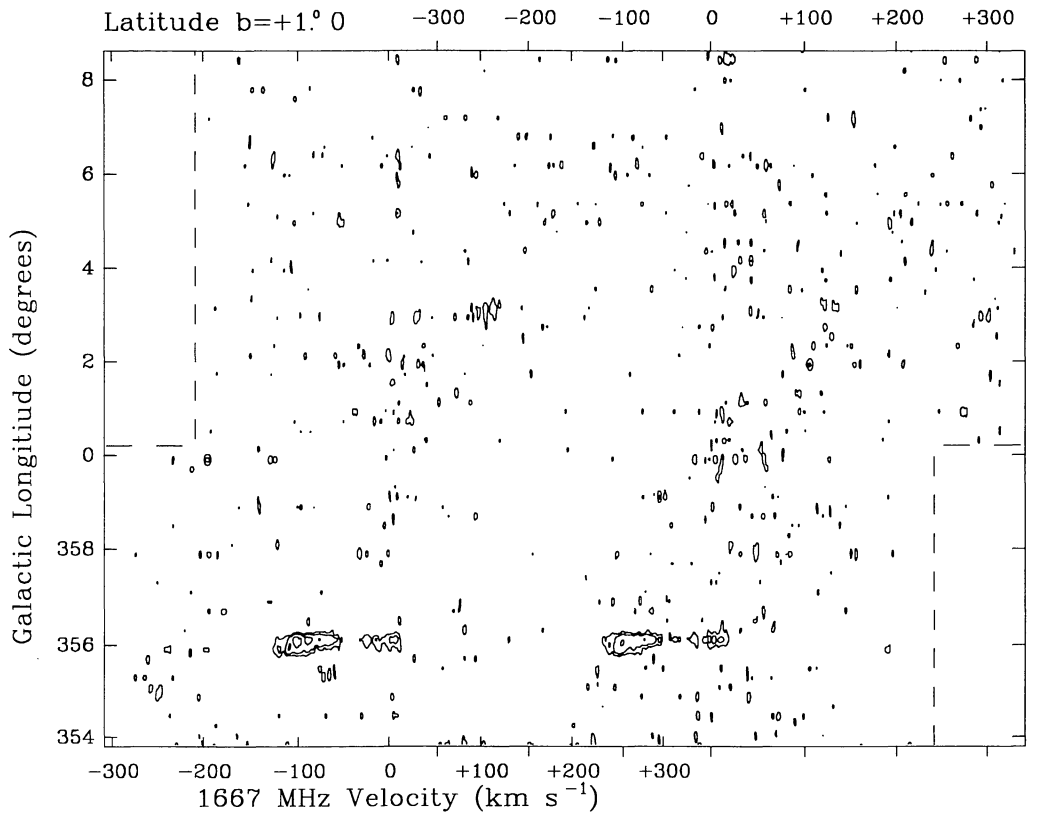

Fig. 2. continued

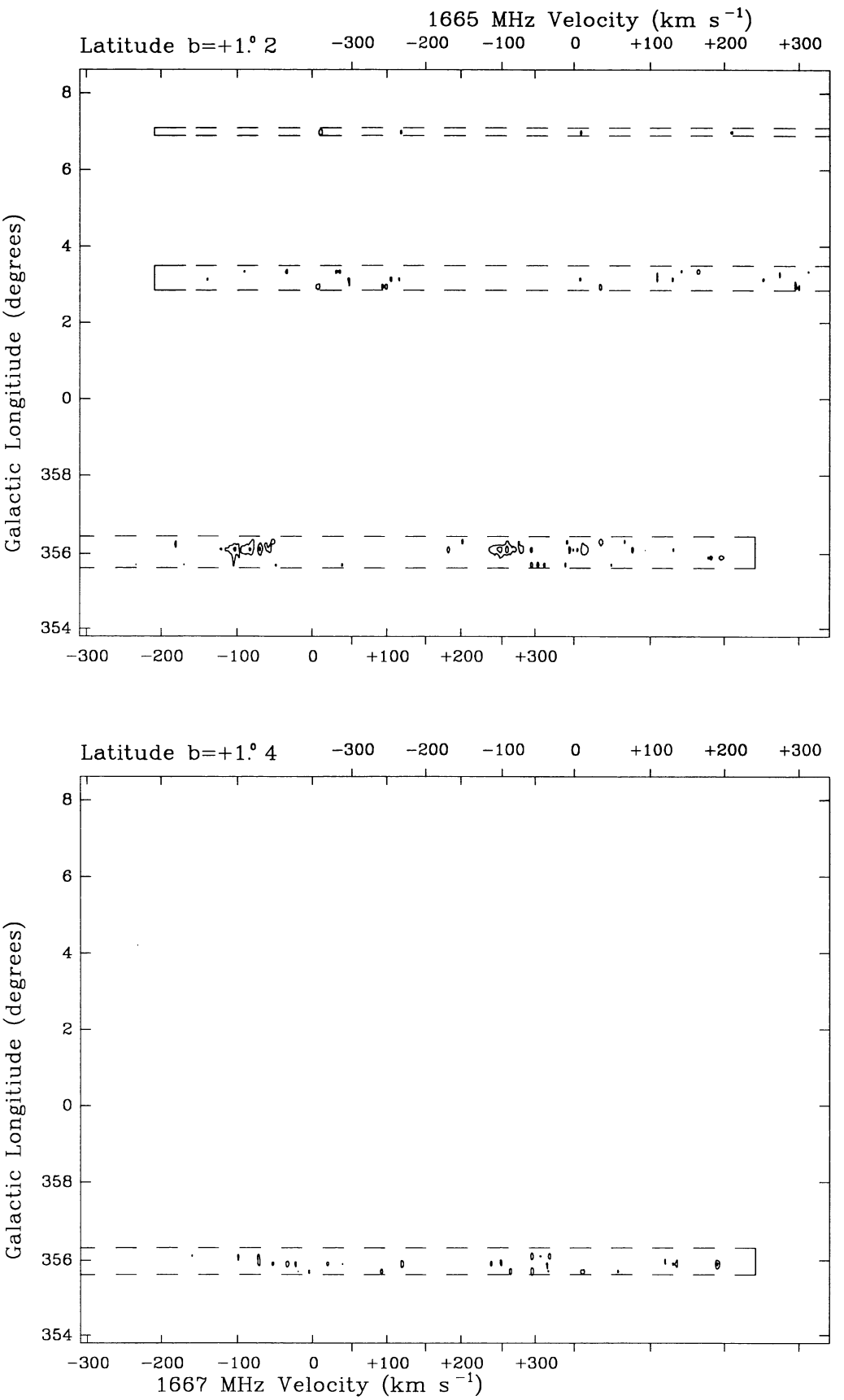

Fig. 2. continued

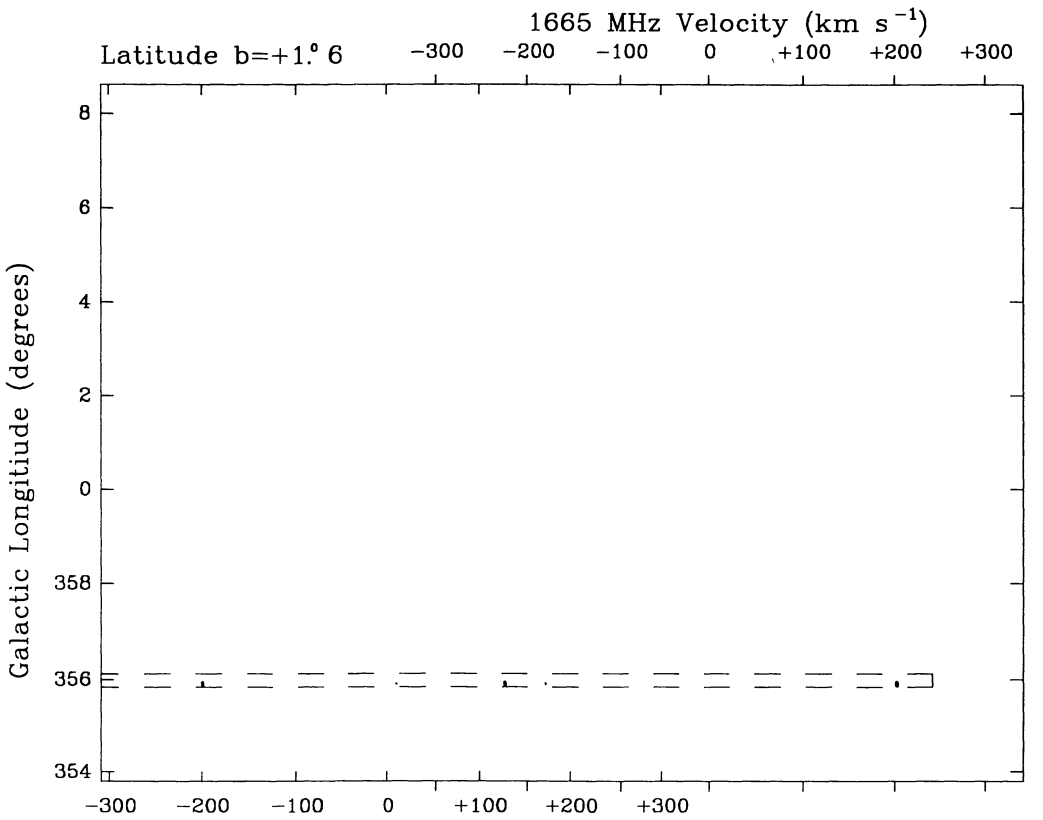

Fig. 2. continued

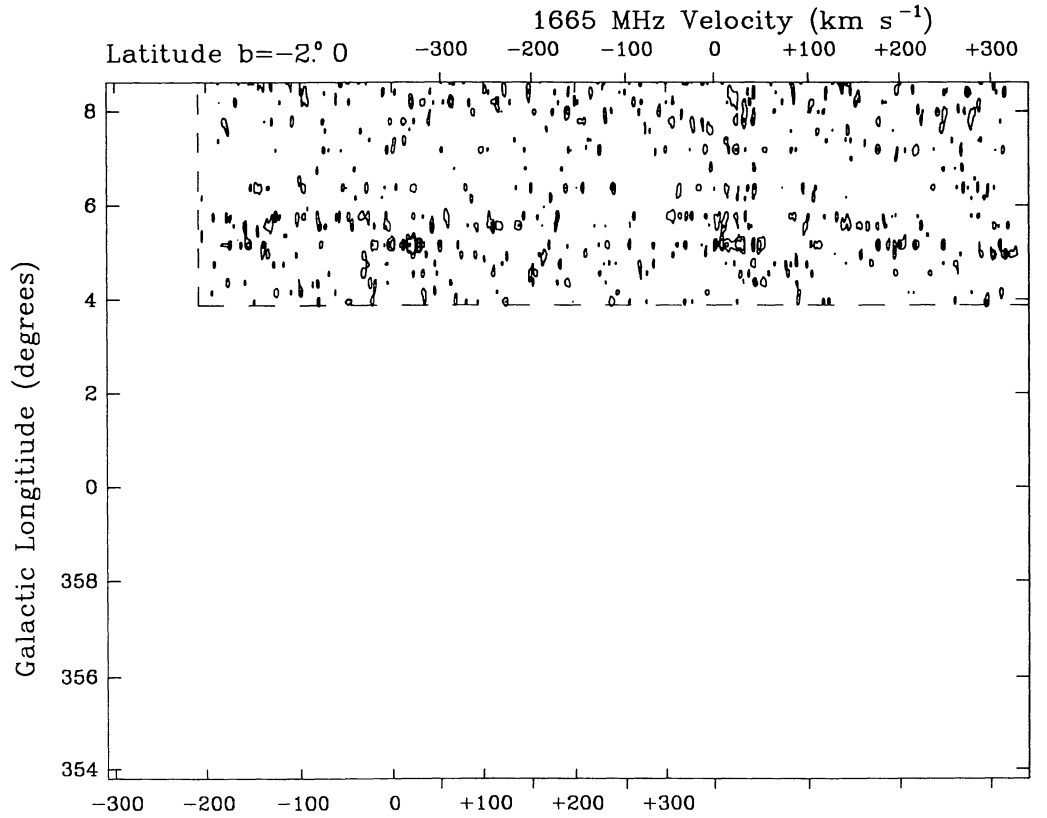

Fig. 3. Longitude–velocity maps of apparent opacity. Between $-0.^{\circ}8 \leq b \leq 0.^{\circ}8$ contour levels are at 0.02, 0.04, 0.08, 0.16, 0.32 and 0.64. Elsewhere the contours are at 0.04, 0.08, 0.16, 0.32 and 0.64. The resolution is 3.1 km s^{-1} × 12′

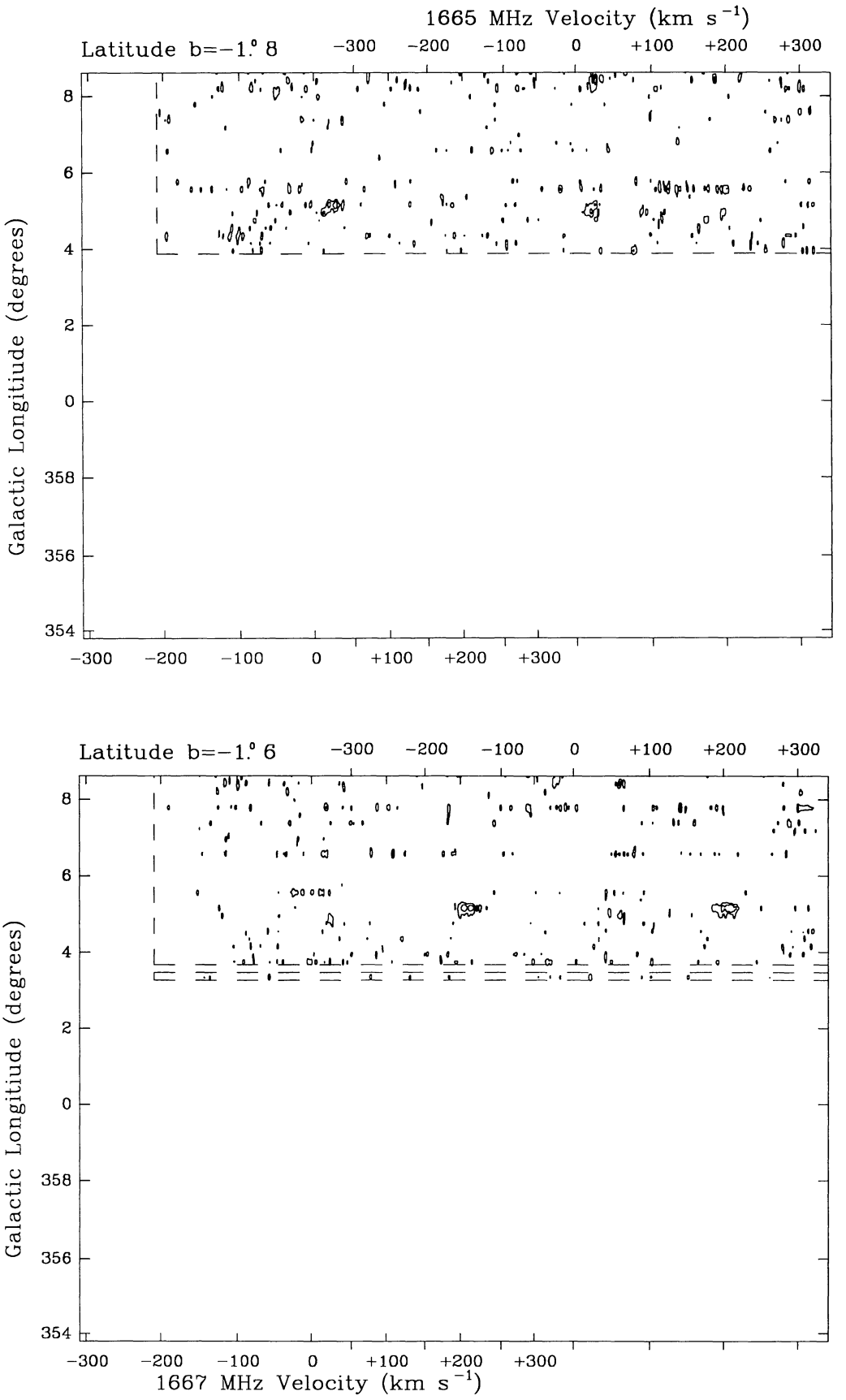

Fig. 3. continued

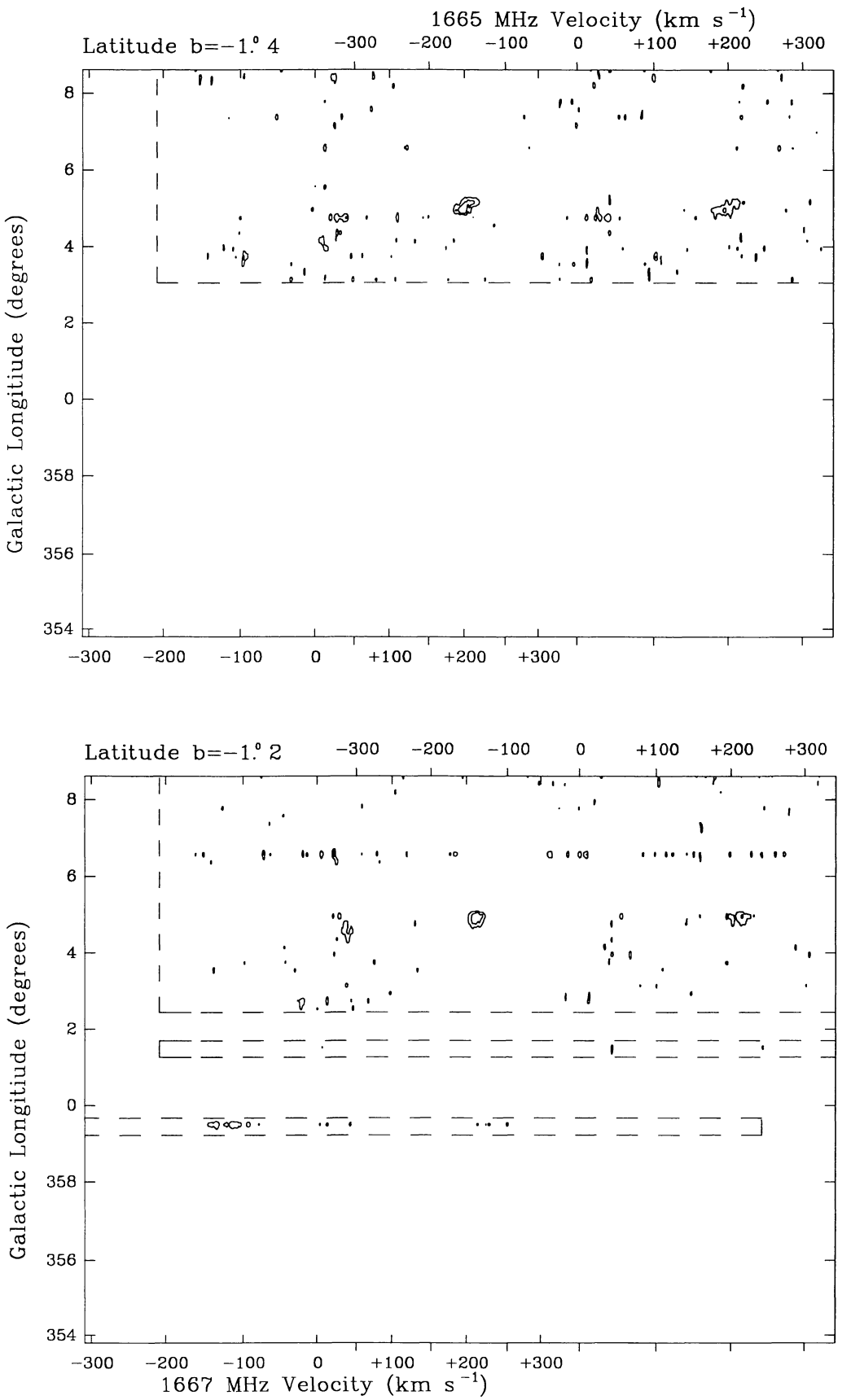

Fig. 3. continued

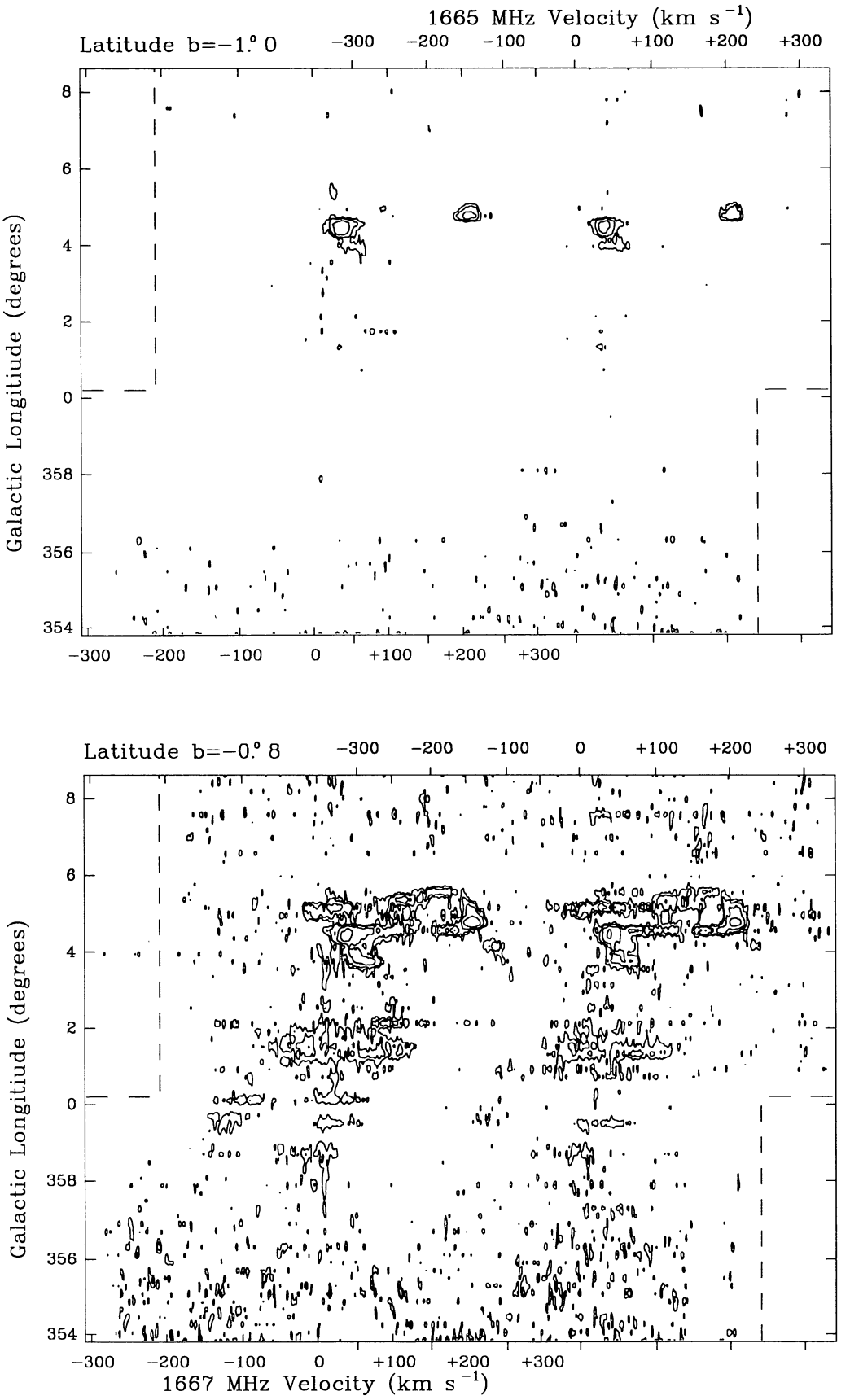

Fig. 3. continued

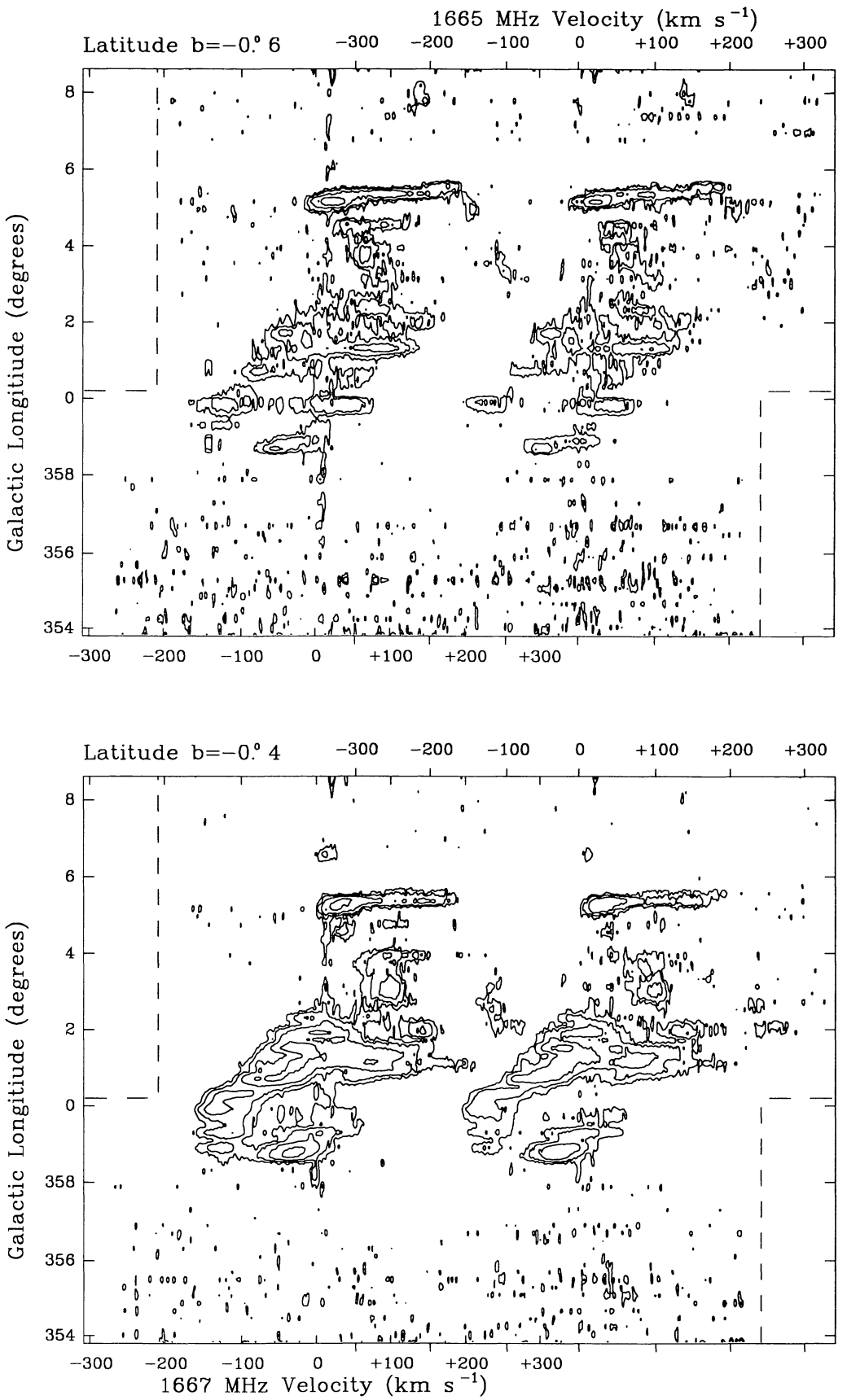

Fig. 3. continued

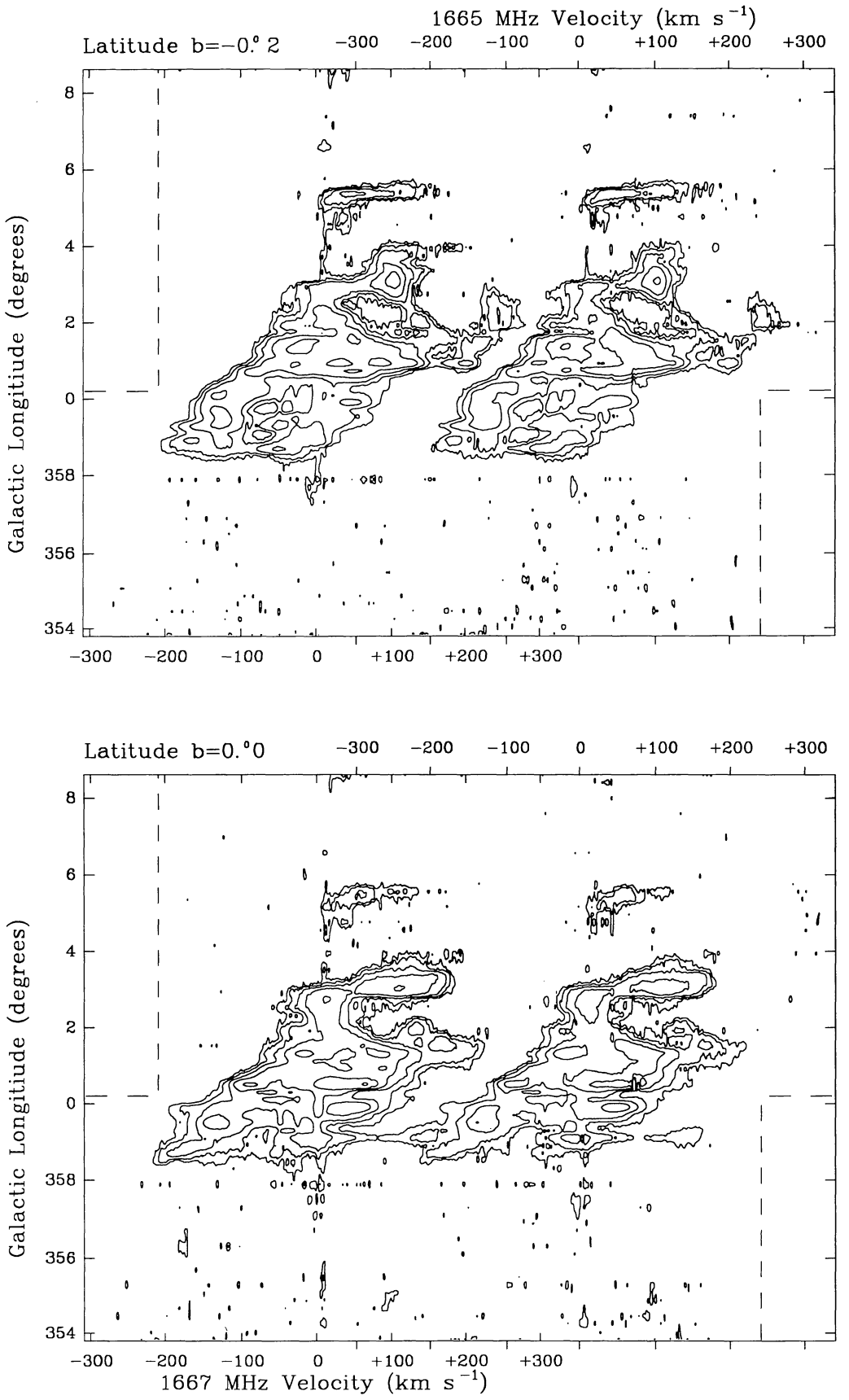

Fig. 3. continued

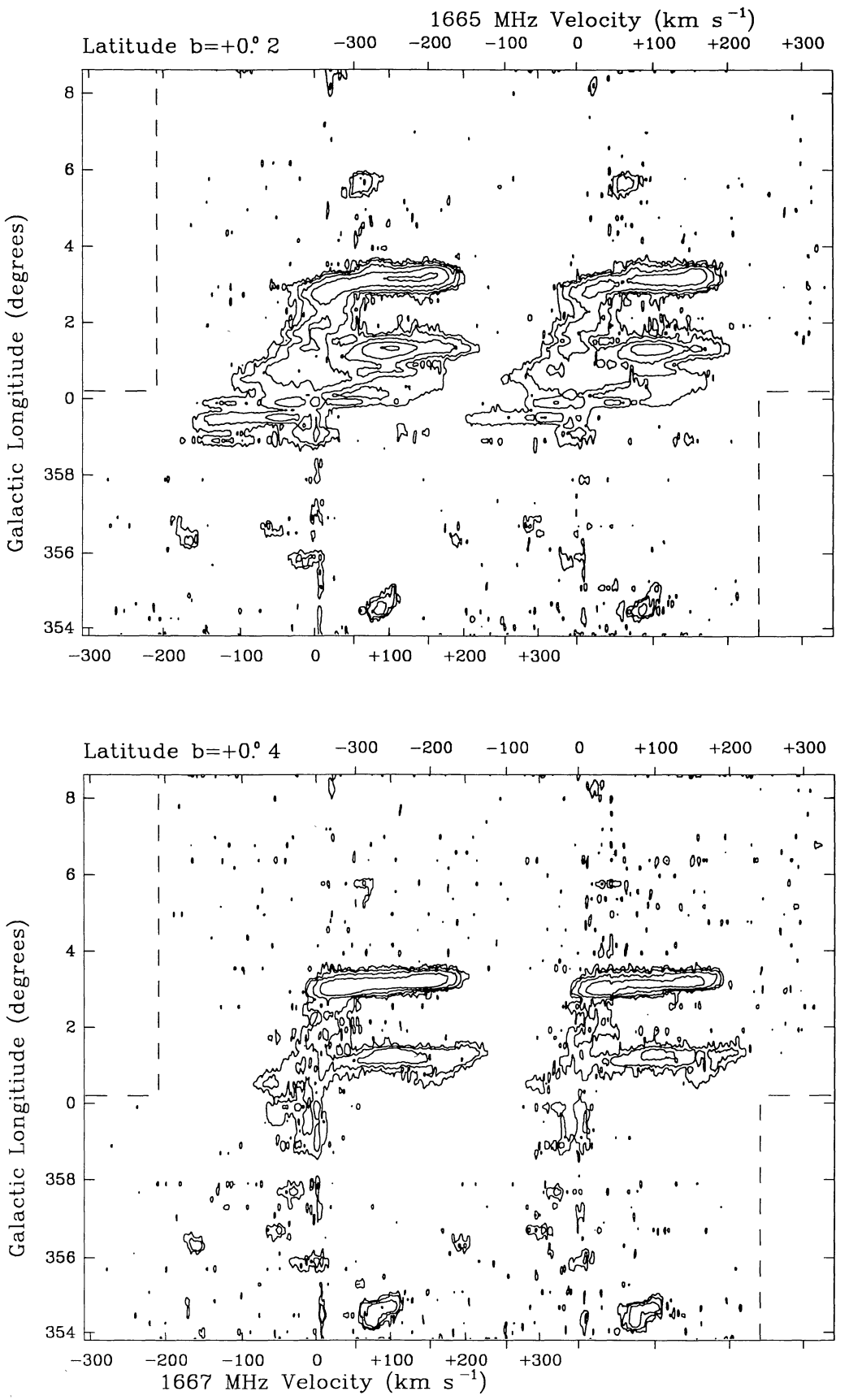

Fig. 3. continued

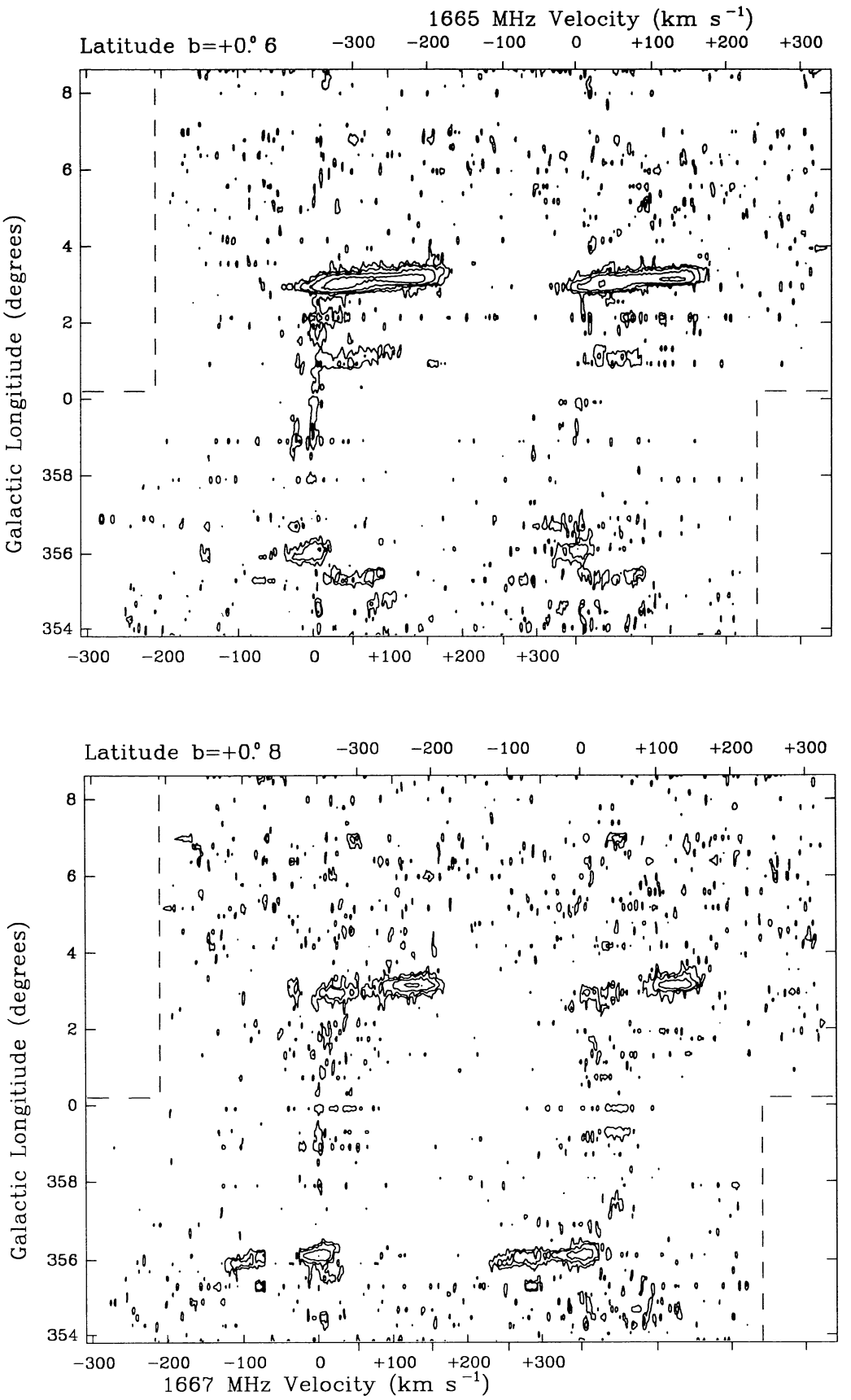

Fig. 3. continued

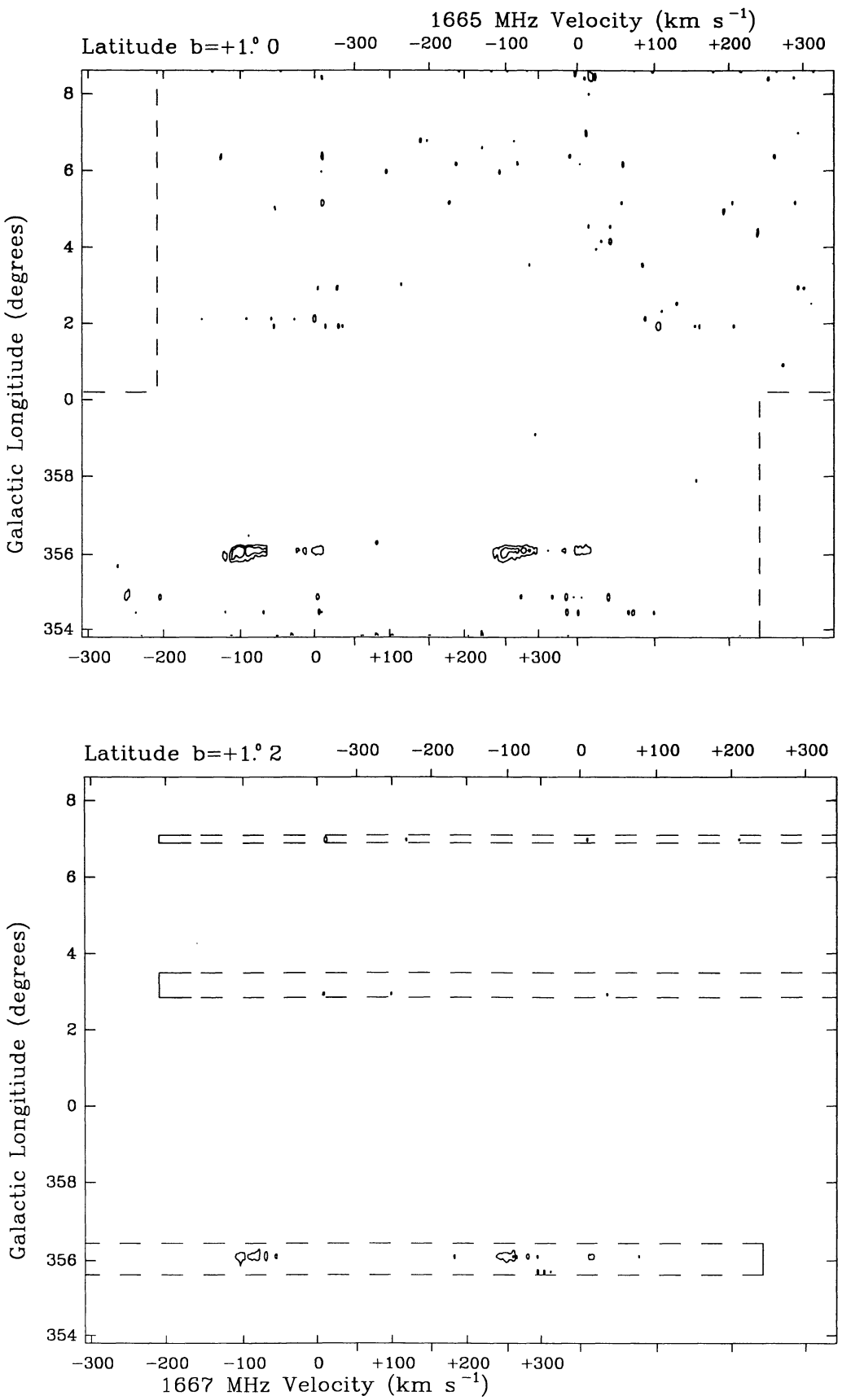

Fig. 3. continued

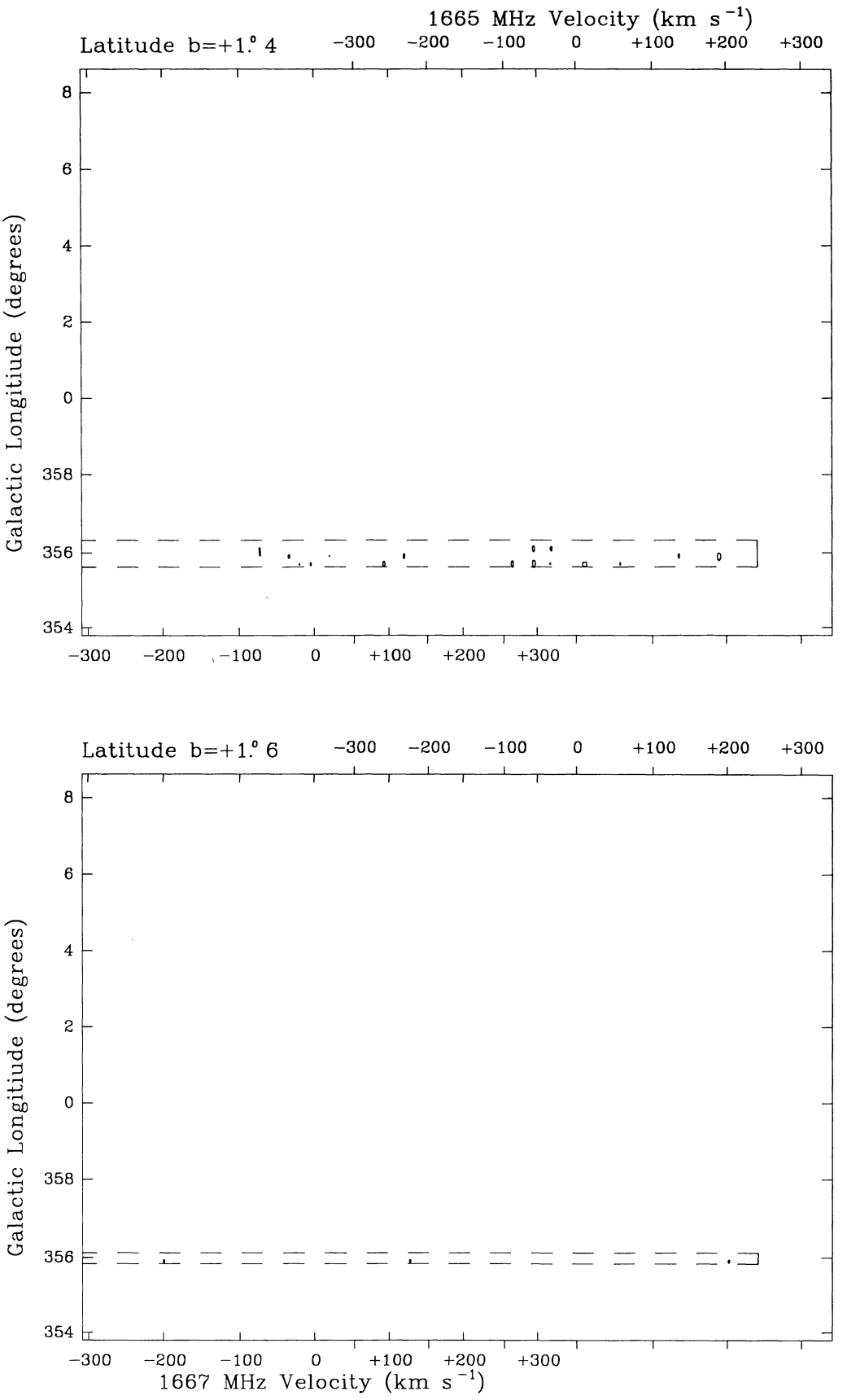

Fig. 3. continued

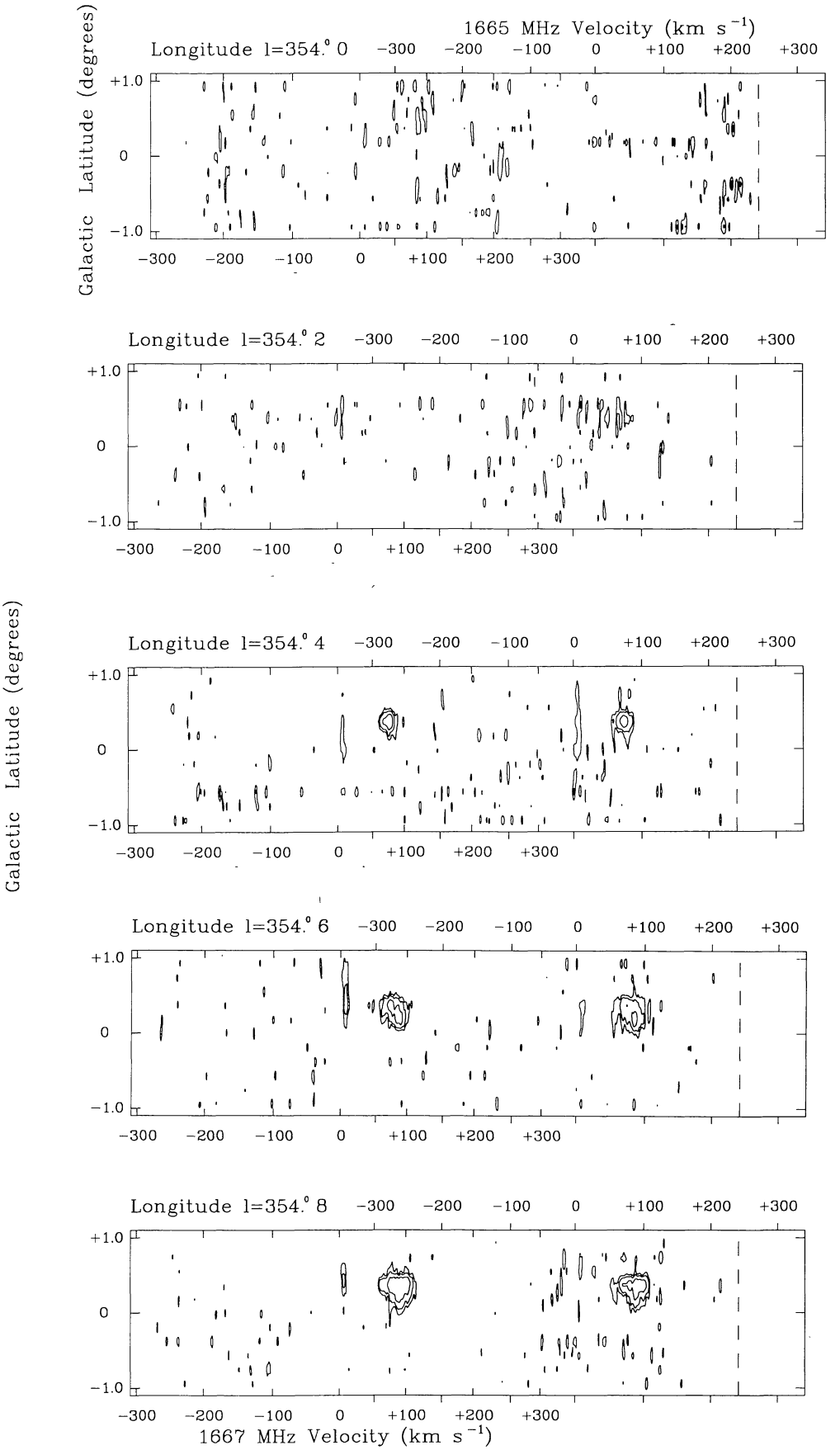

Fig. 4. Latitude-velocity maps of the OH absorption. Contour levels are in units of antenna temperature and set at intervals of −0.16, −0.32, −0.64, −1.28, −2.56, −5.12, −10.24, −20.48 and −40.96 K. The resolution is 3.1 km s^{-1} × 12′

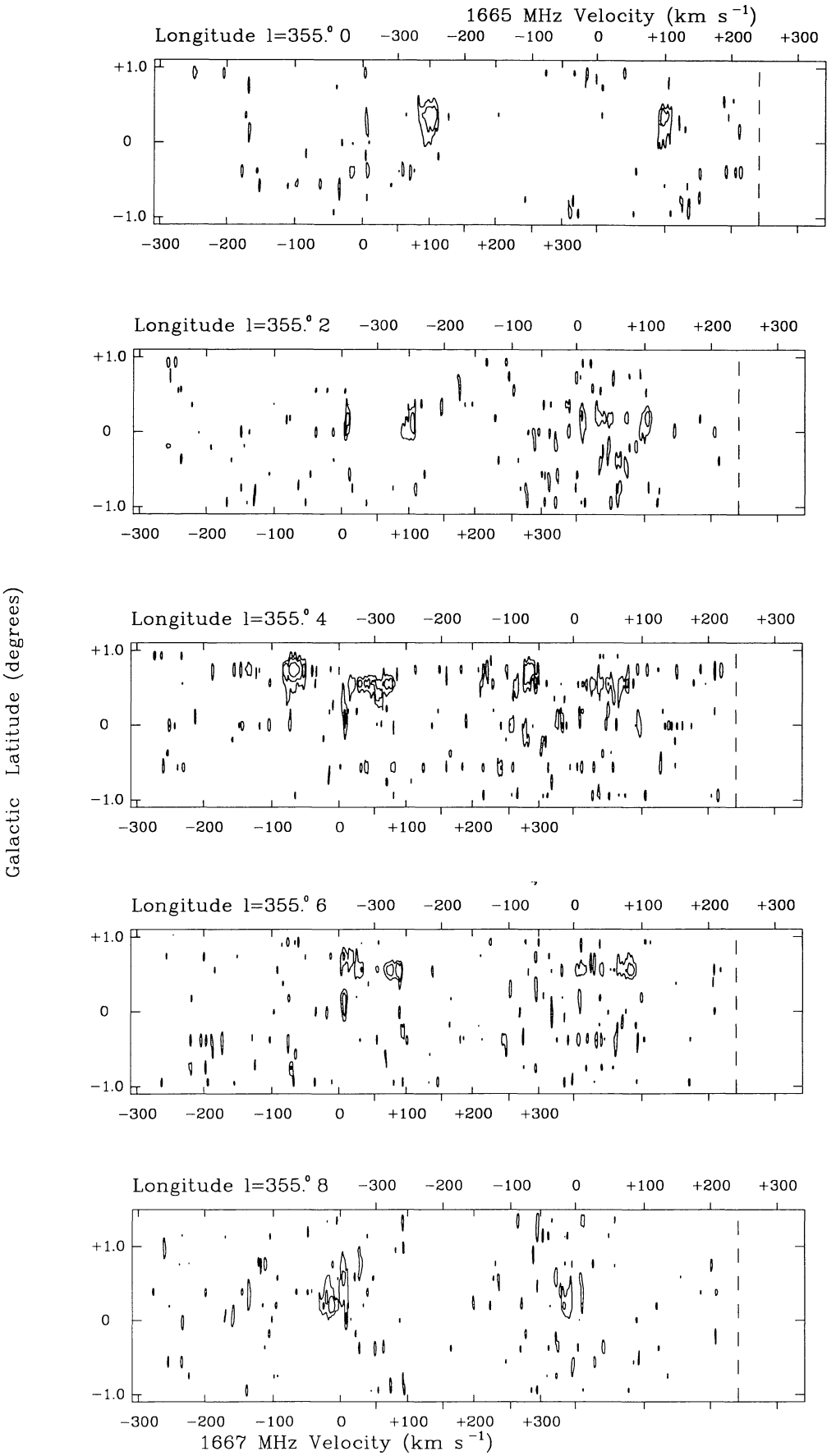

Fig. 4. continued

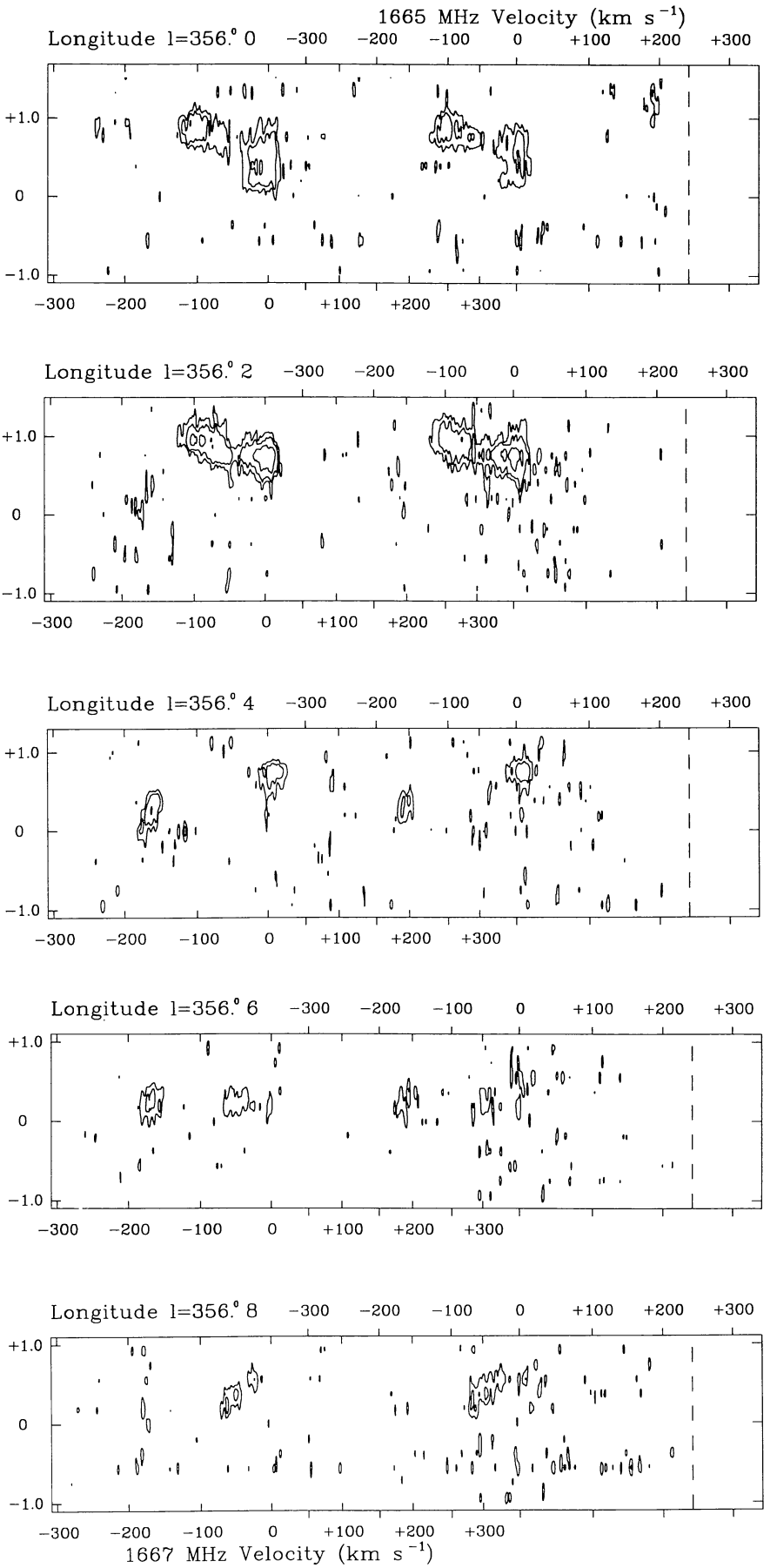

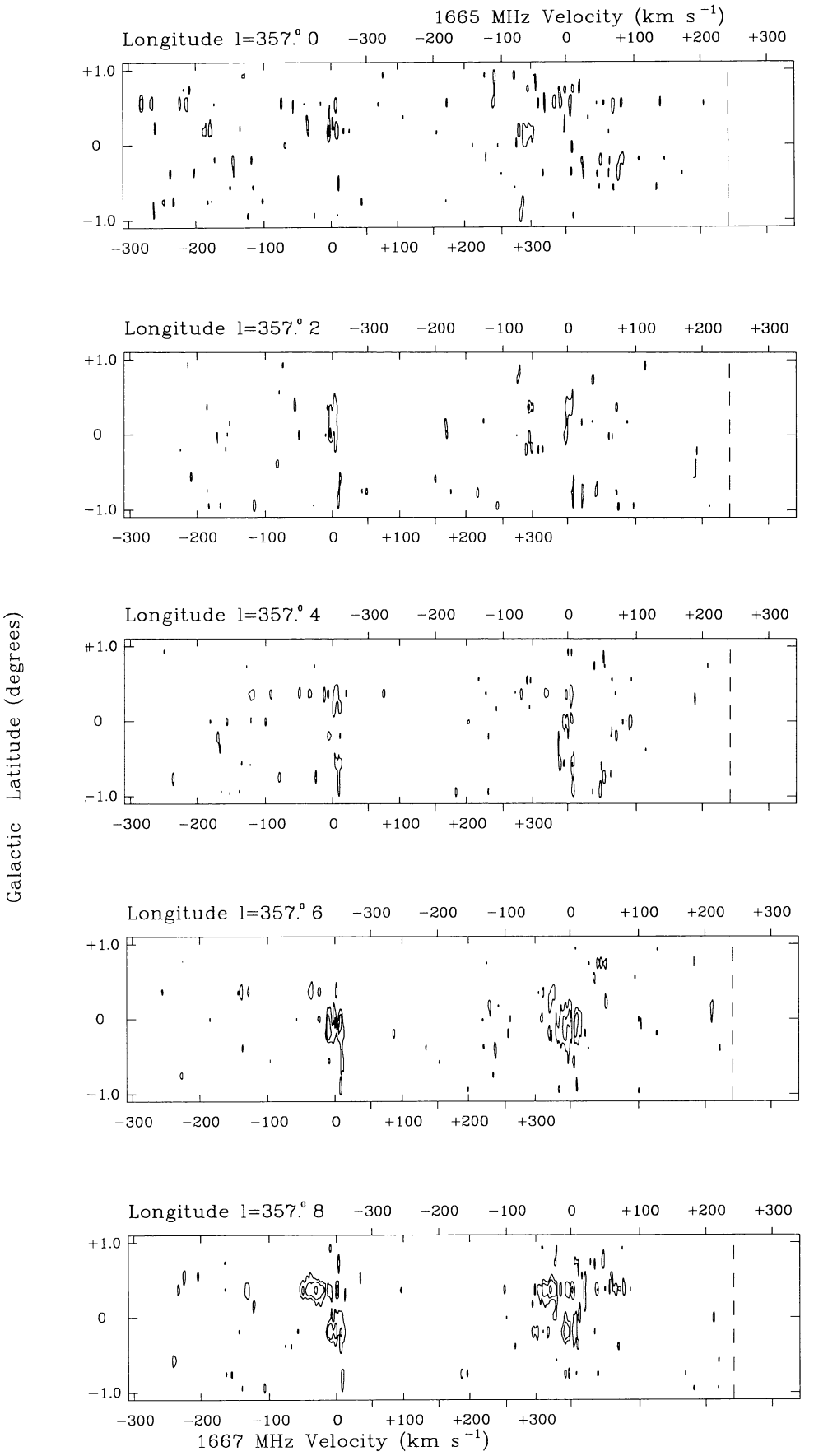

Fig. 4. continued

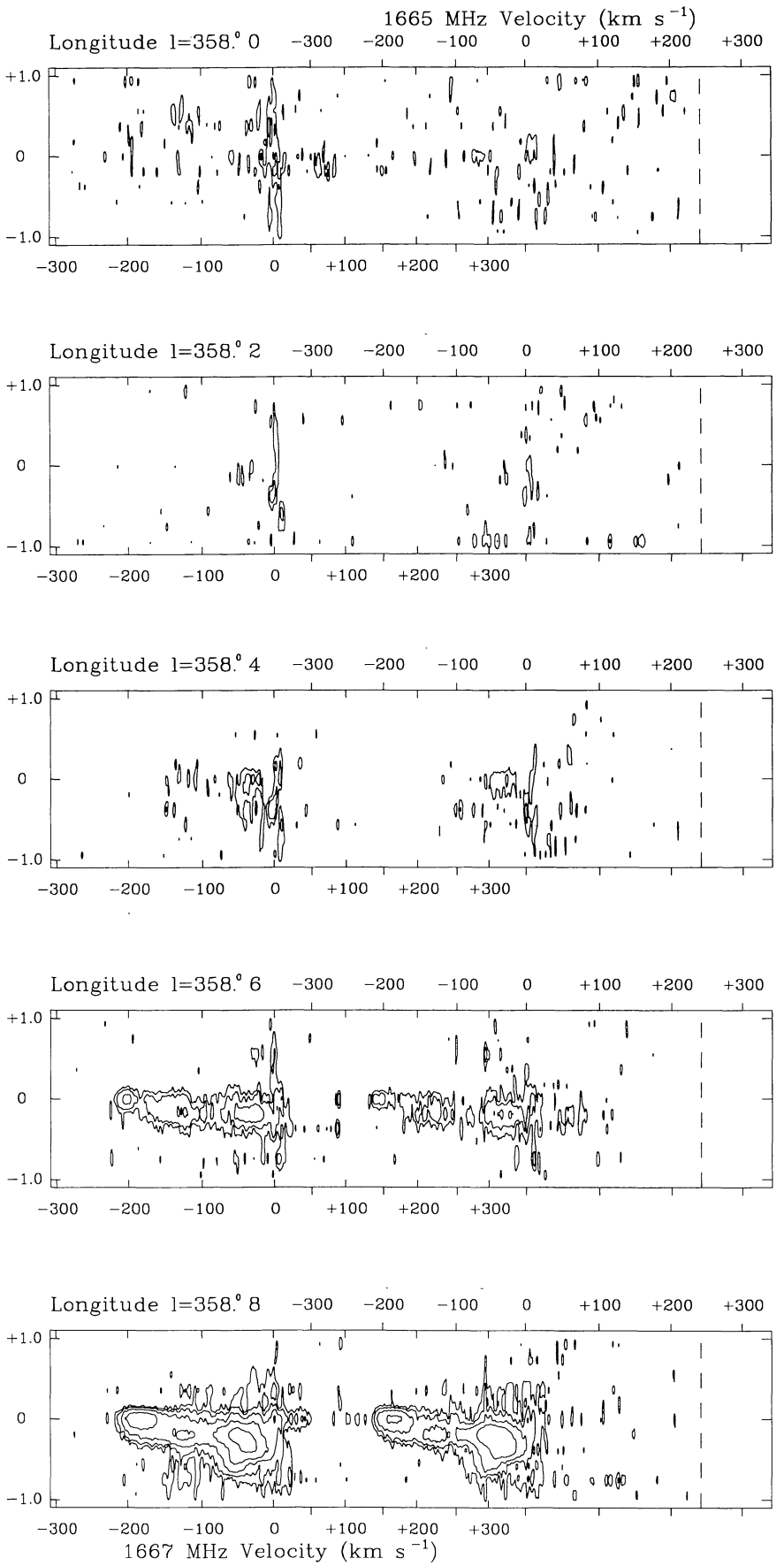

Fig. 4. continued

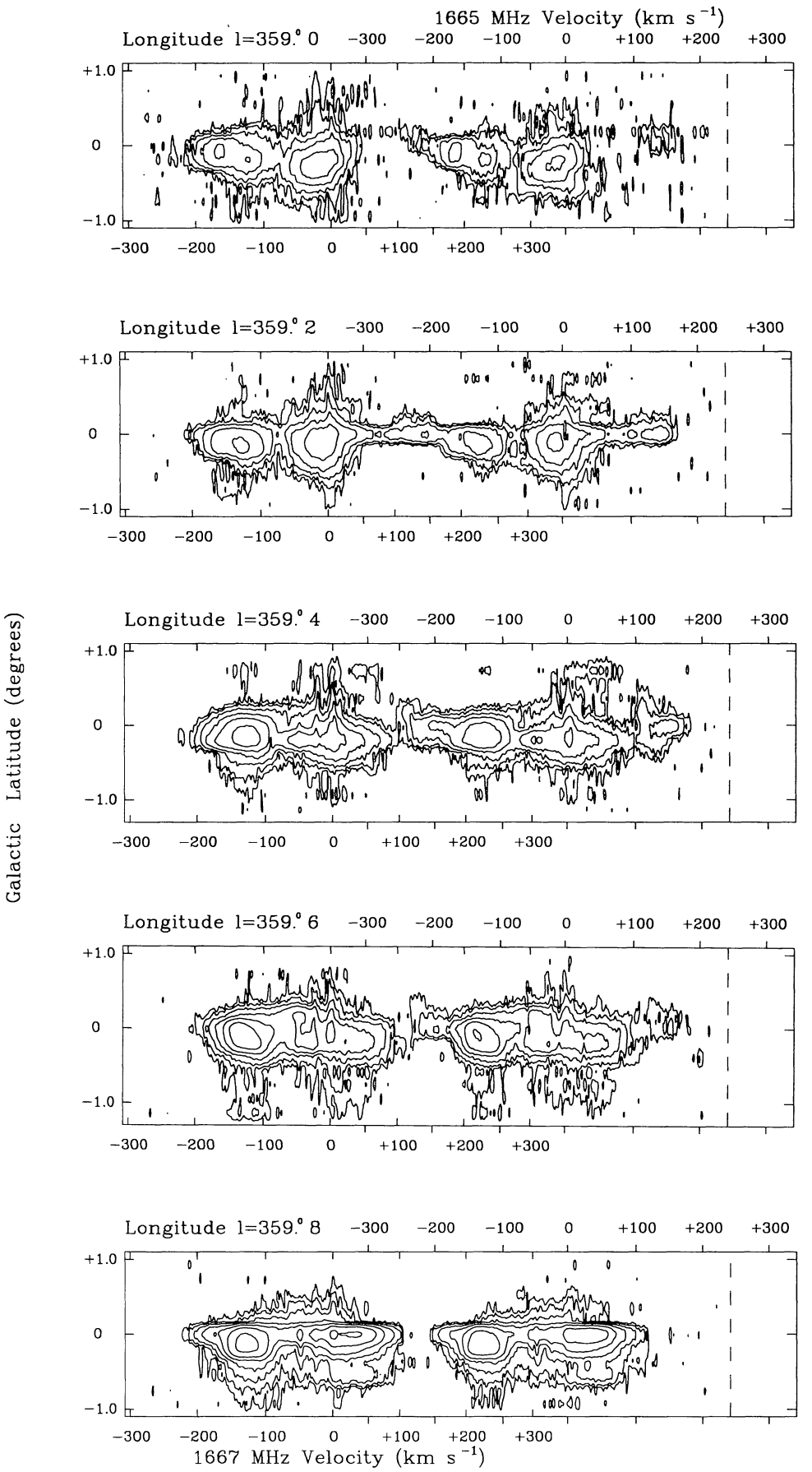

Fig. 4. continued

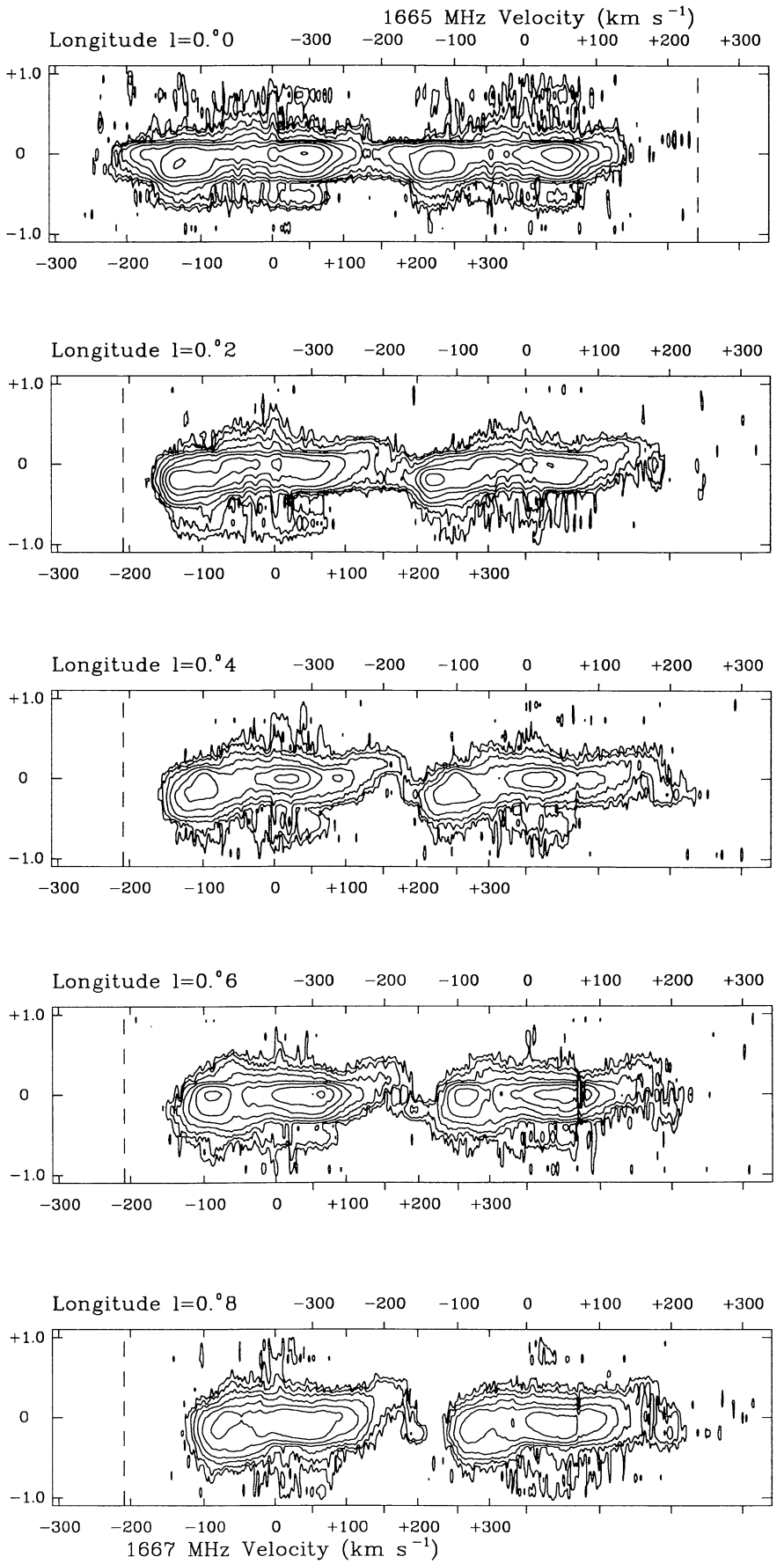

Fig. 4. continued

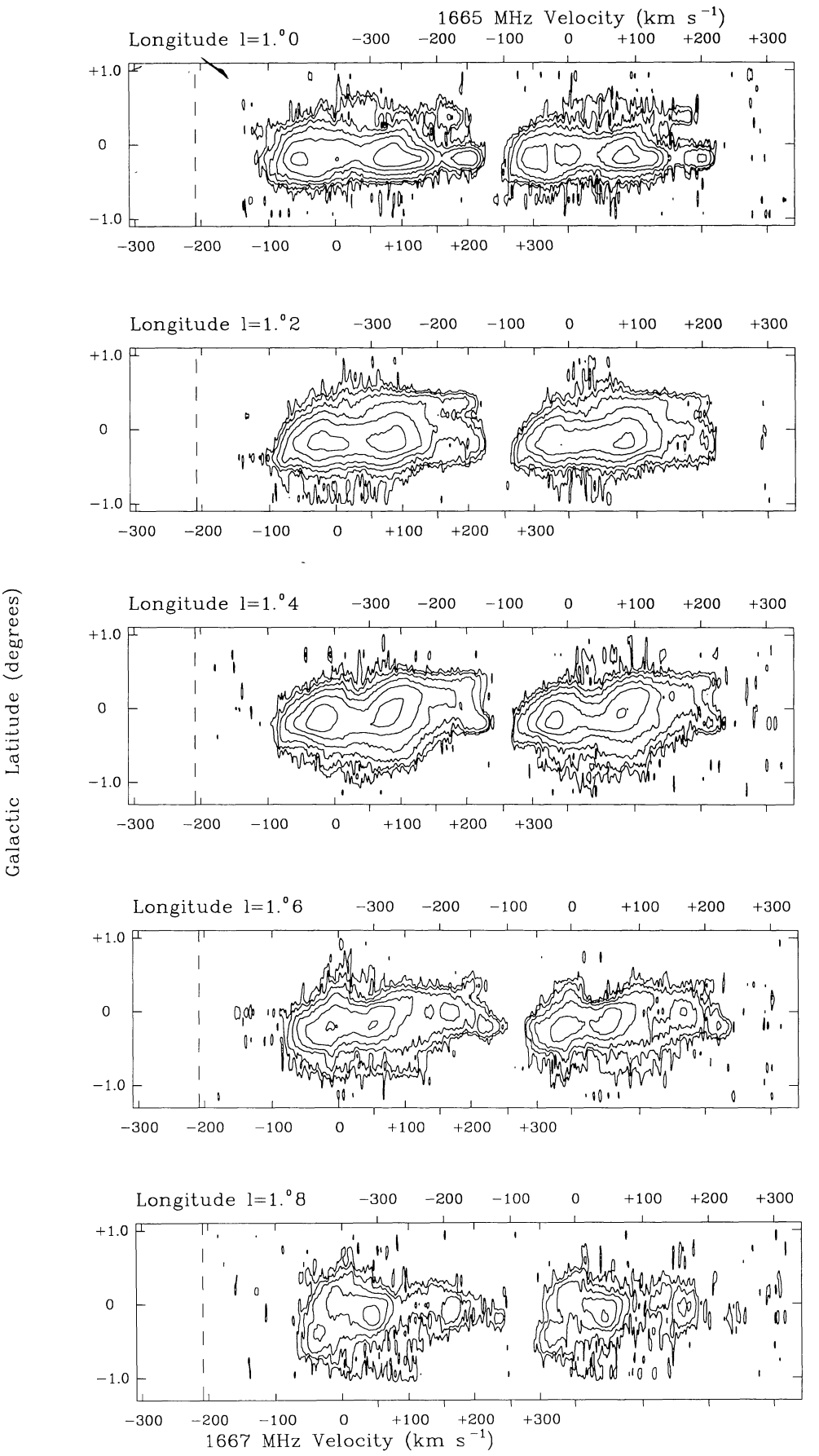

Fig. 4. continued

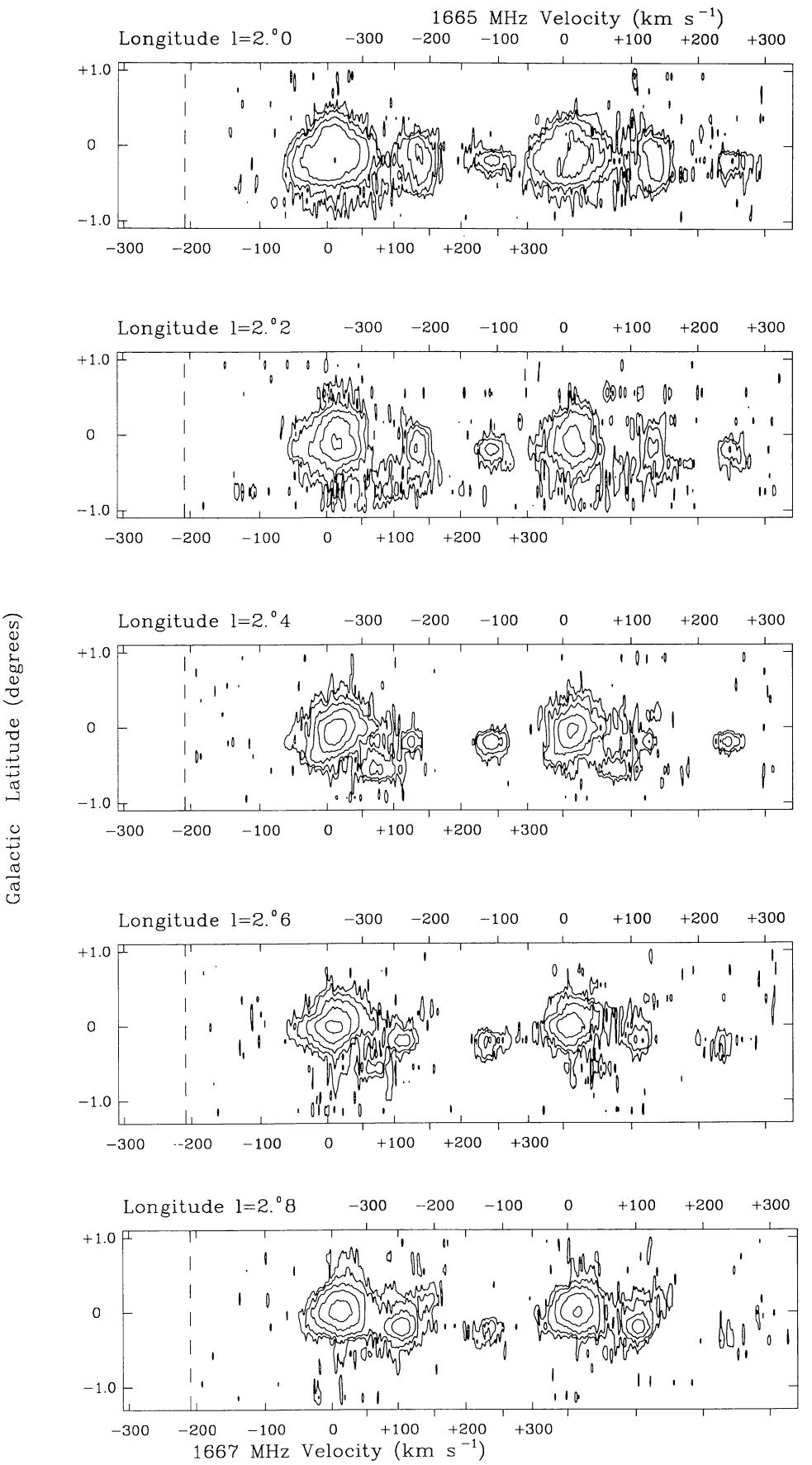

Fig. 4. continued

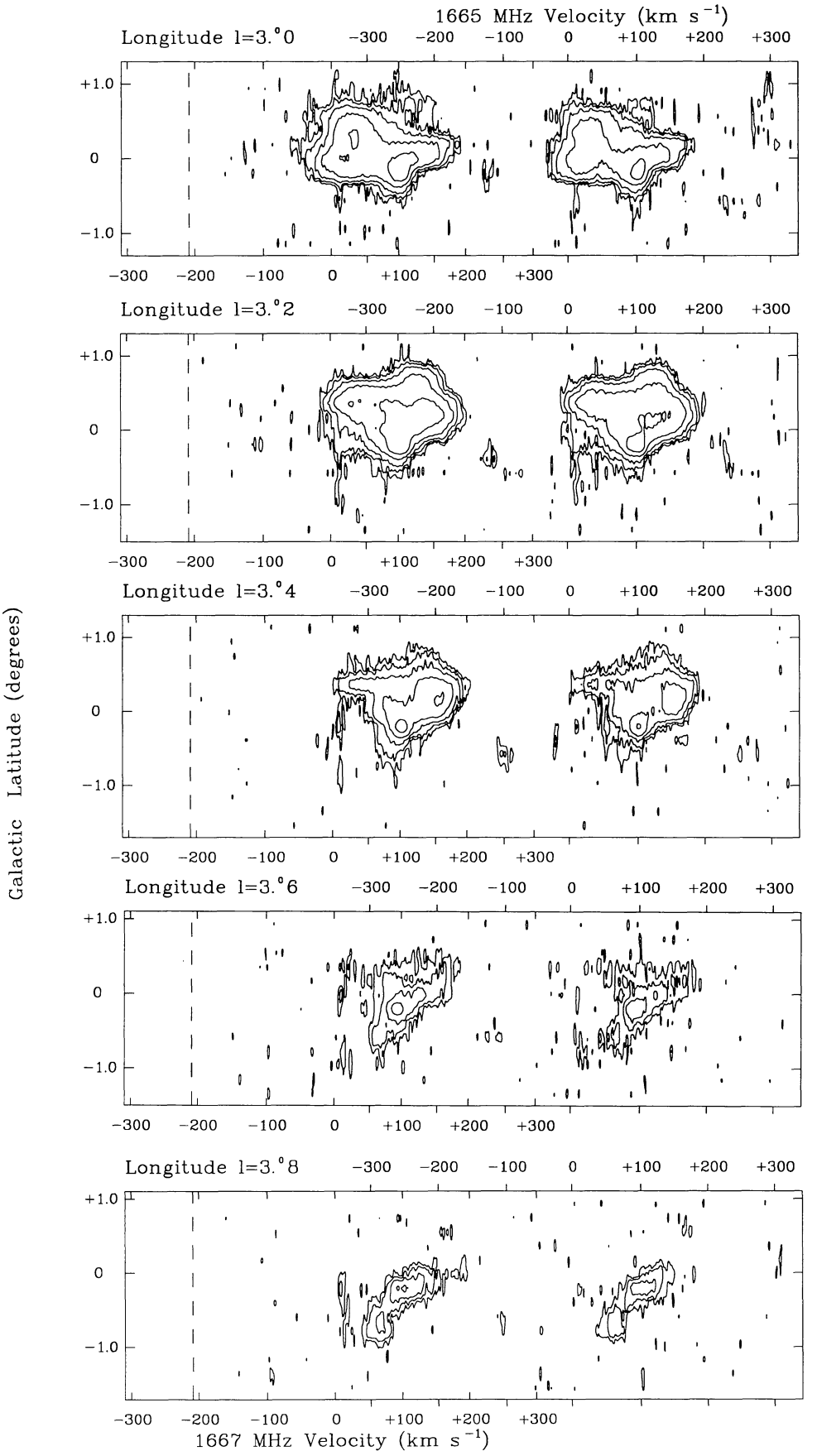

Fig. 4. continued

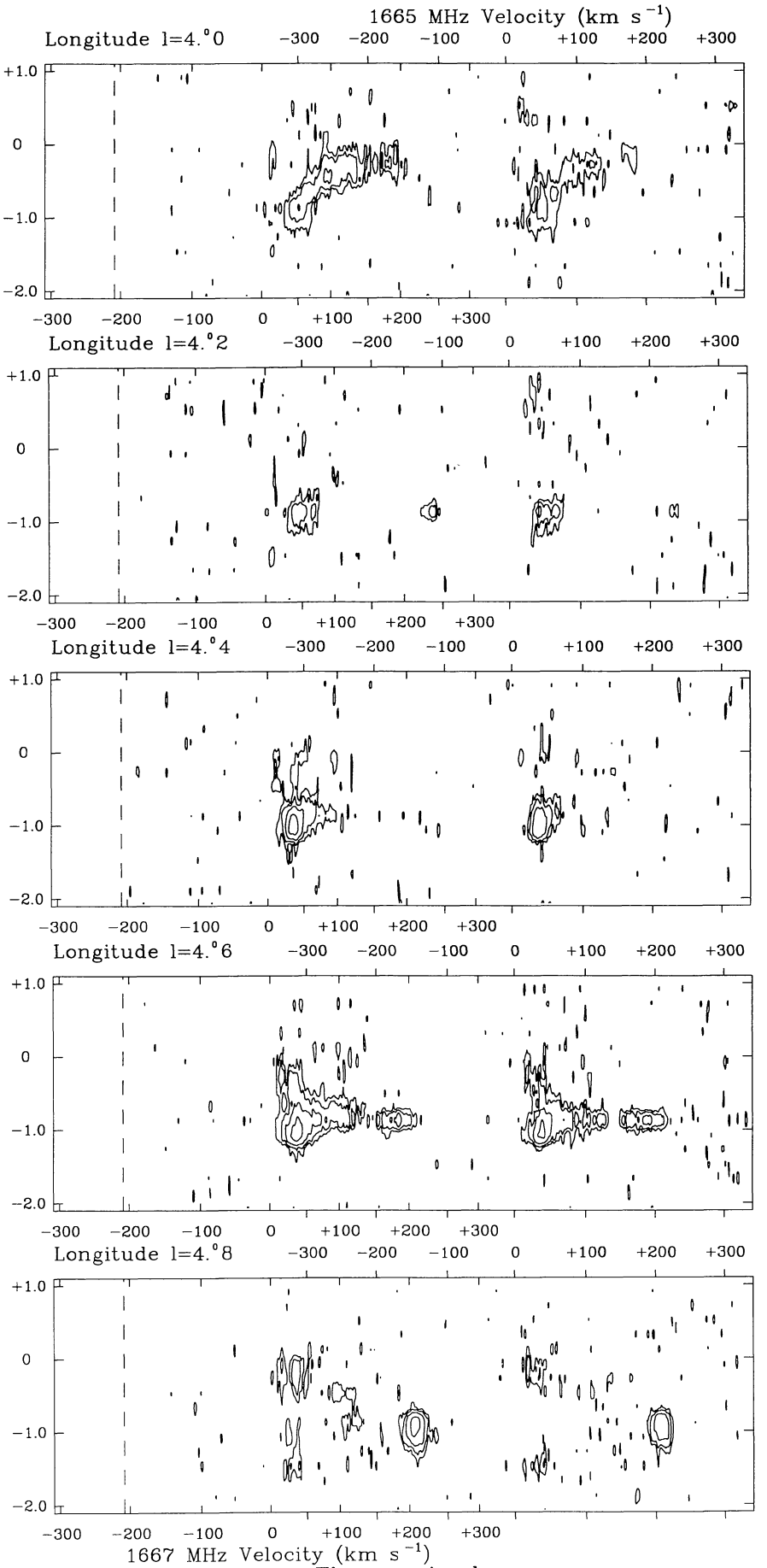

Fig. 4. continued

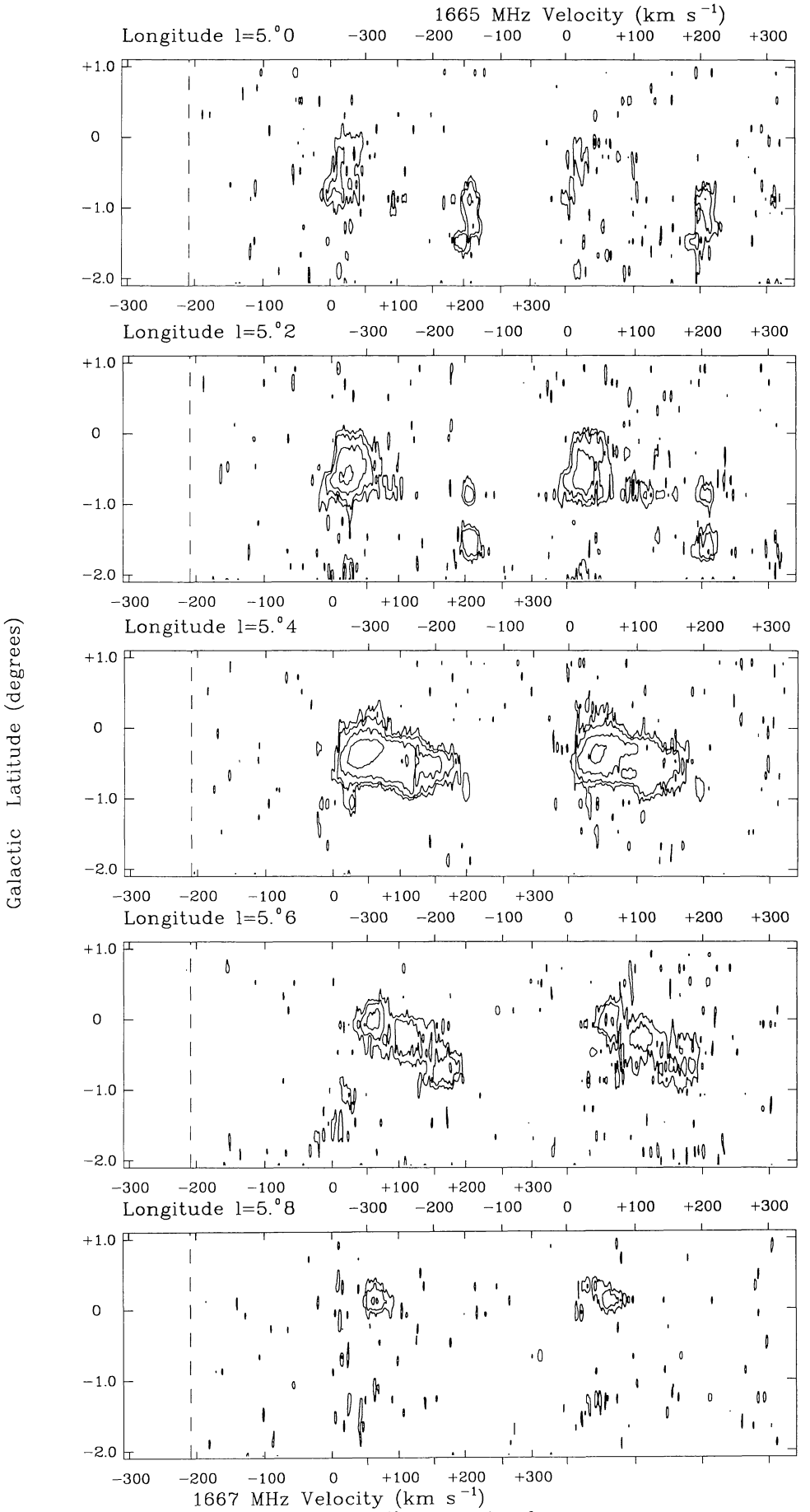

Fig. 4. continued

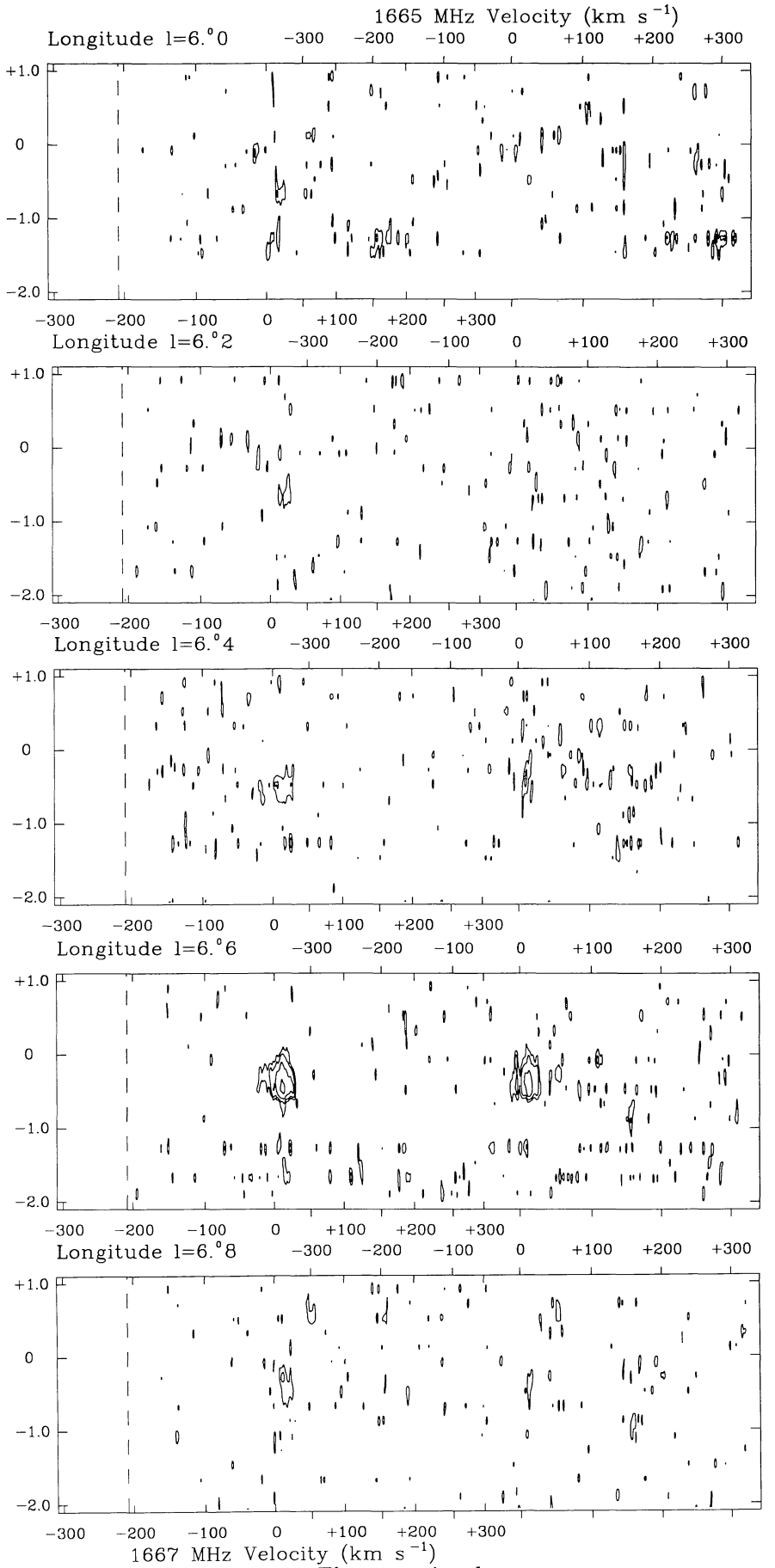

Fig. 4. continued

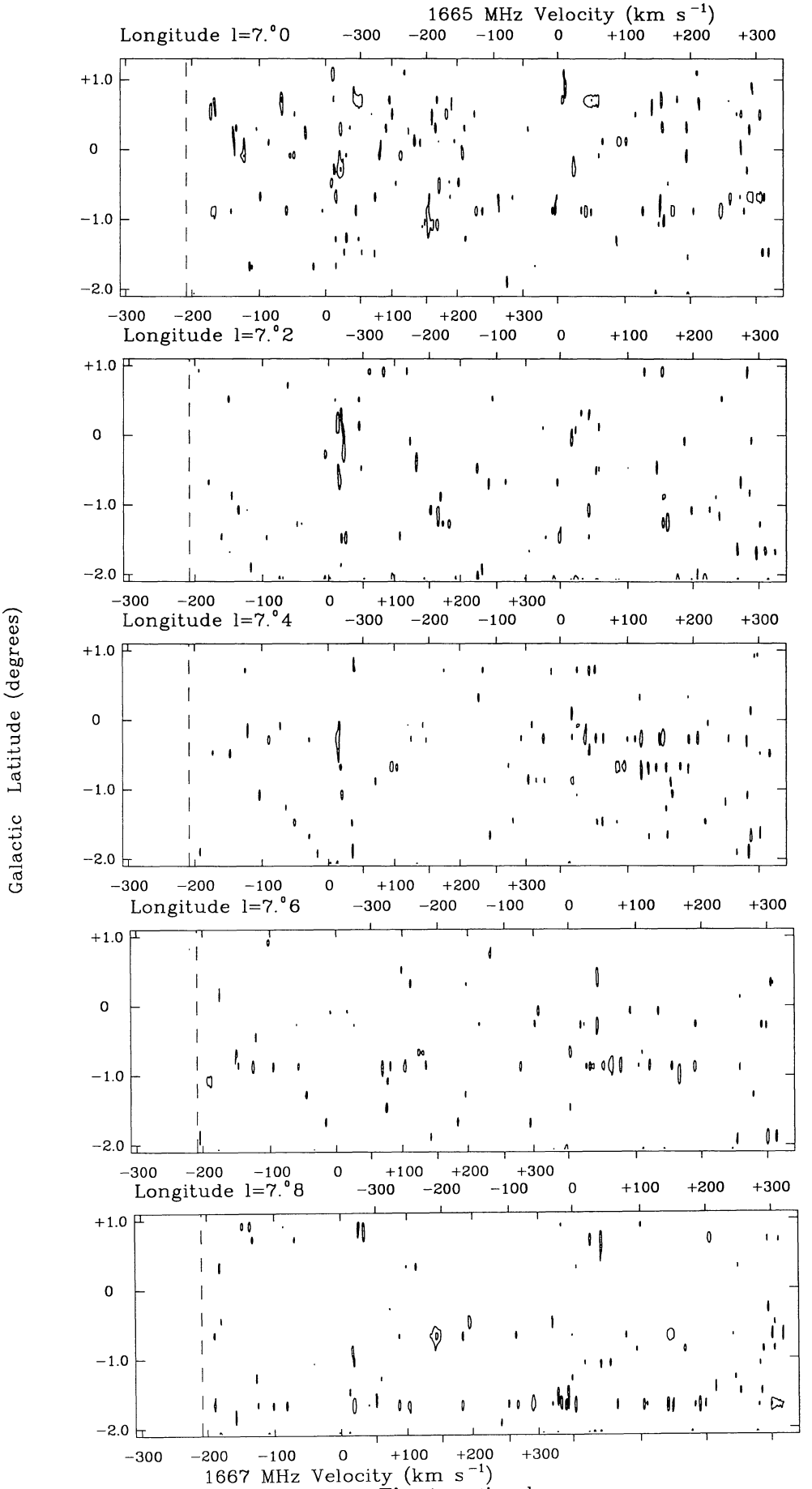

Fig. 4. continued

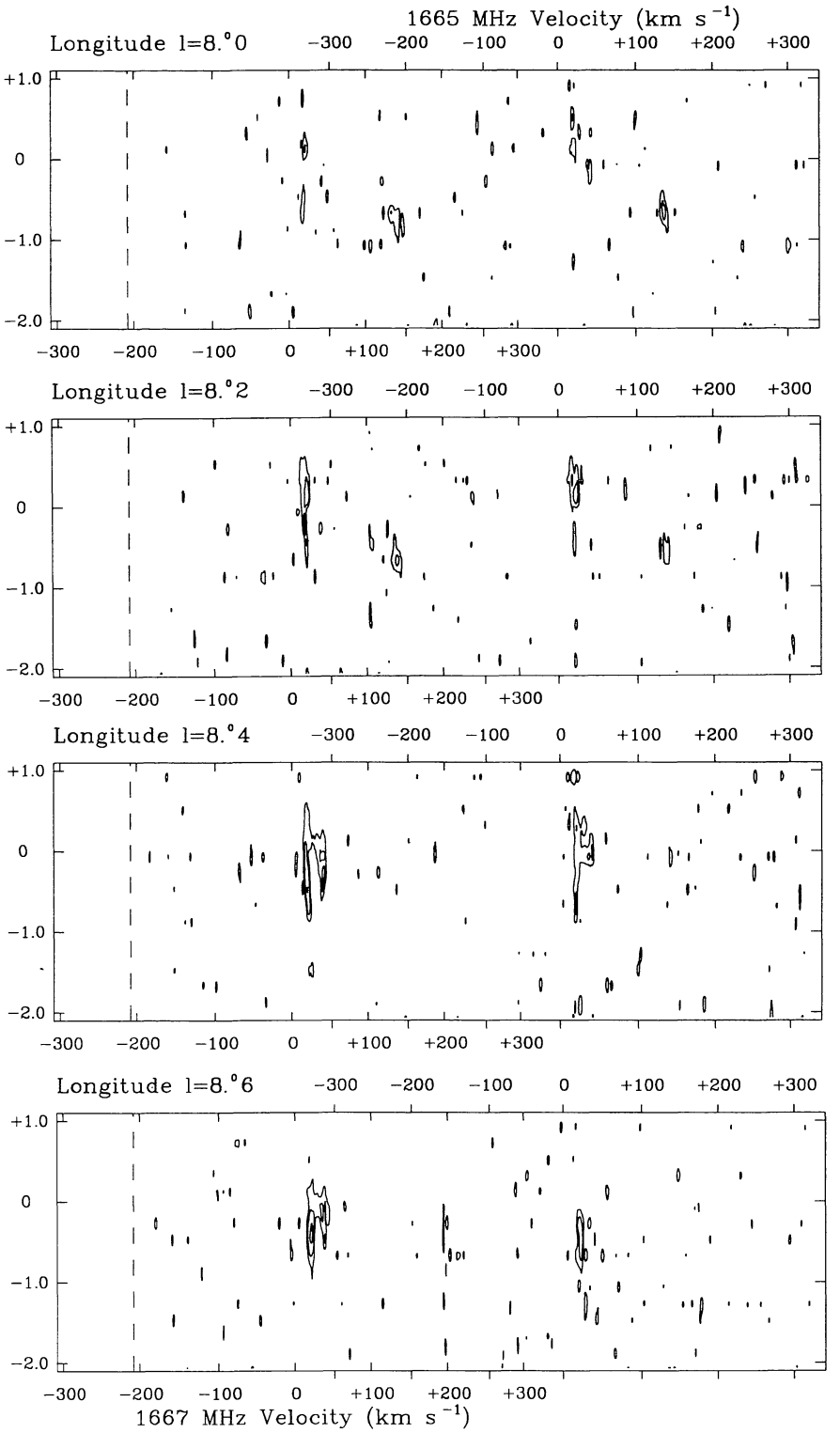

Fig. 4. continued

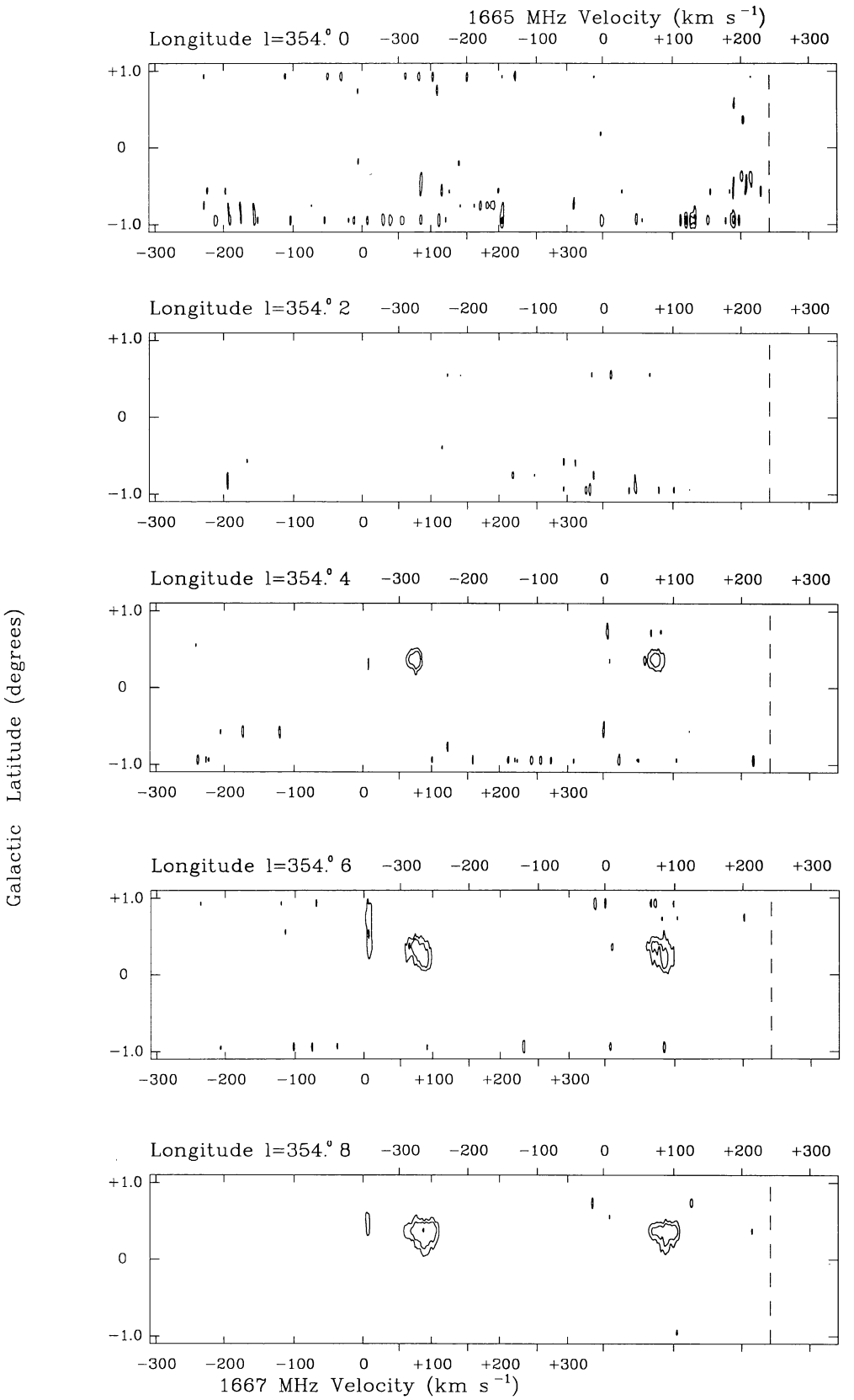

Fig. 5. Latitude–velocity maps of apparent opacity. Between $356.°2 \leq l \leq 3.°8$ contour levels are at 0.02, 0.04, 0.08, 0.16, 0.32 and 0.64. Elsewhere the contours are at 0.04, 0.08, 0.16, 0.32 and 0.64. The resolution is 3.1 km s^{-1} × 12′

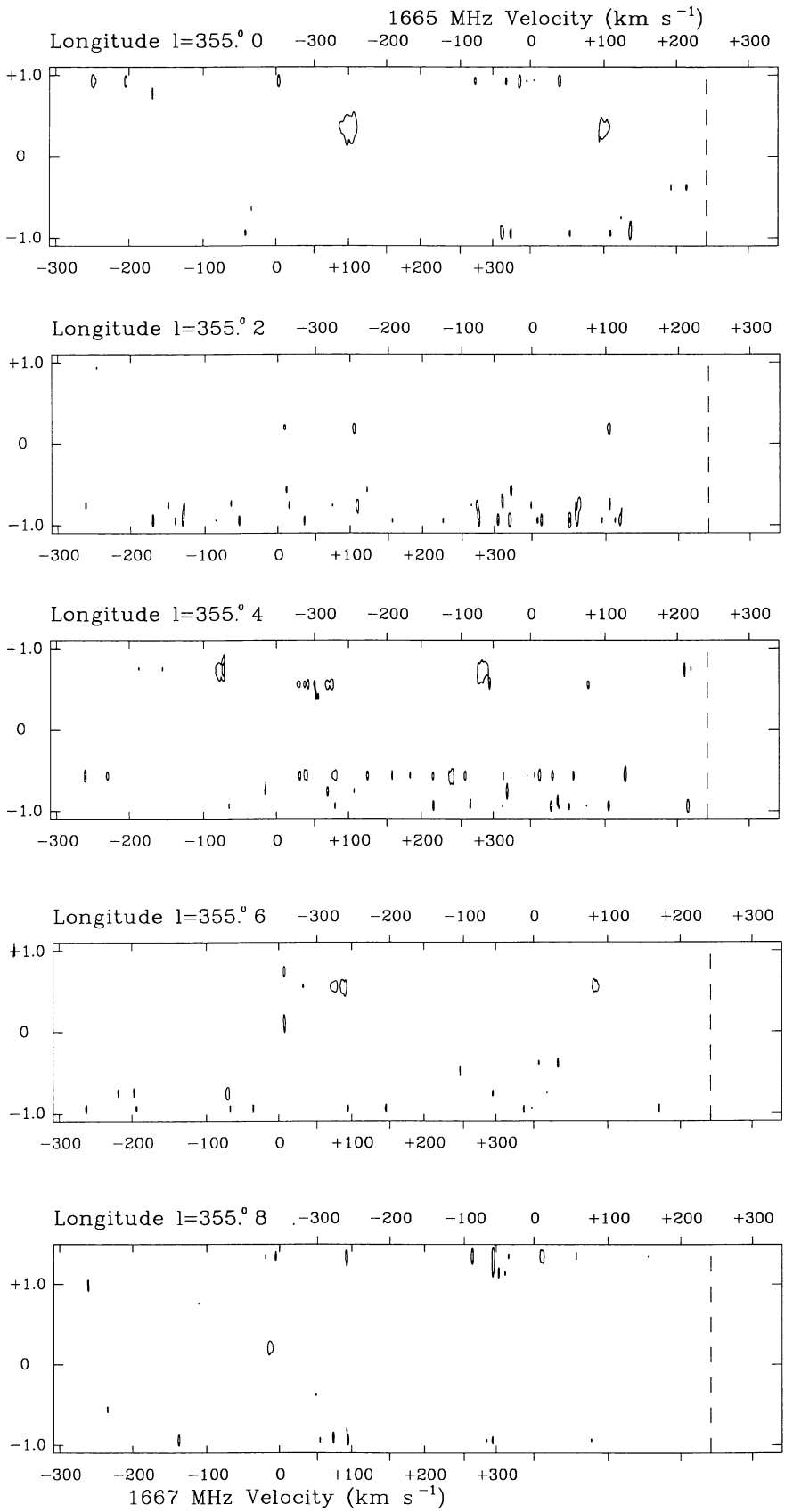

Fig. 5. continued

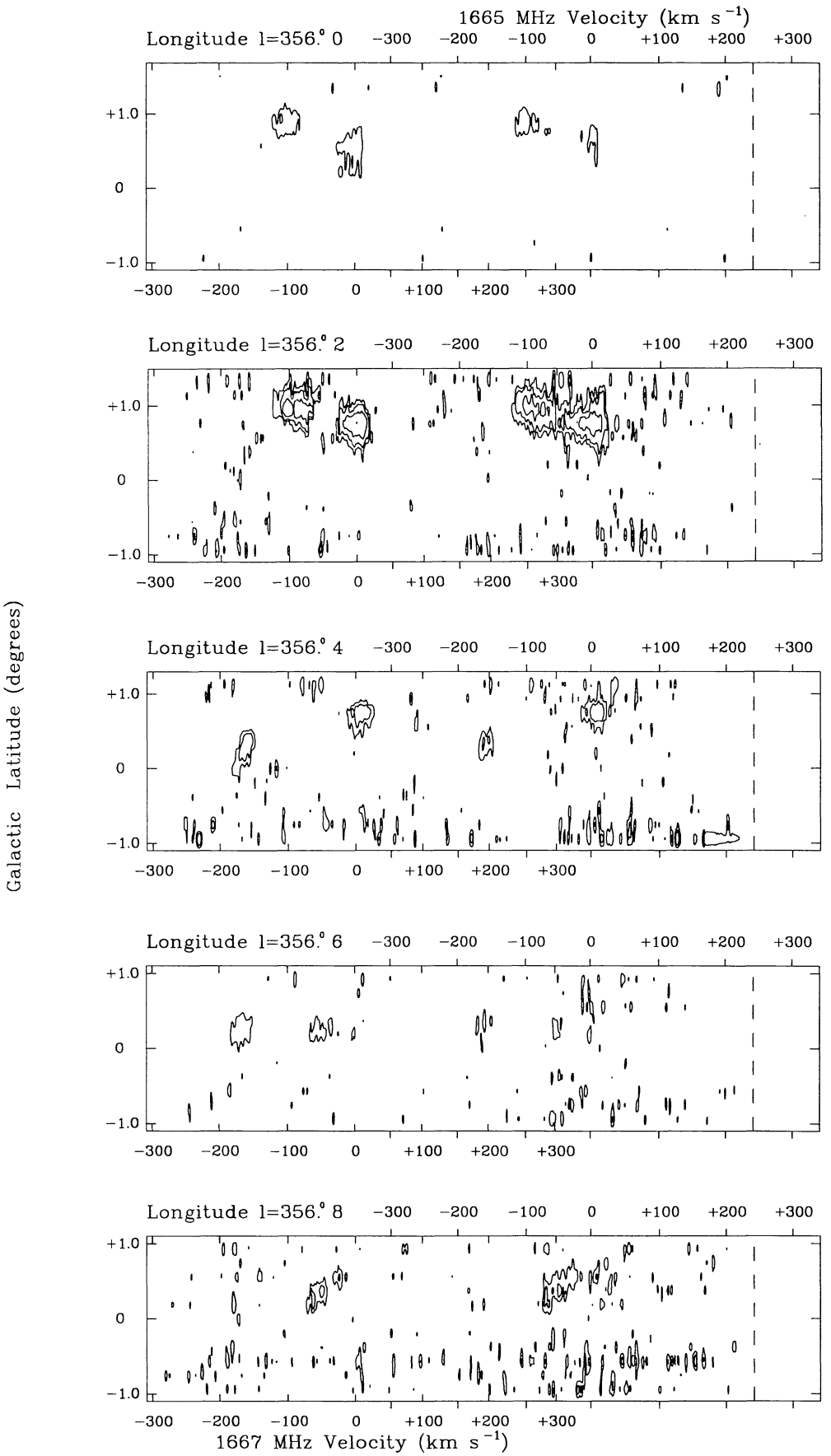

Fig. 5. continued

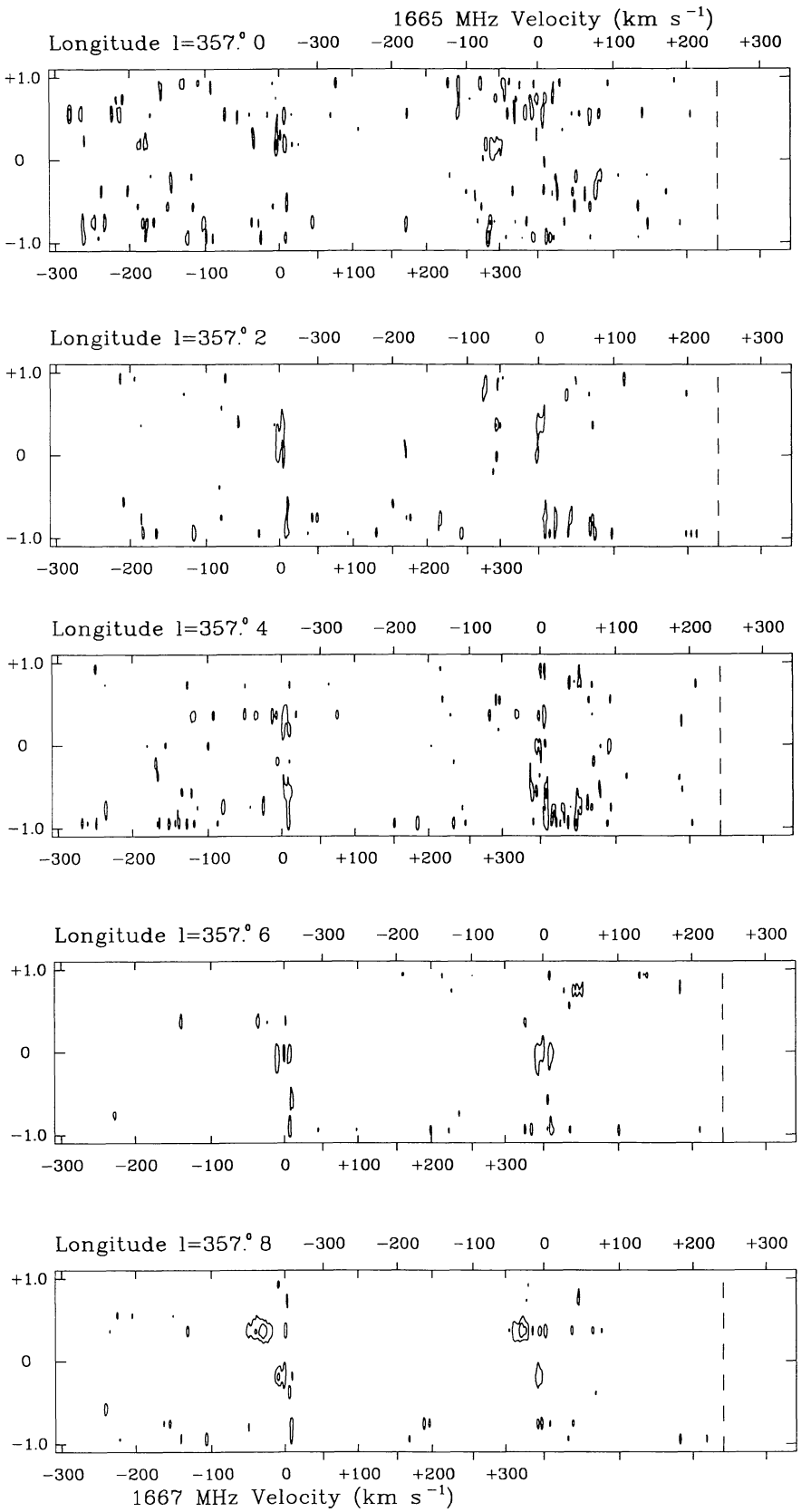

Fig. 5. continued

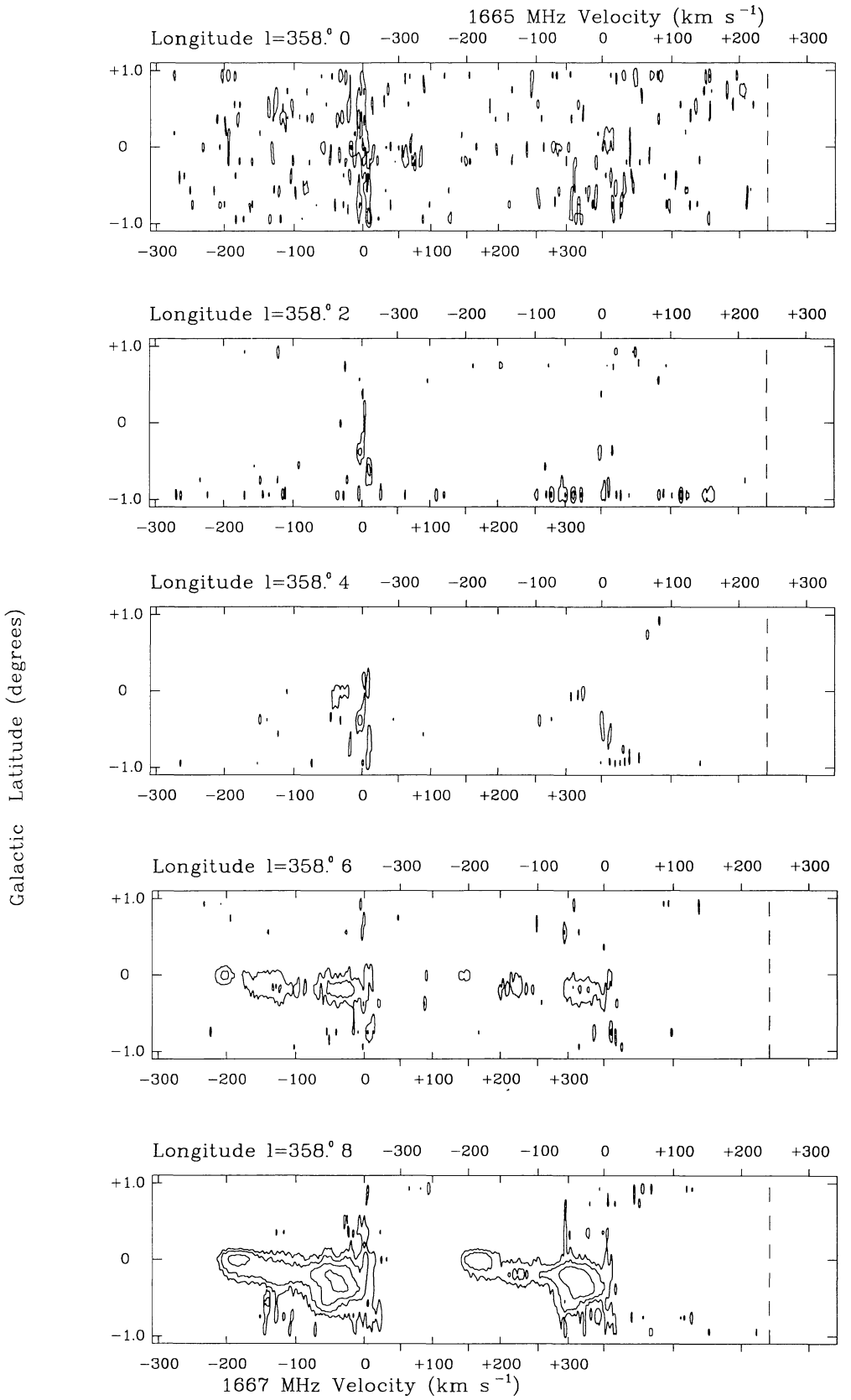

Fig. 5. continued

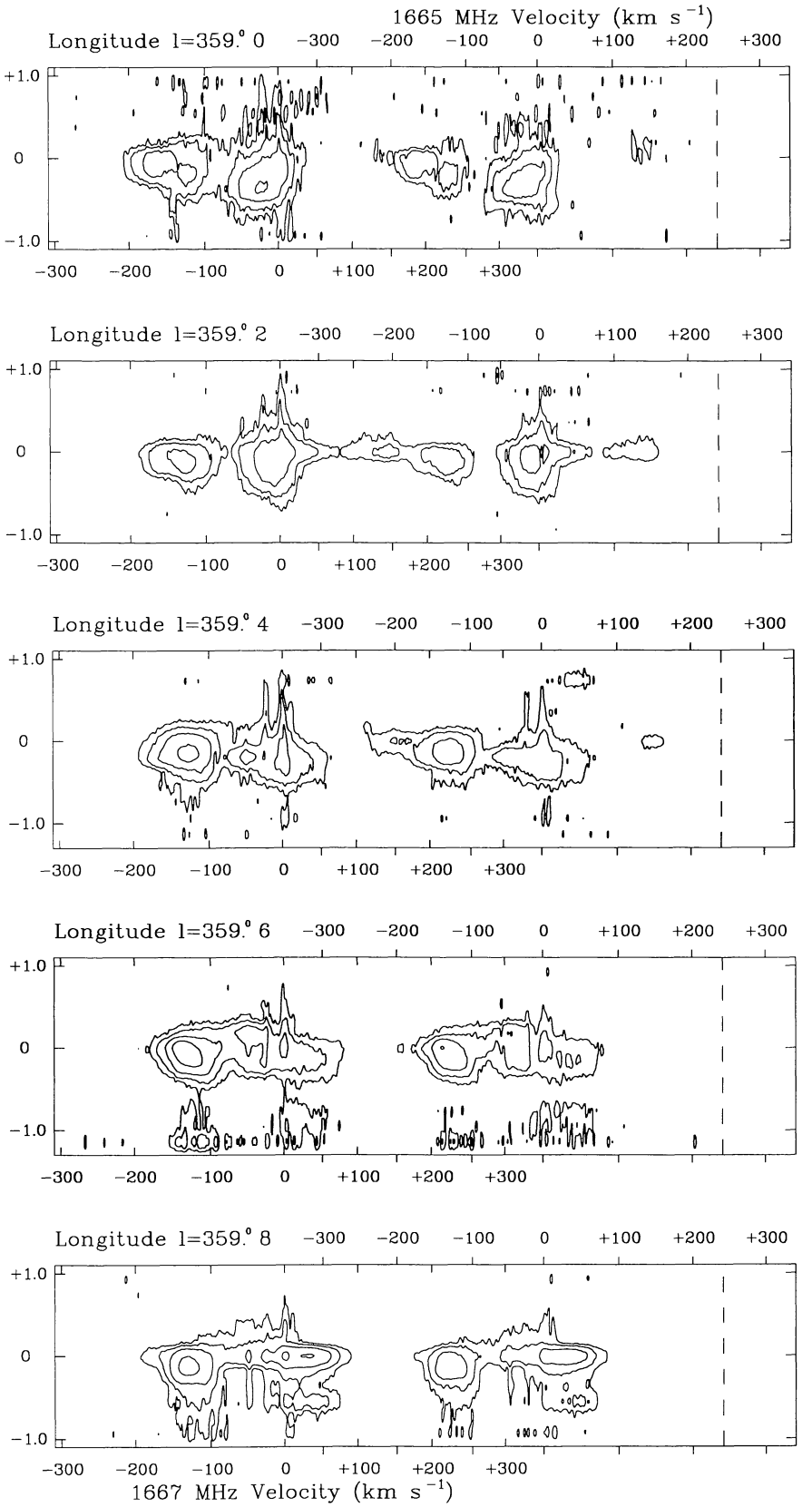

Fig. 5. continued

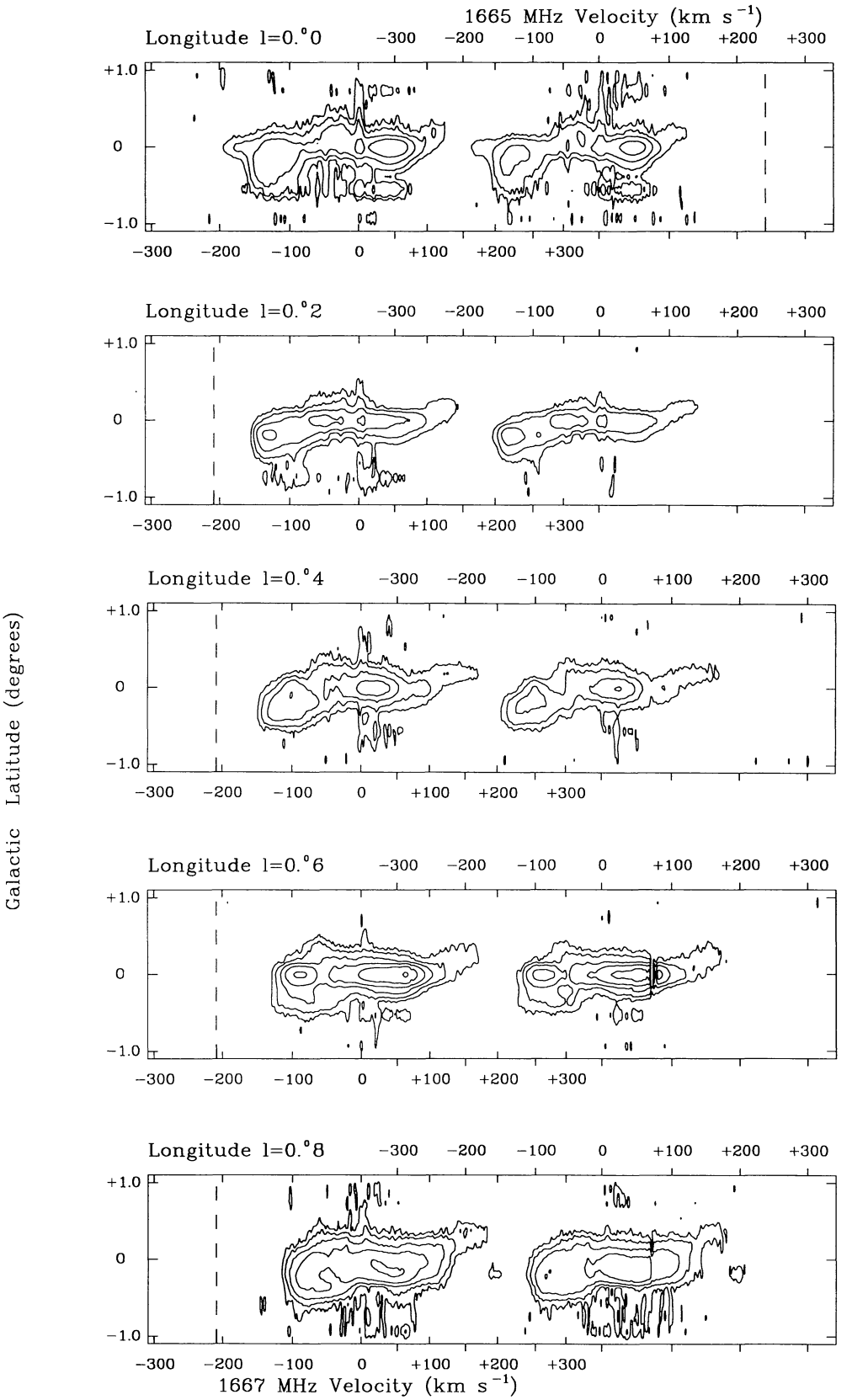

Fig. 5. continued

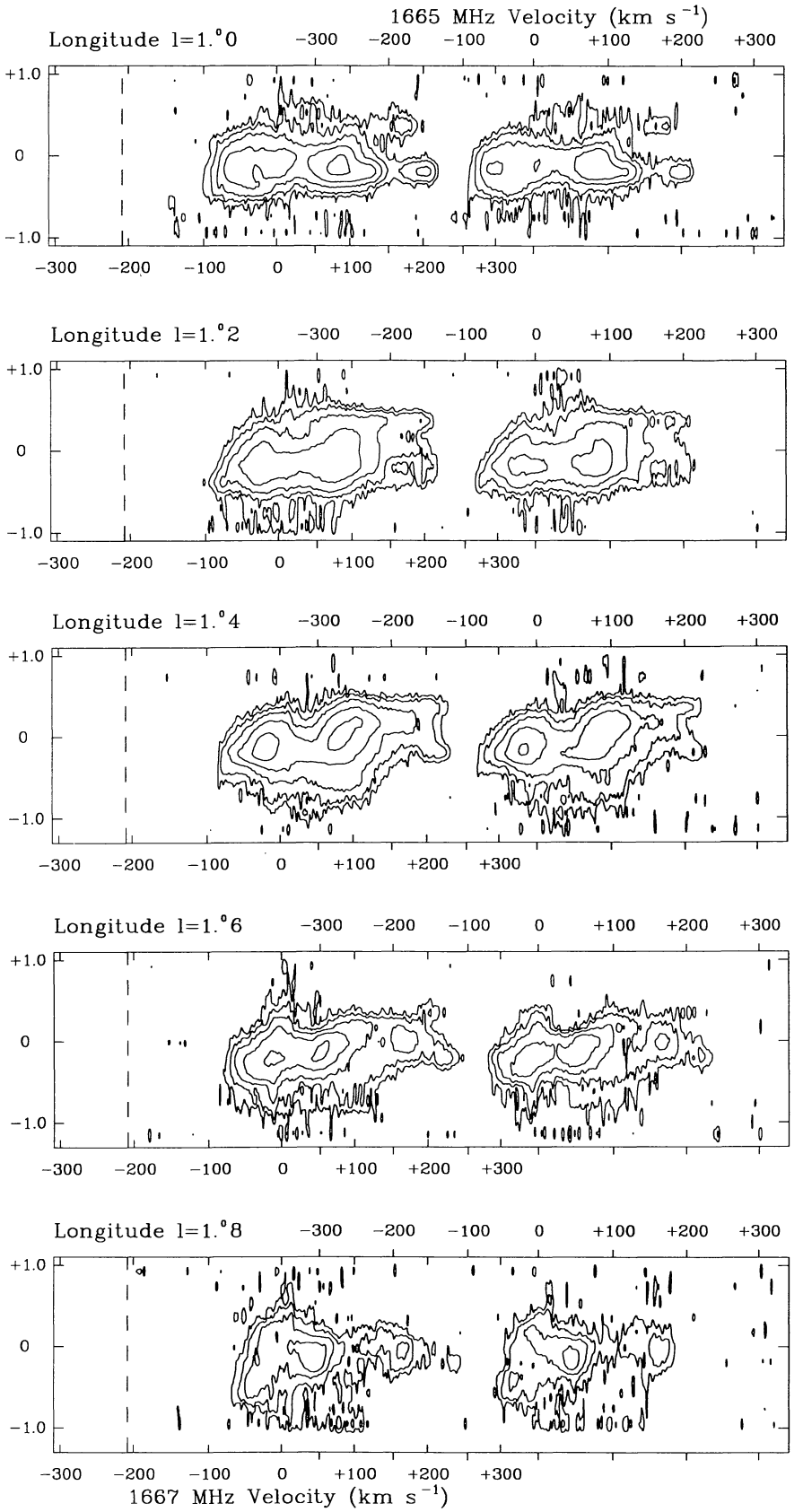

Fig. 5. continued

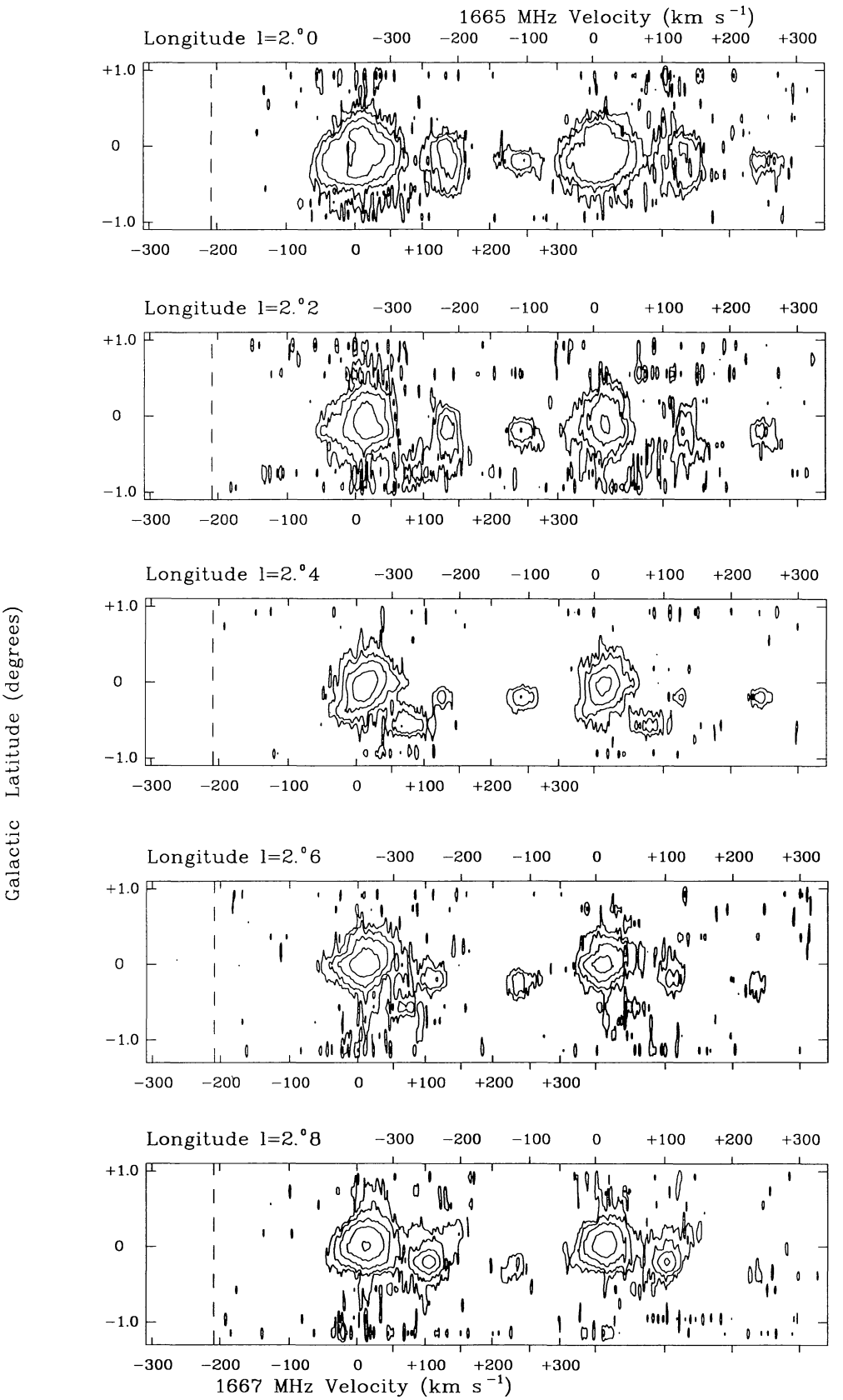

Fig. 5. continued

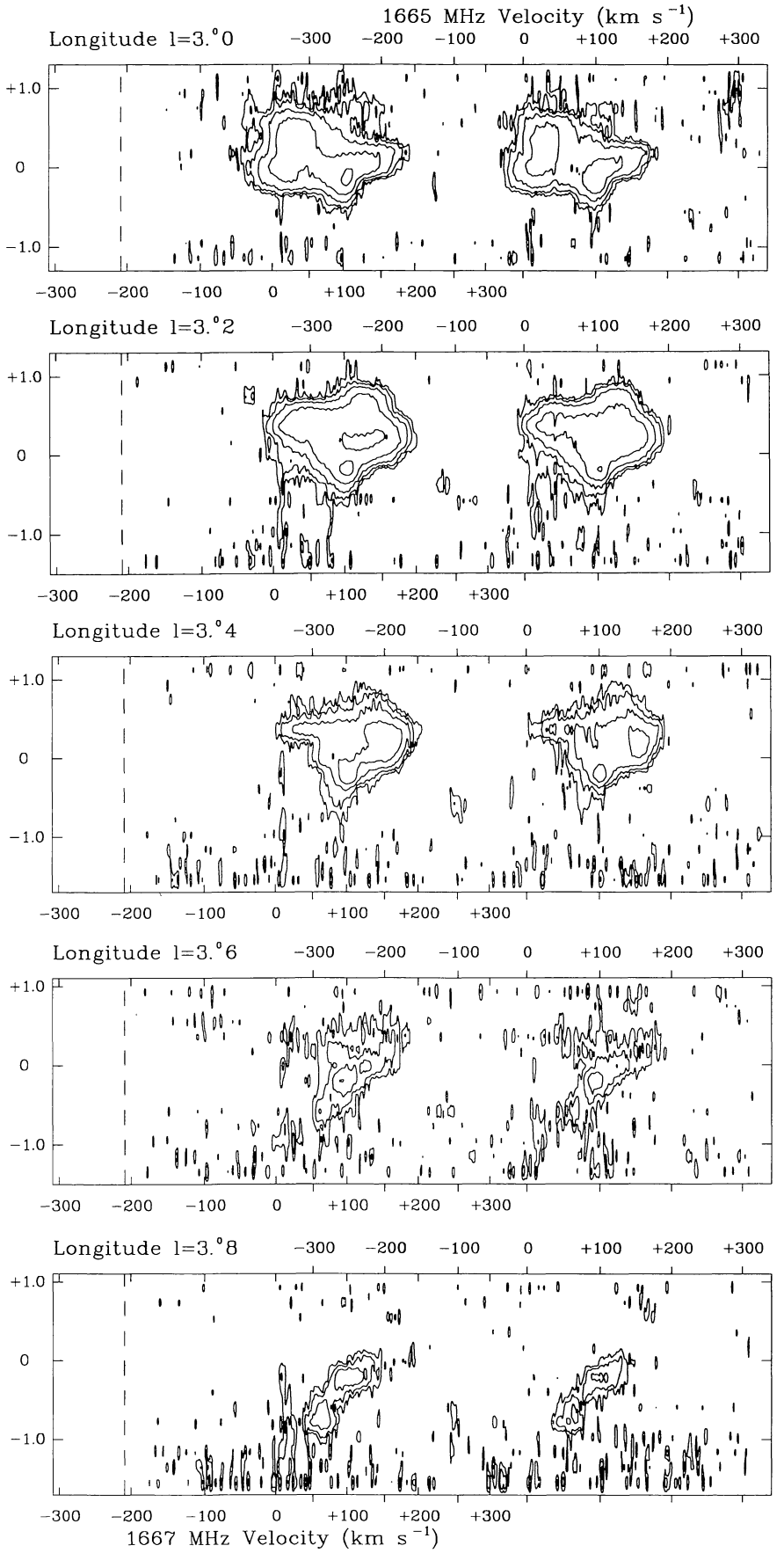

Fig. 5. continued

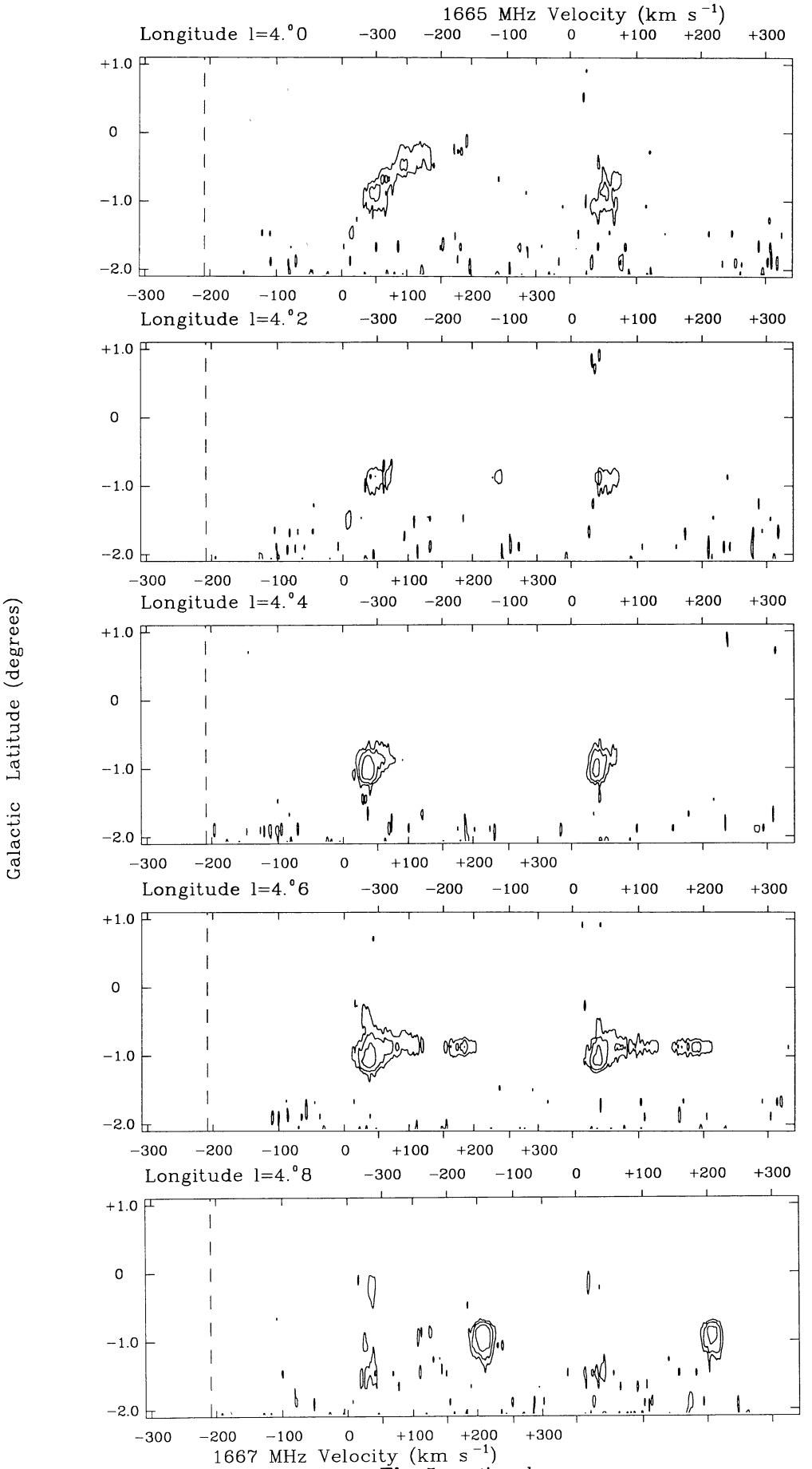

Fig. 5. continued

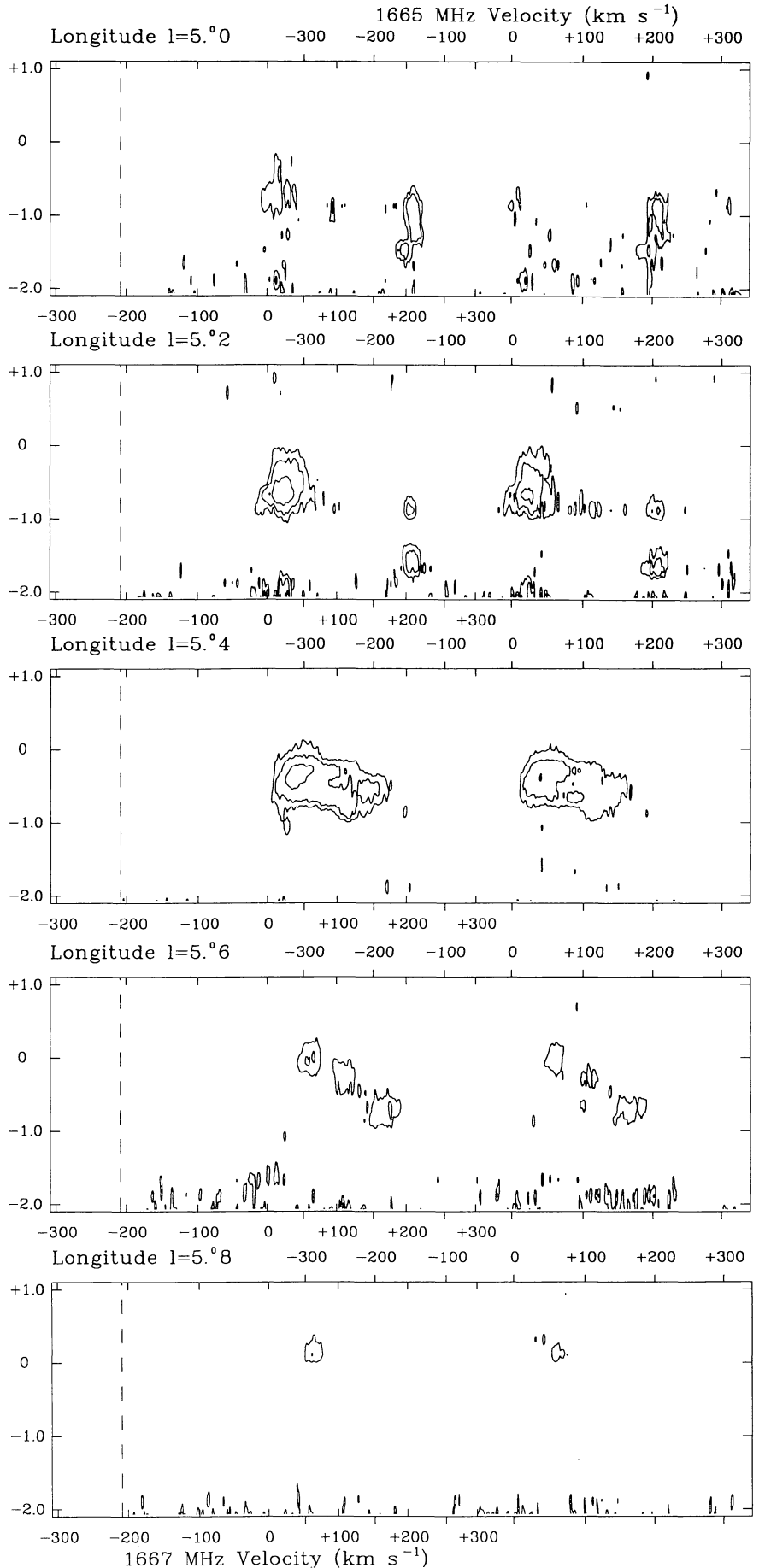

Fig. 5. continued

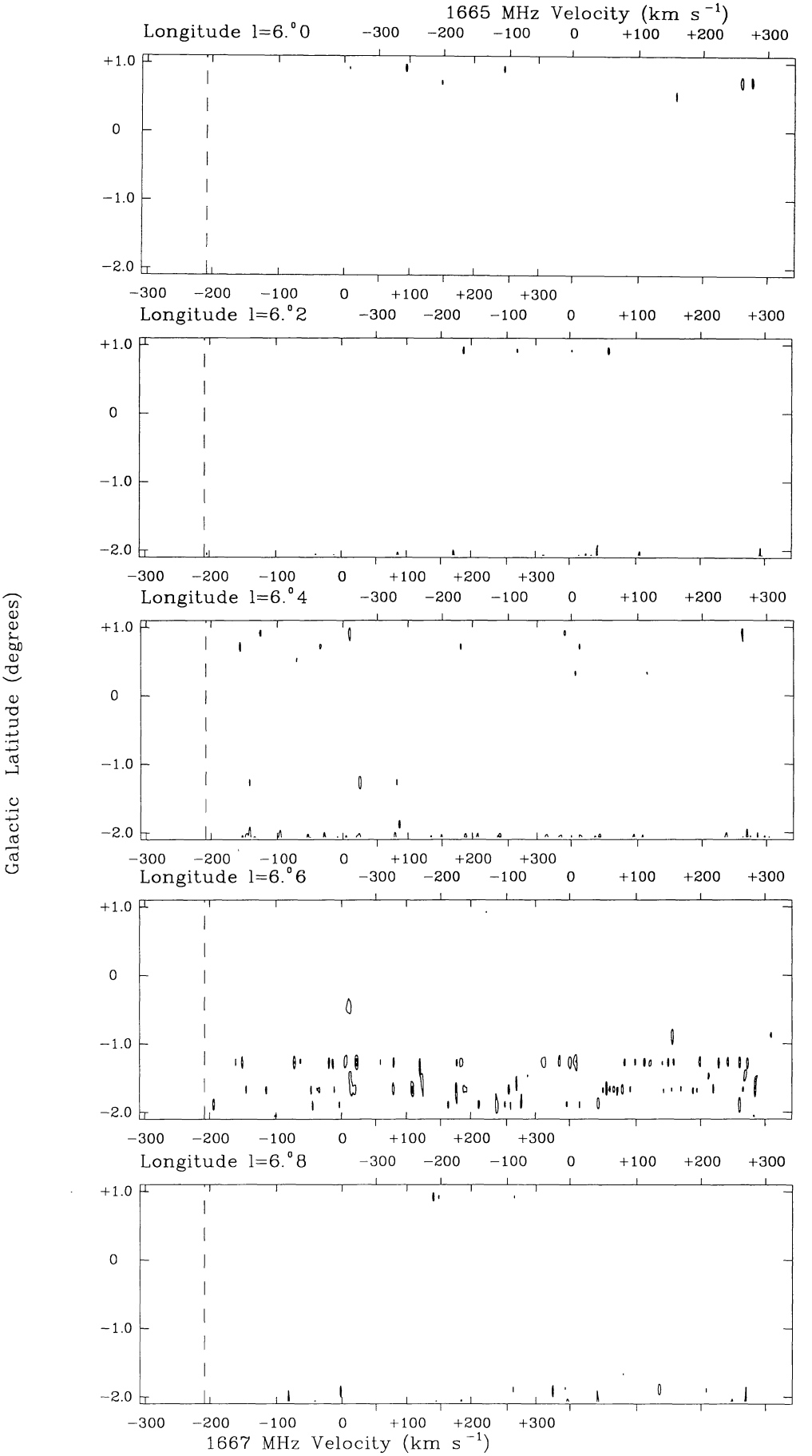

Fig. 5. continued

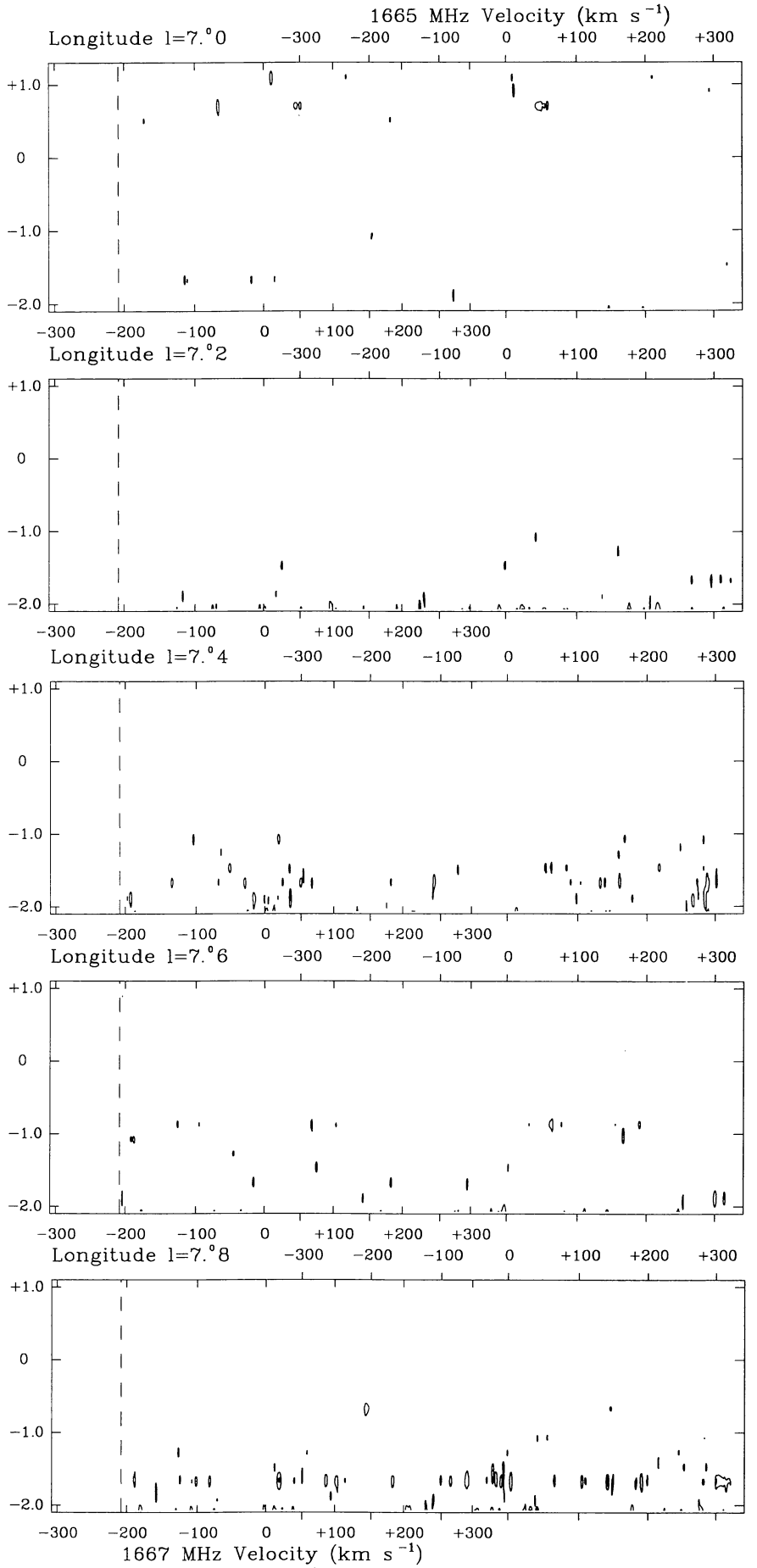

Fig. 5. continued

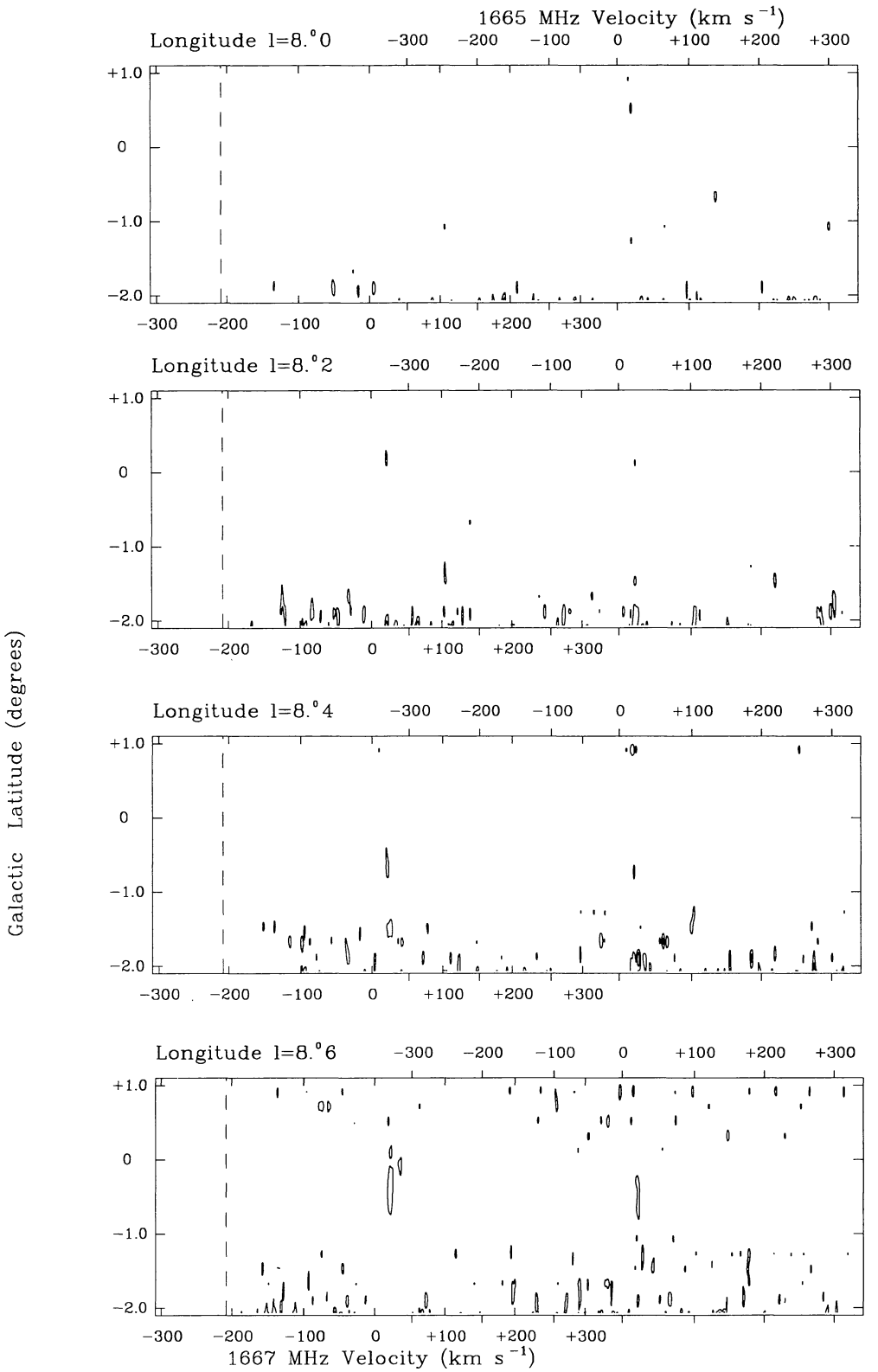

Fig. 5. continued

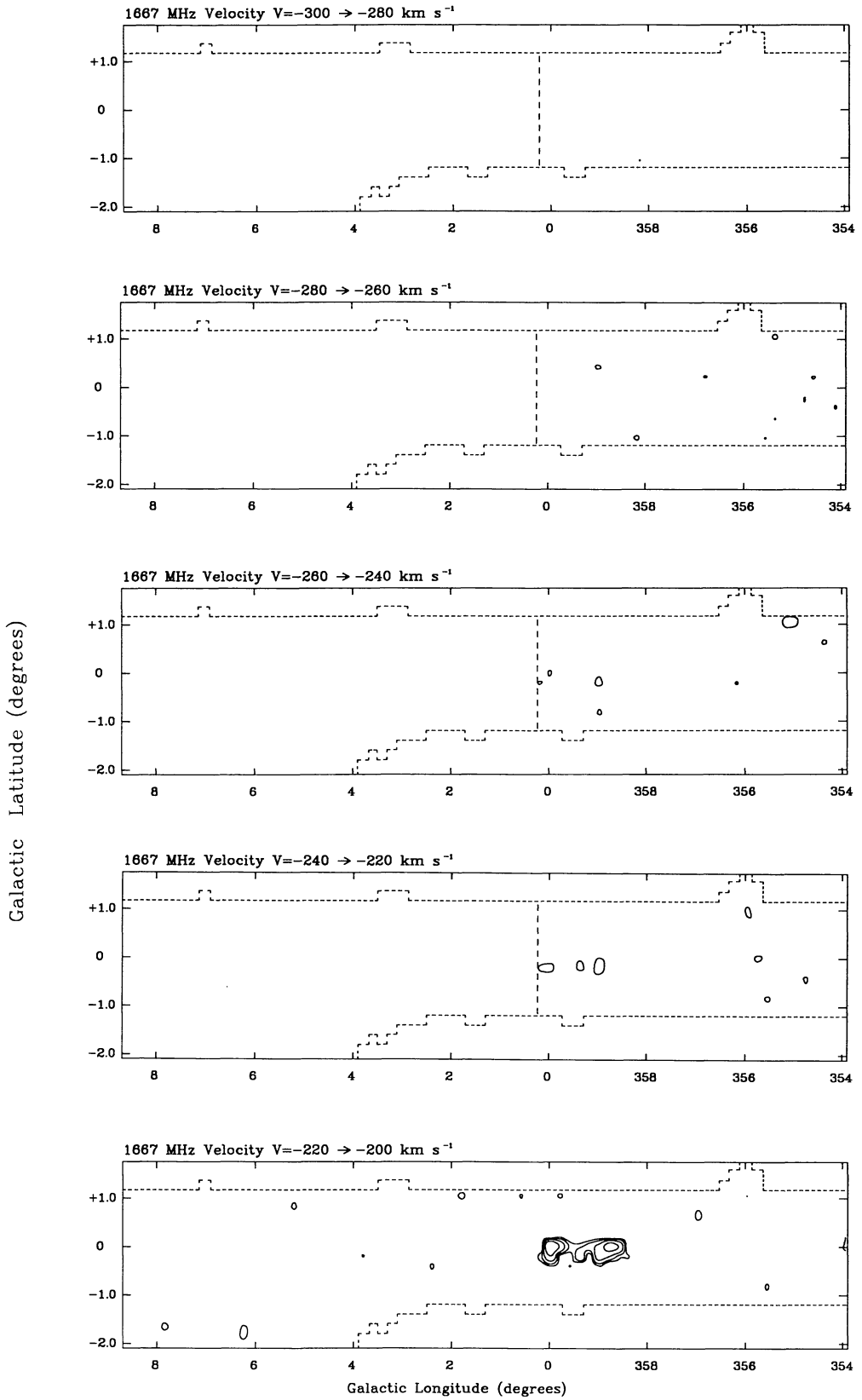

Fig. 6. Longitude-latitude maps of OH line temperature from the 1667 MHz line integrated over 20 km s^{-1} intervals. Contour levels are set at −1, −2, −4, −8, −16, −32, −64, −128 and −256 K km s^{-1}

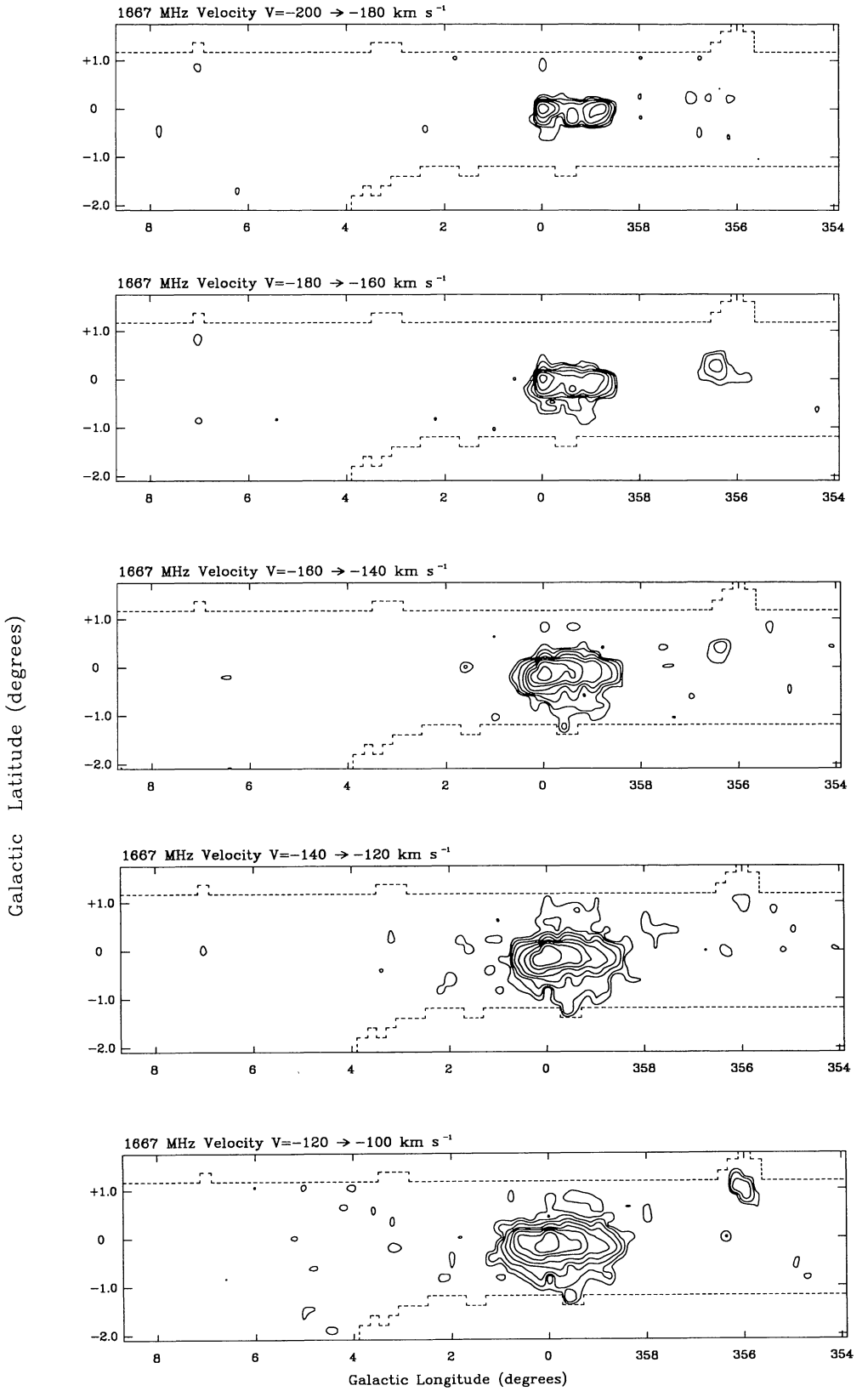

Fig. 6. continued

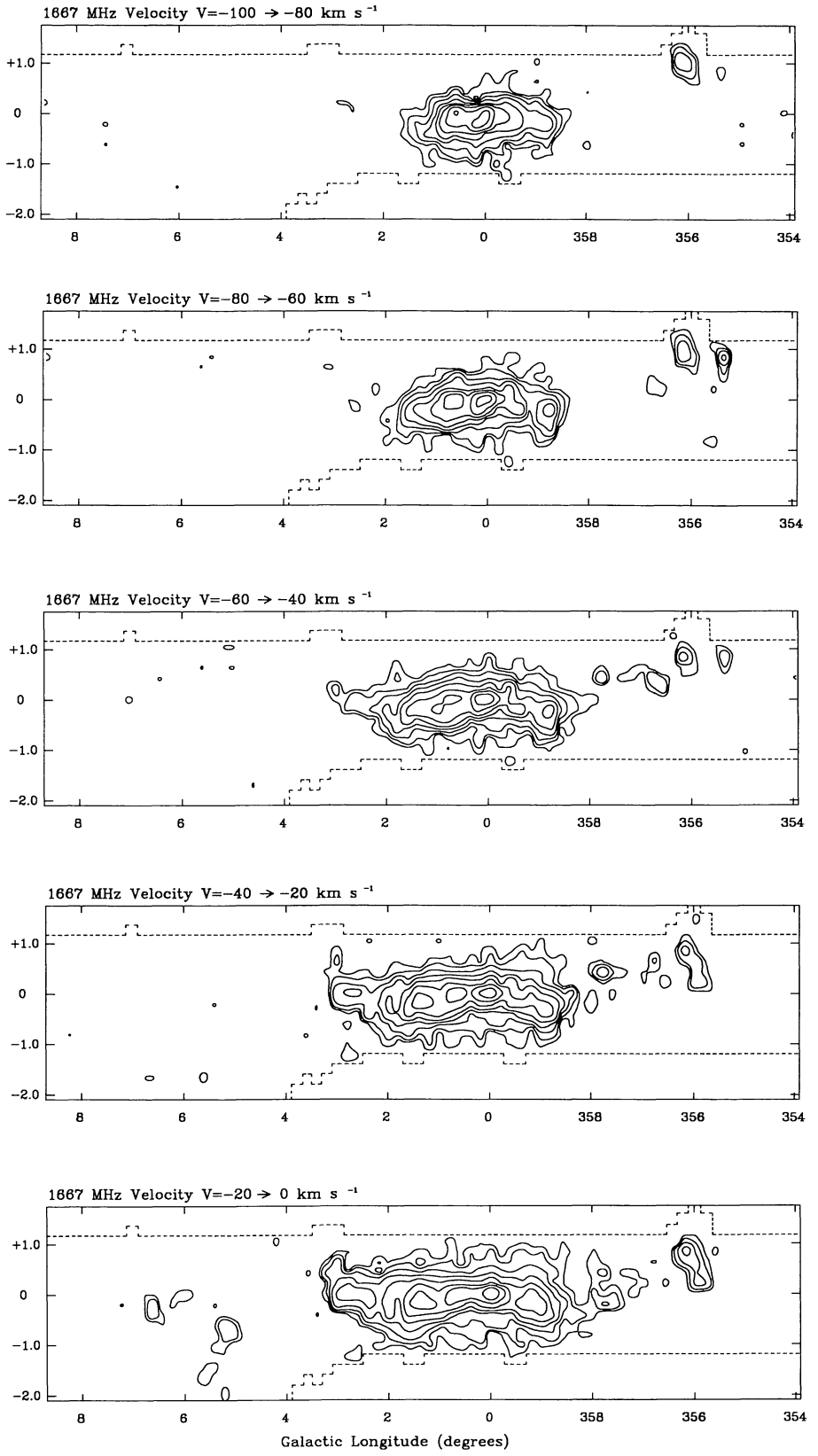

Fig. 6. continued

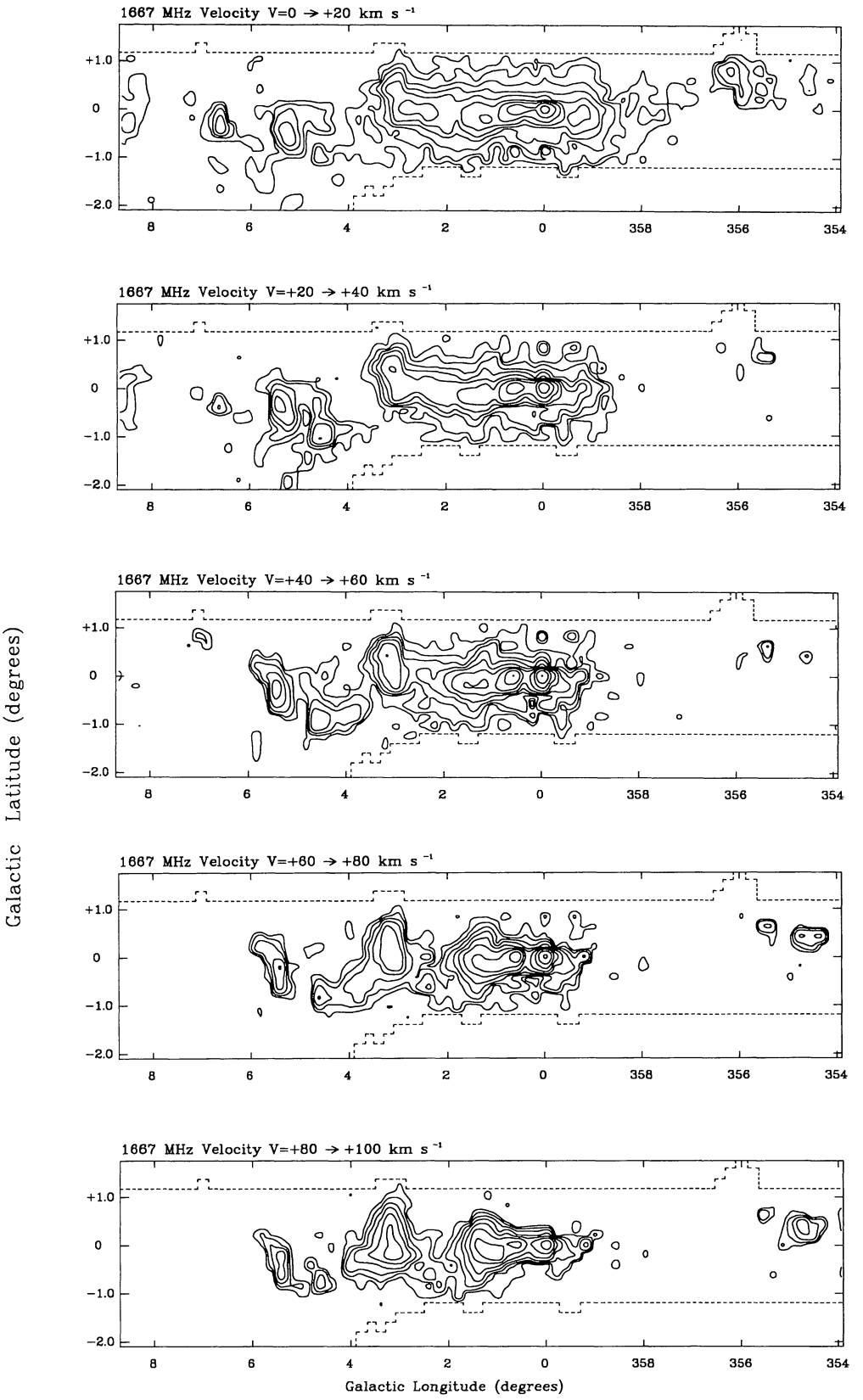

Fig. 6. continued

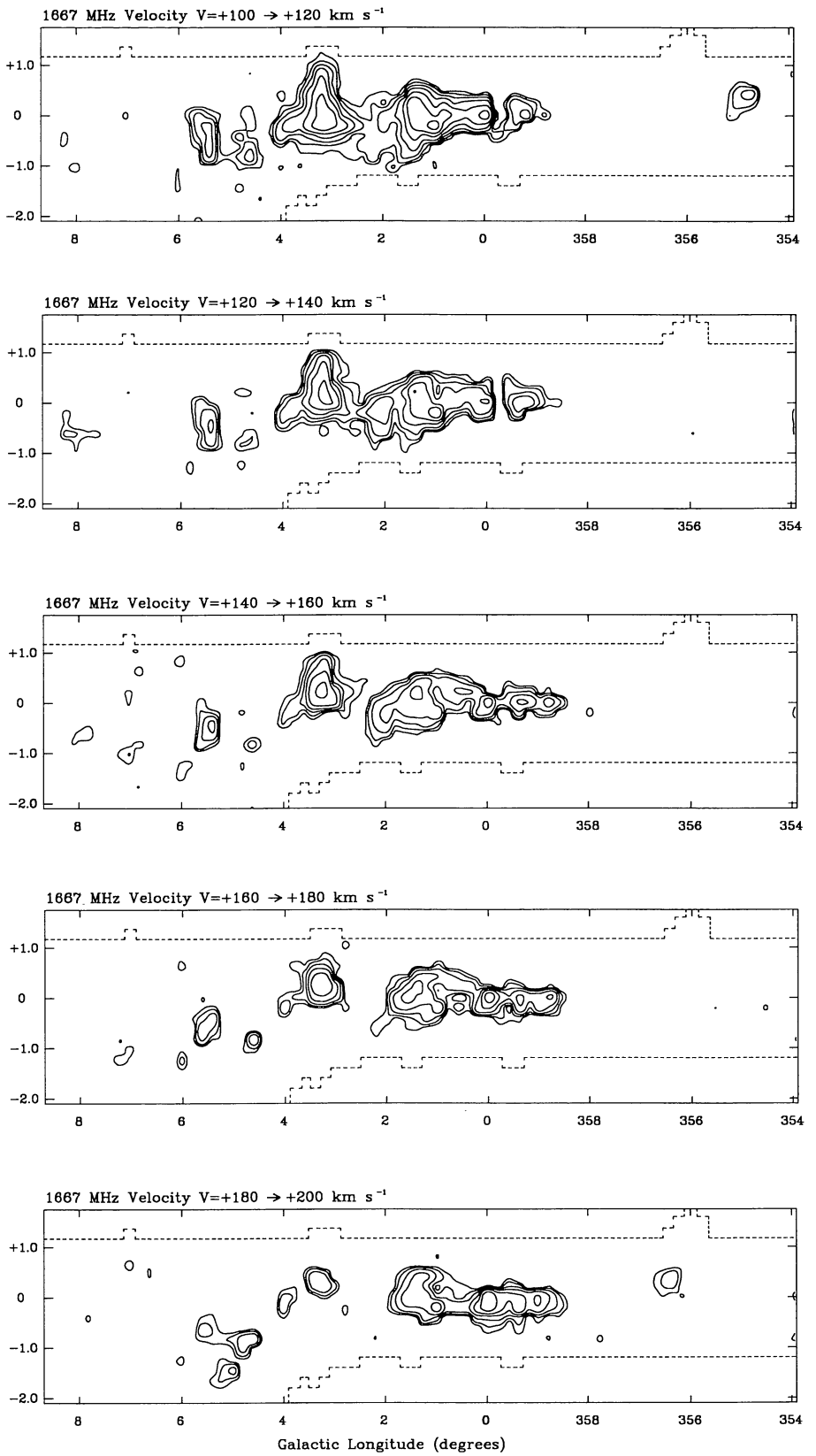

Fig. 6. continued

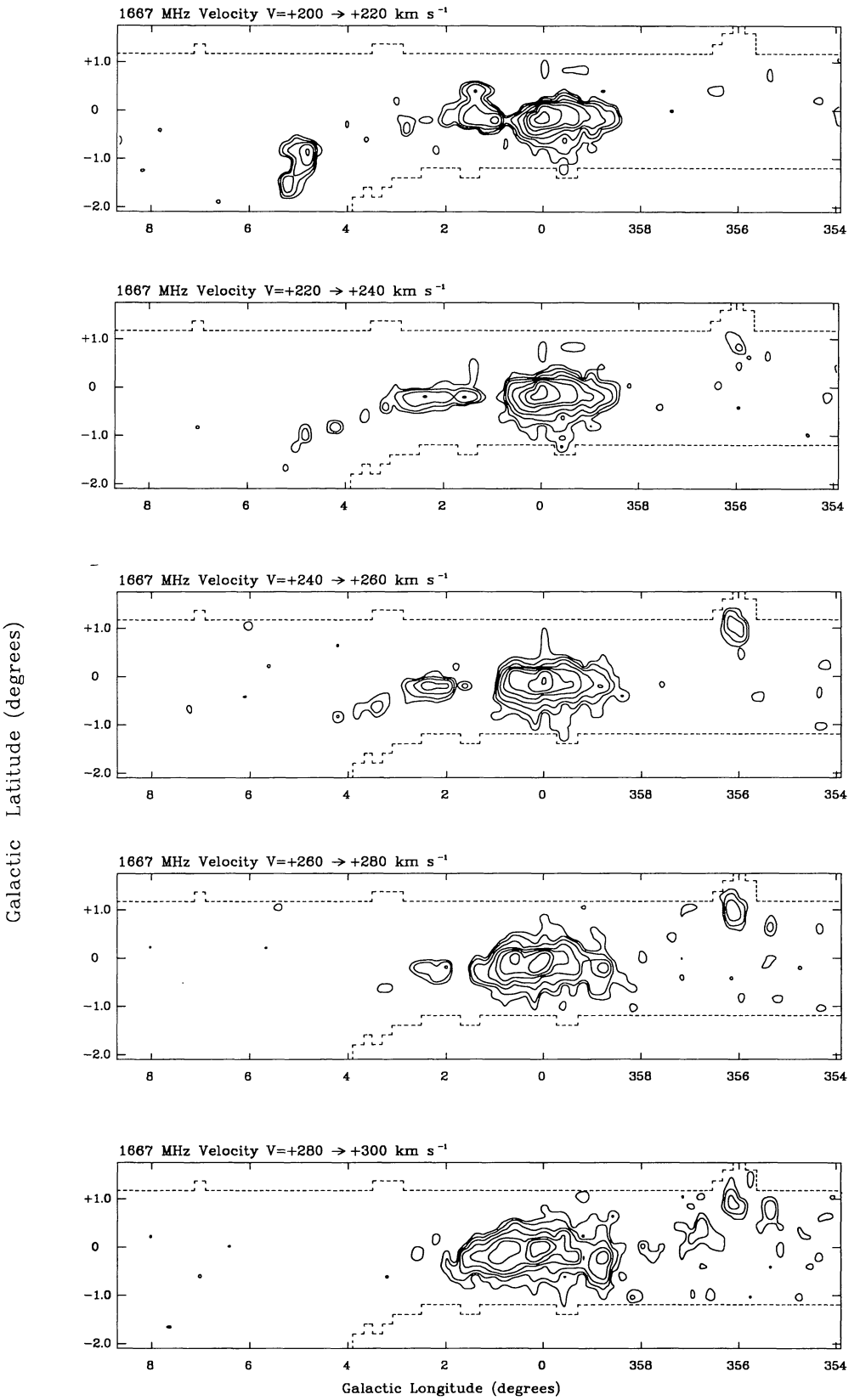

Fig. 6. continued

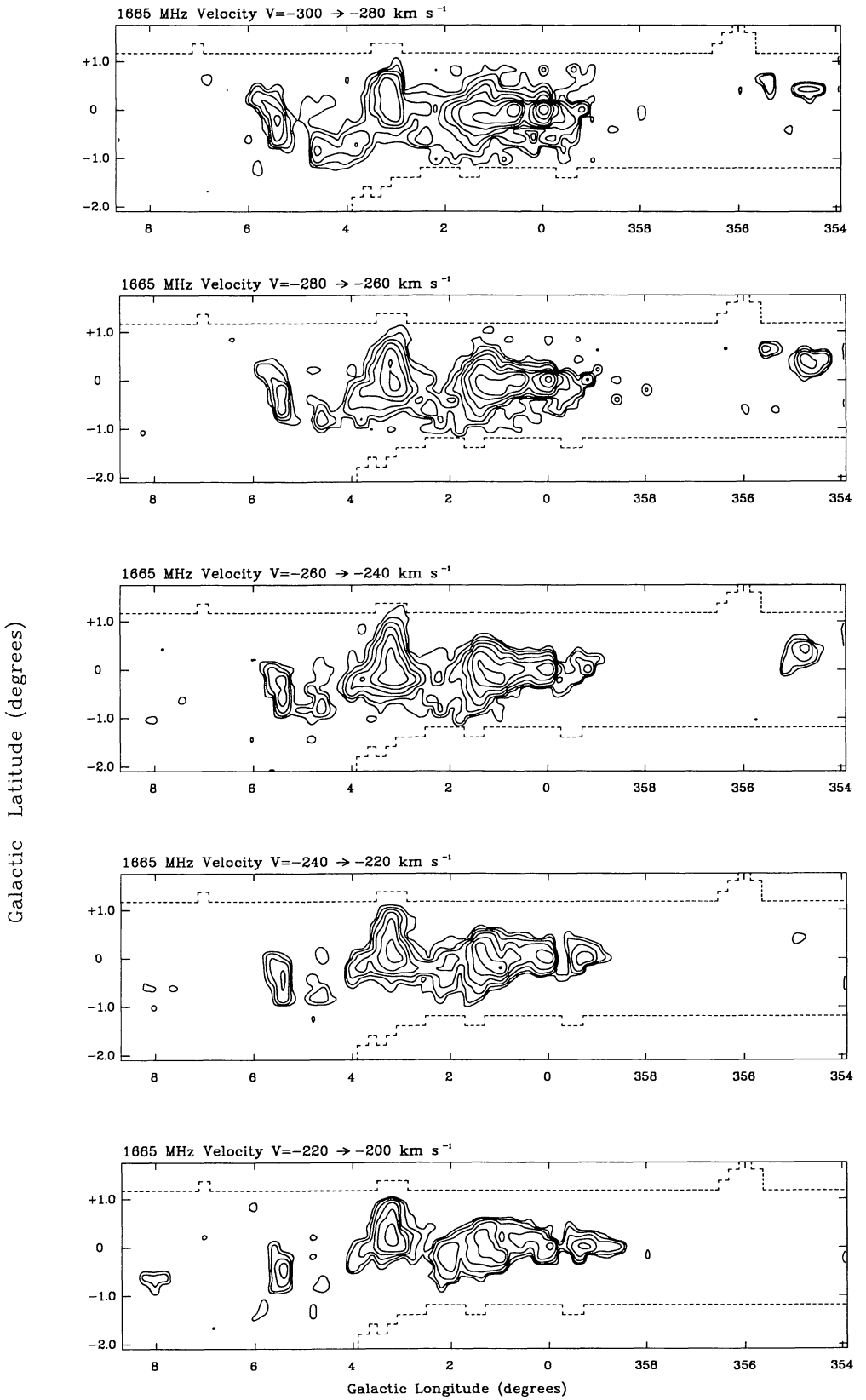

Fig. 7. Longitude–Latitude maps of OH line temperature from the 1665 MHz line integrated over 20 km s^{-1} intervals. Contour levels are set at −1, −2, −4, −8, −16, −32, −64, −128 and −256 K km s^{-1}

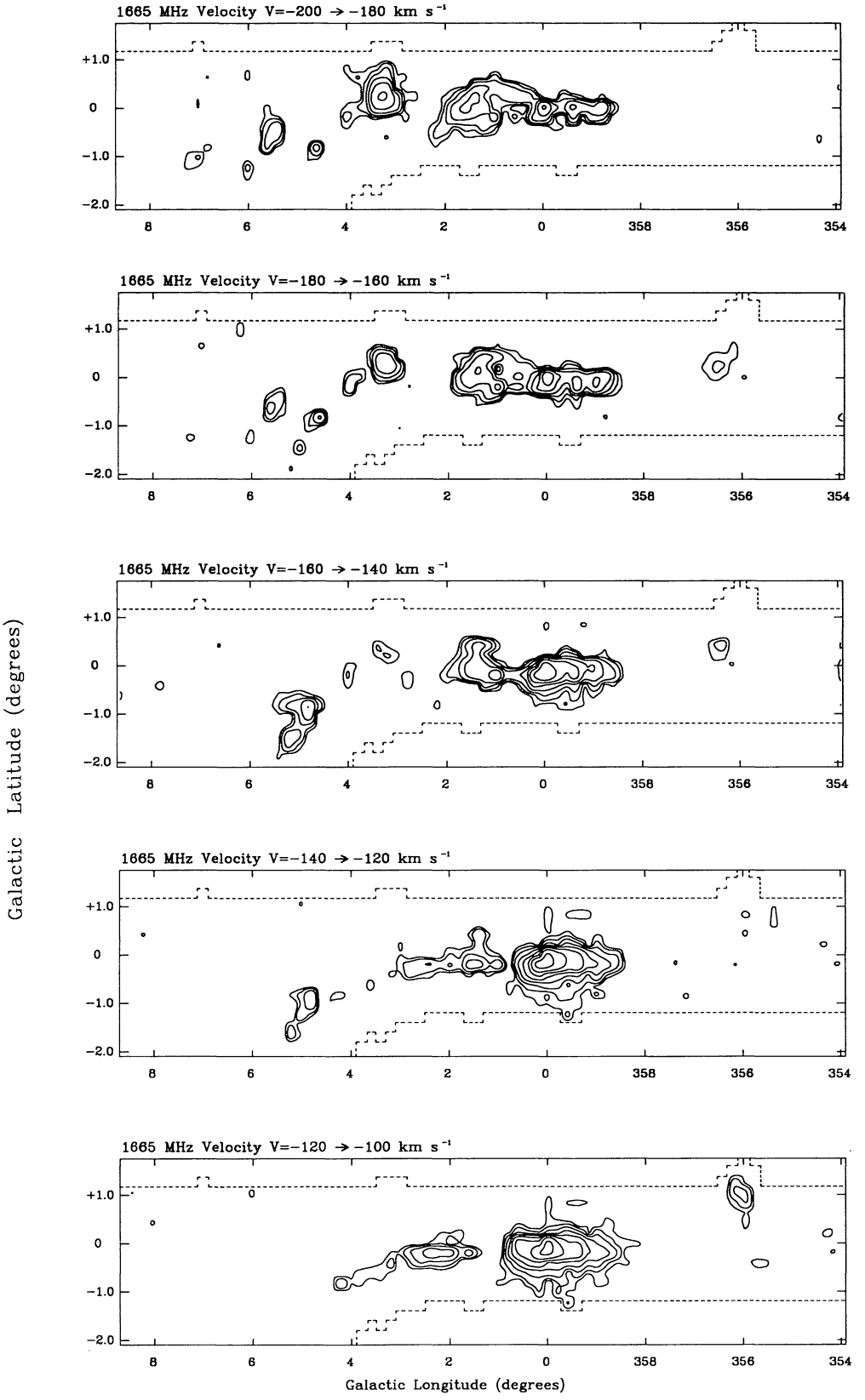

Fig. 7. continued

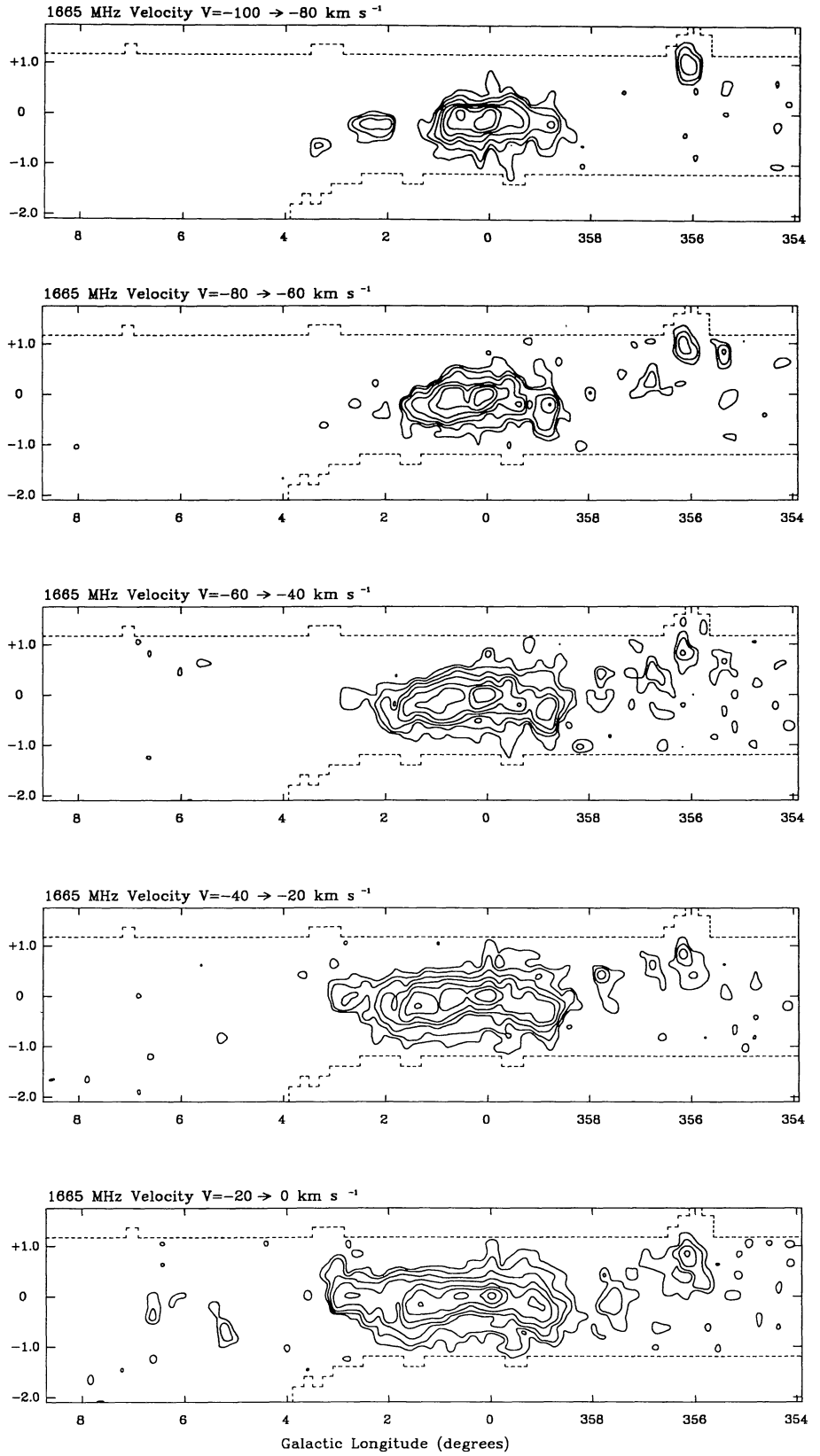

Fig. 7. continued

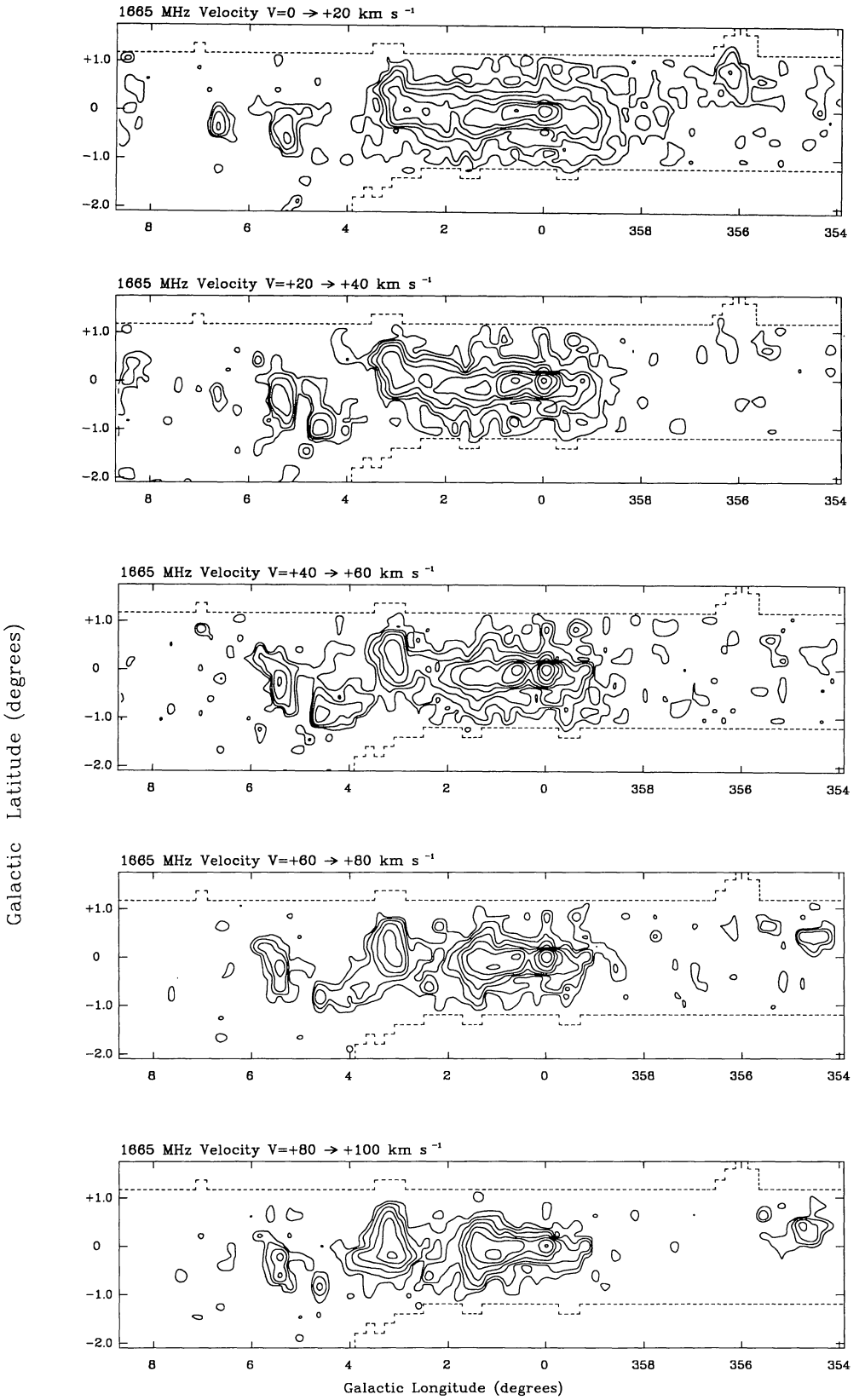

Fig. 7. continued

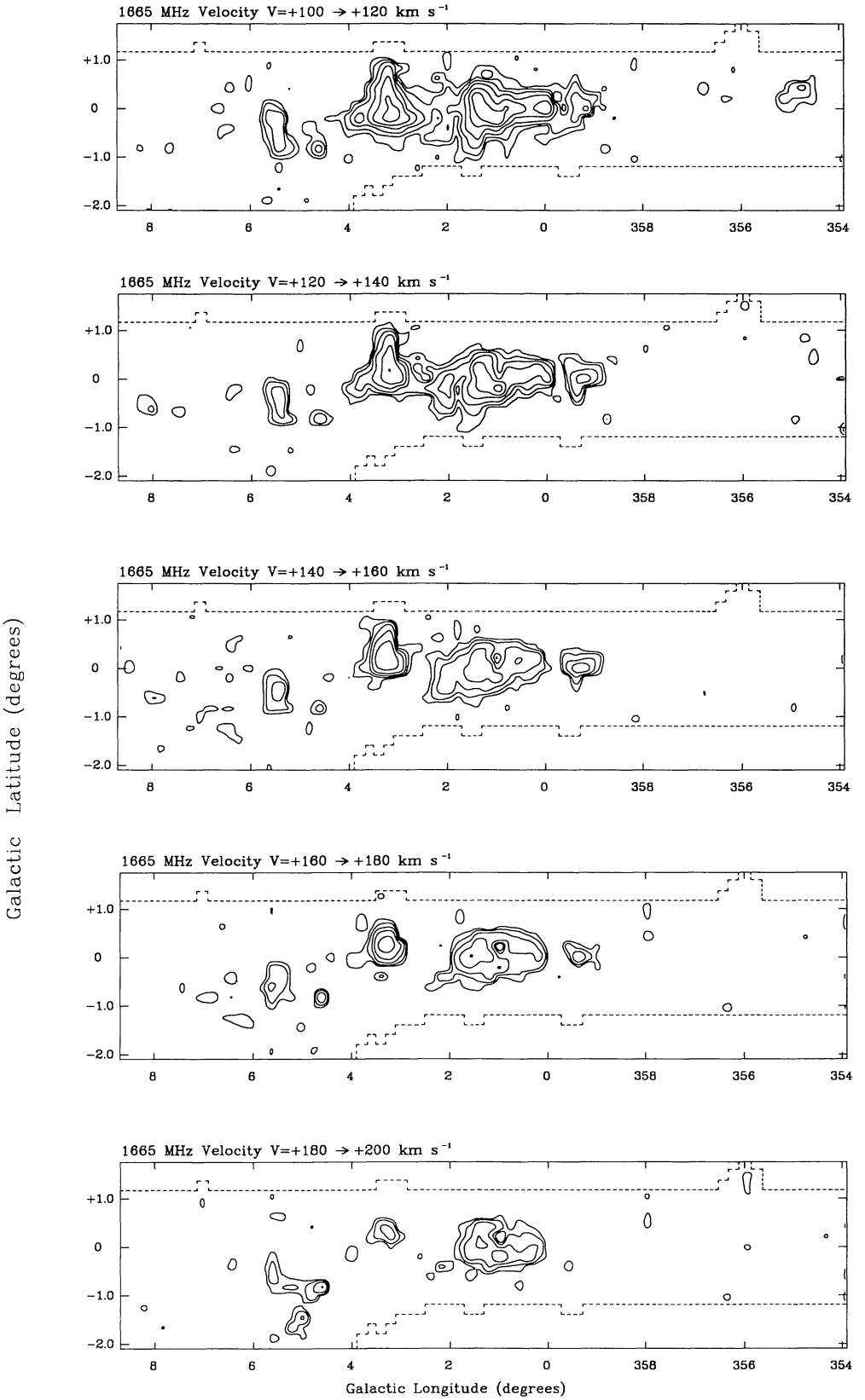

Fig. 7. continued

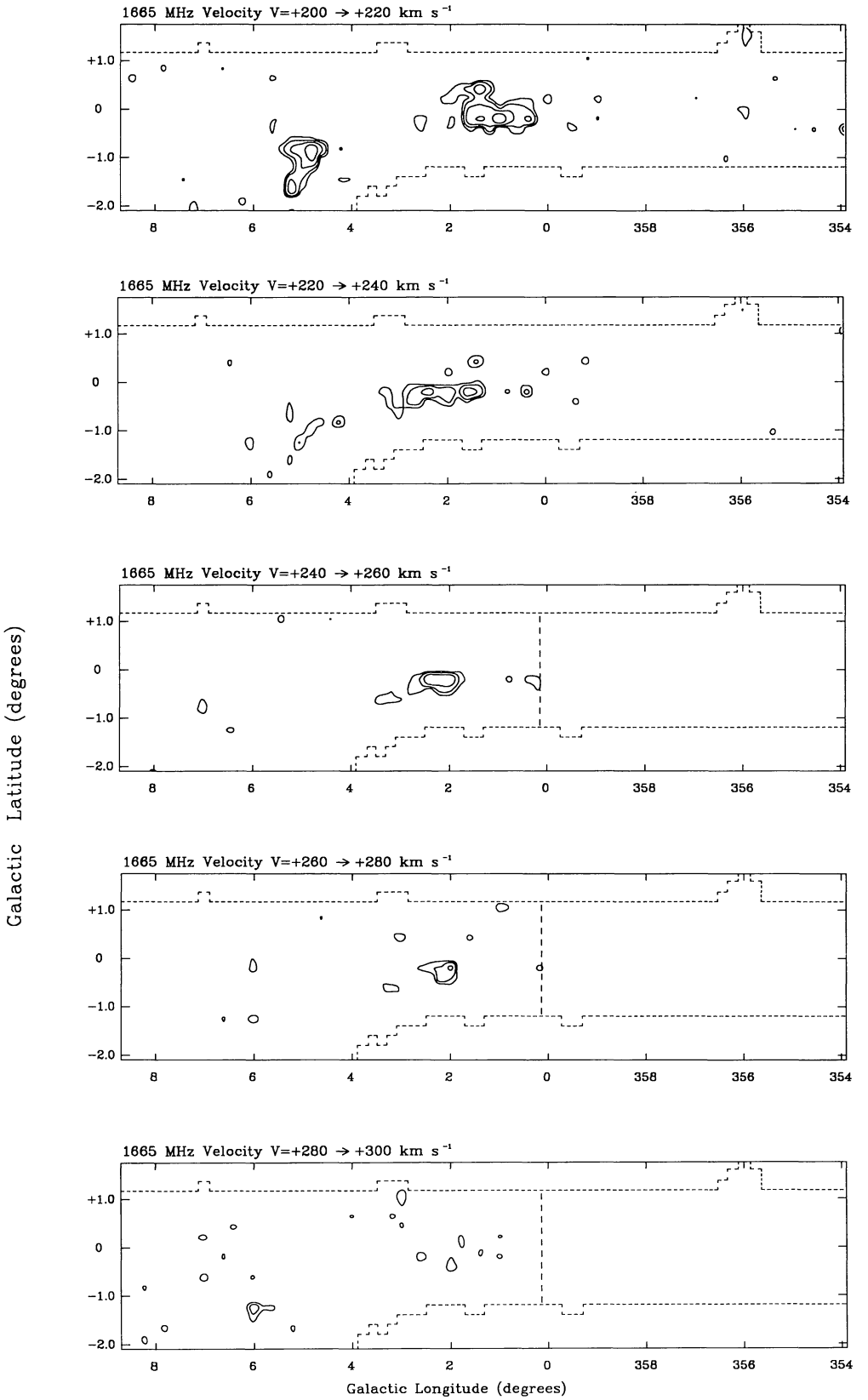

Fig. 7. continued

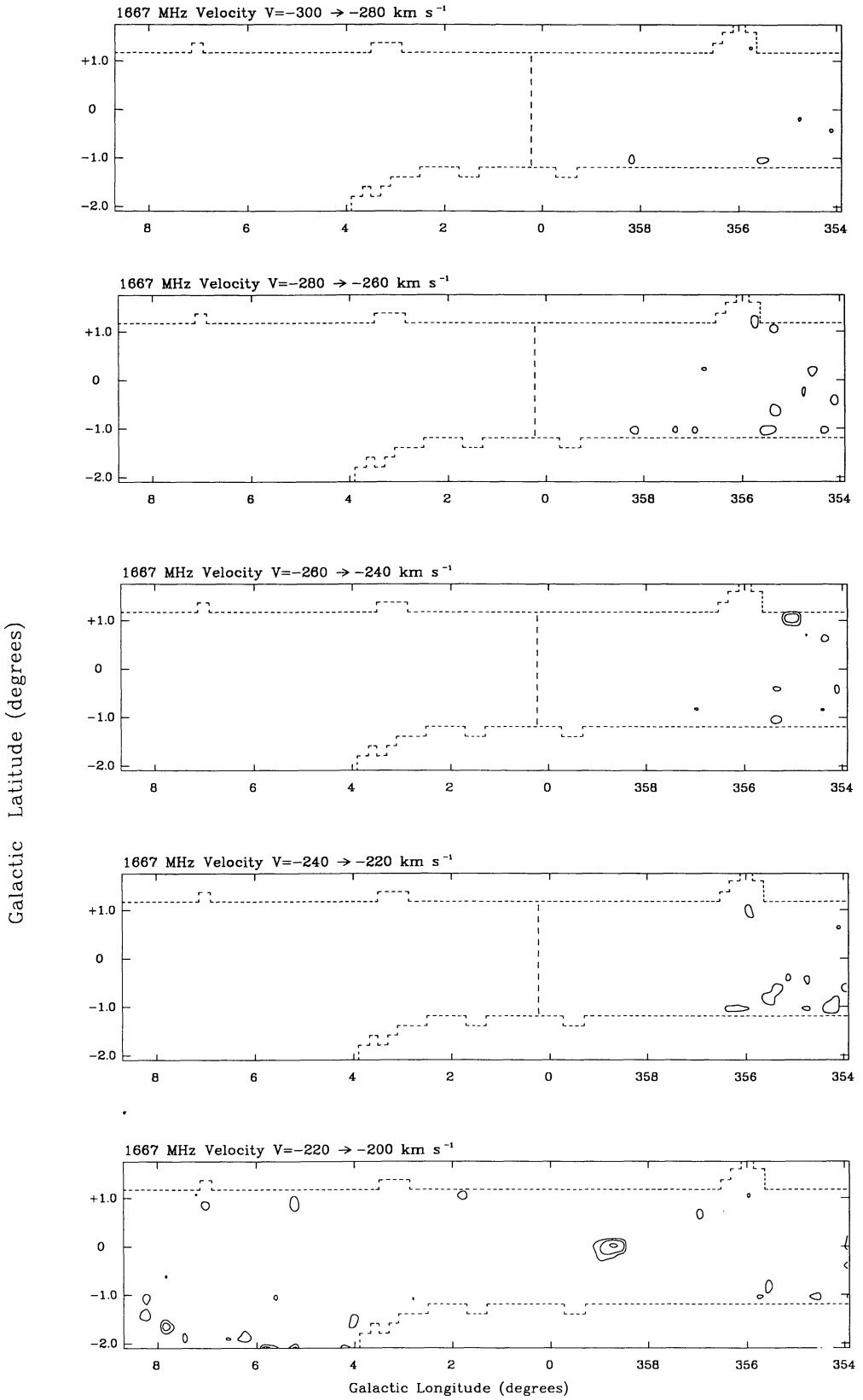

Fig. 8. Longitude–Latitude maps of OH apparent opacity from the 1667 MHz line averaged over 20 km s^{-1} intervals. Contour levels are set at 0.01, 0.02, 0.04, 0.08, 0.16, 0.32 and 0.64

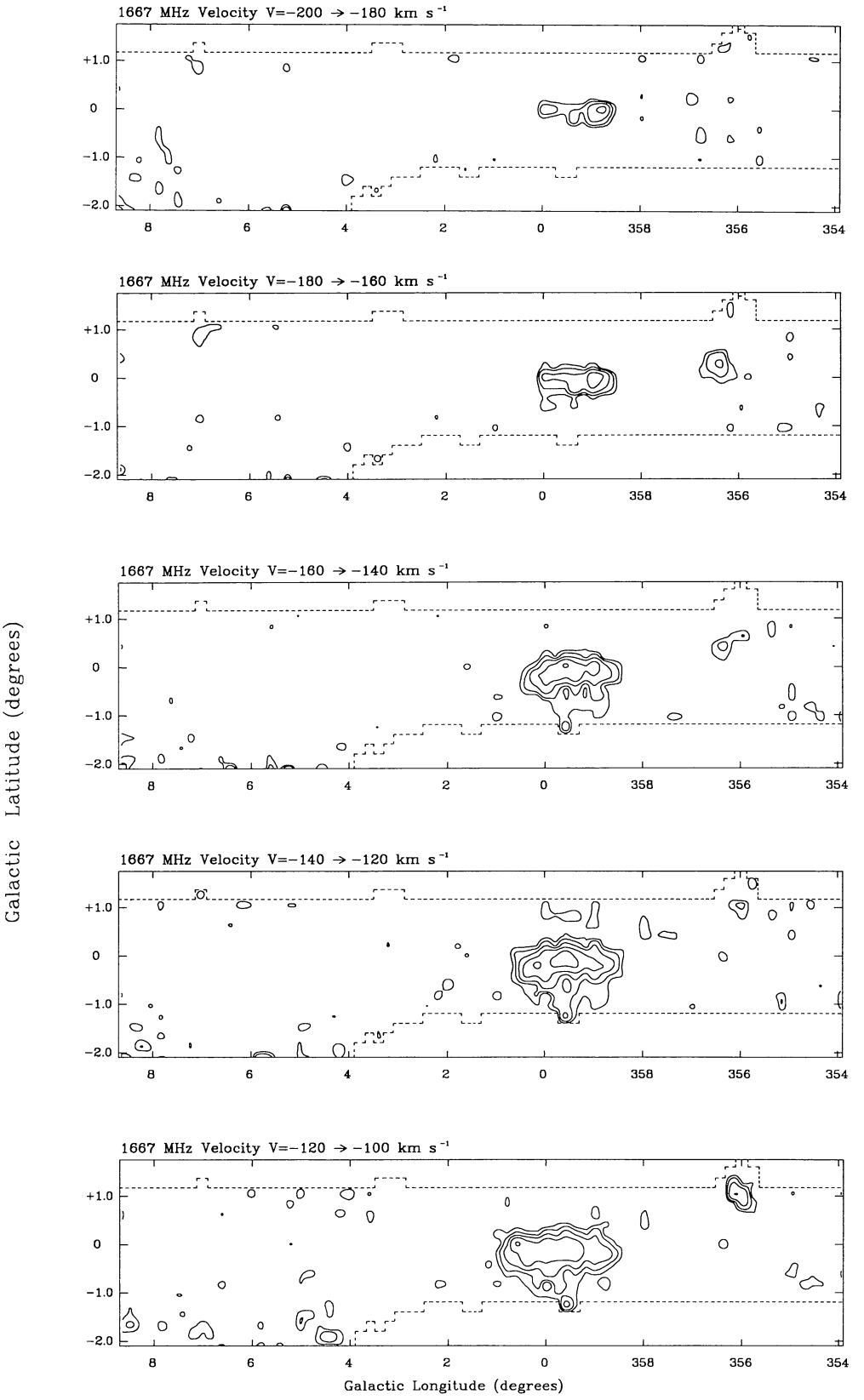

Fig. 8. continued

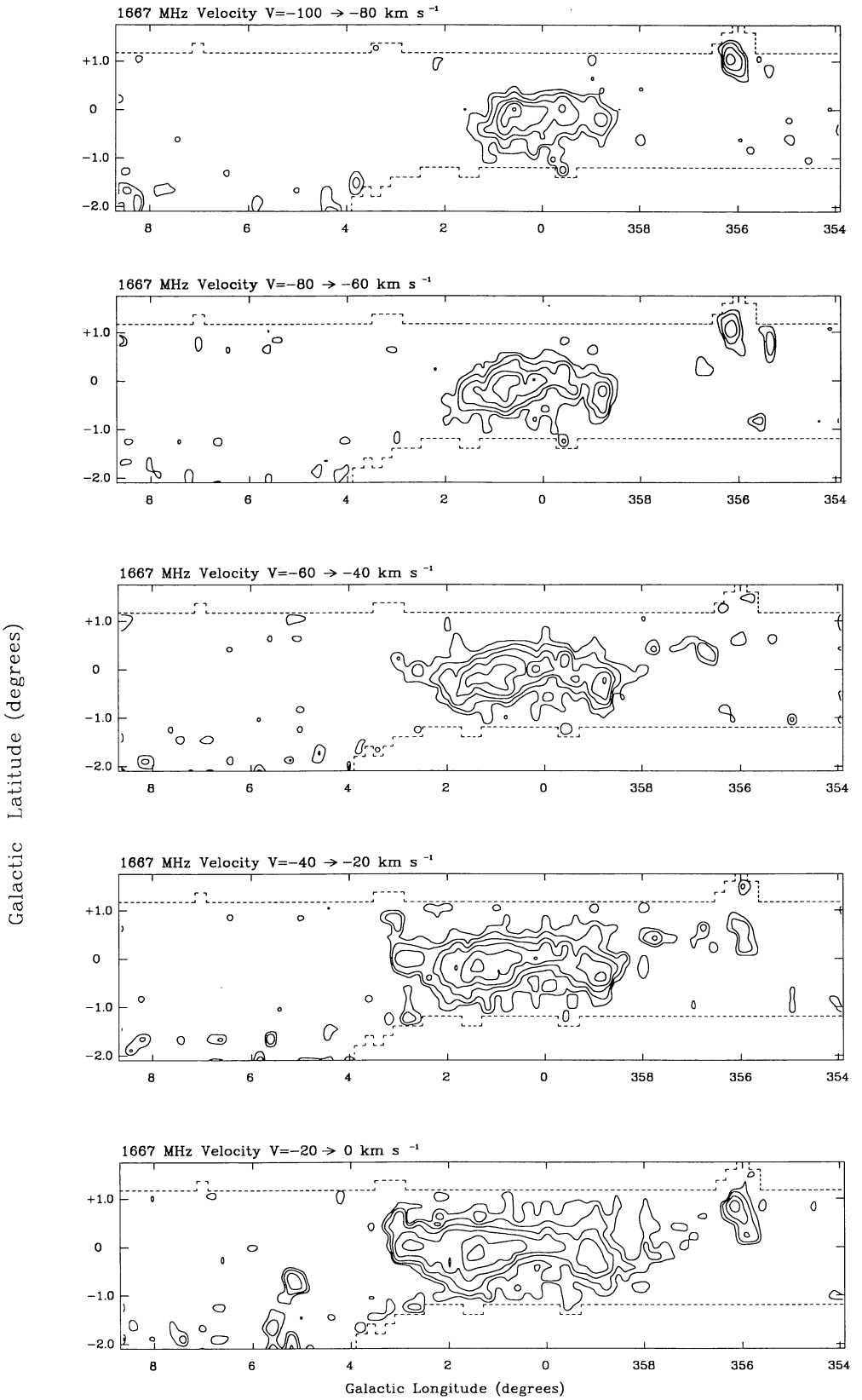

Fig. 8. continued

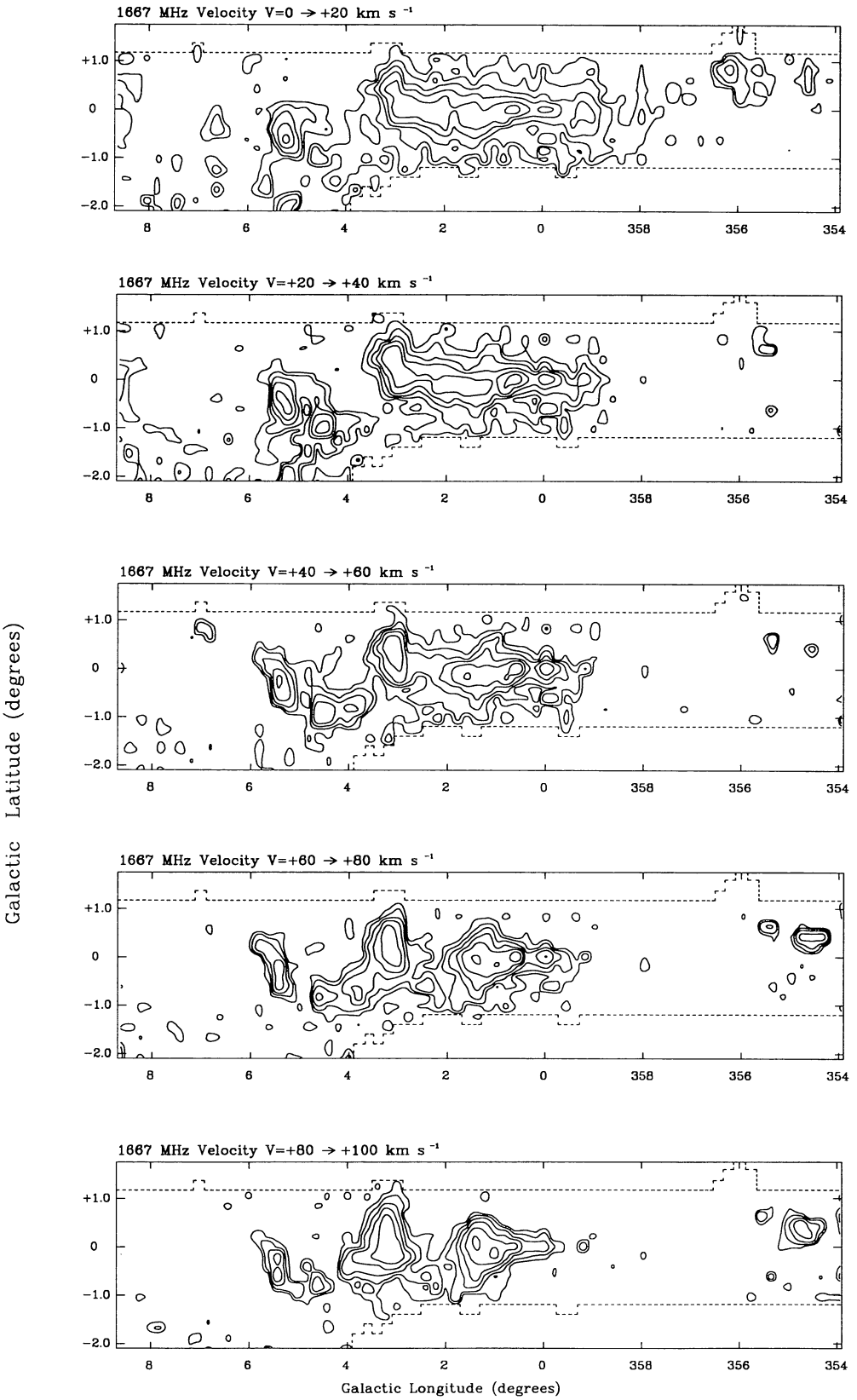

Fig. 8. continued

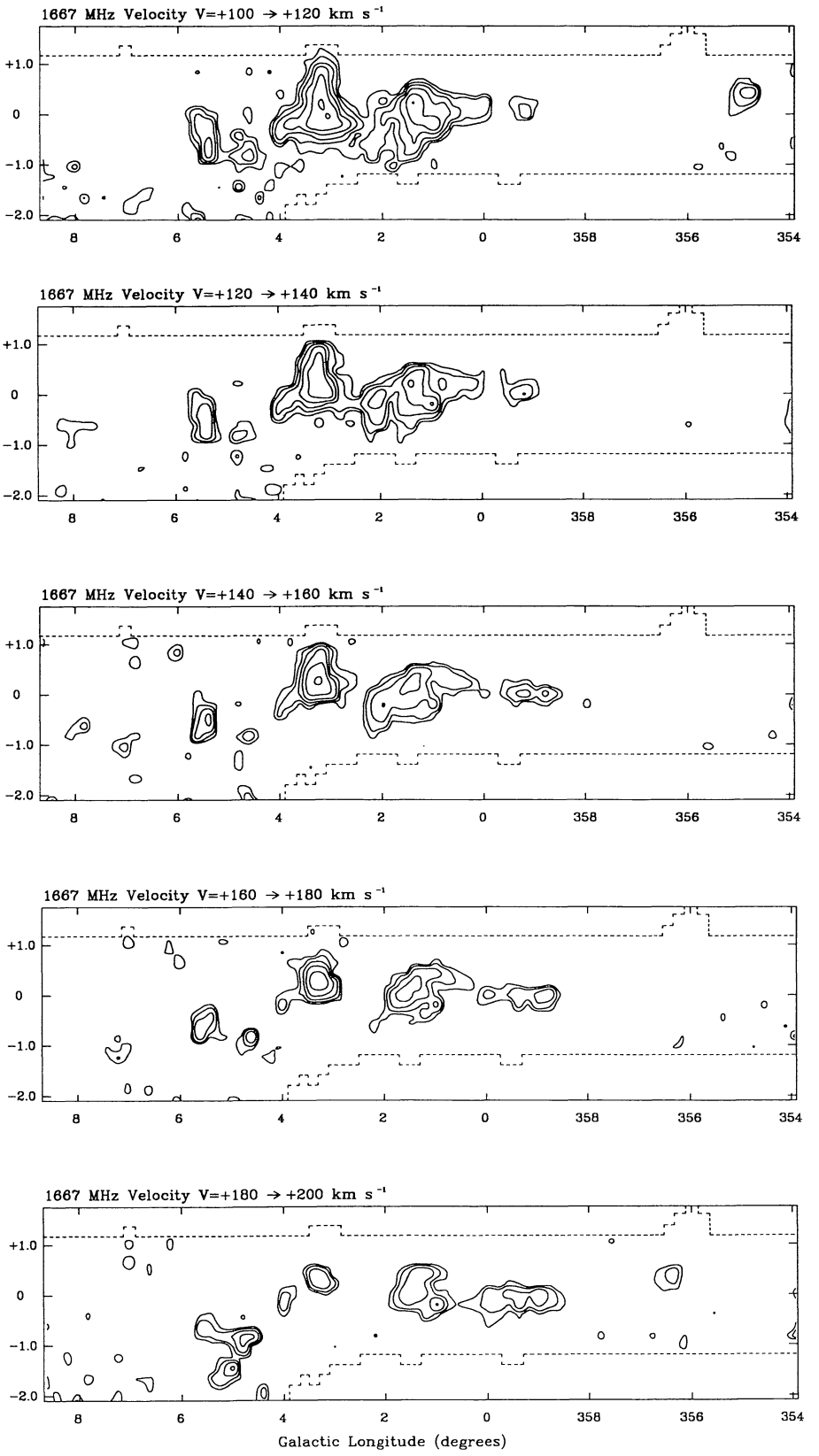

Fig. 8. continued

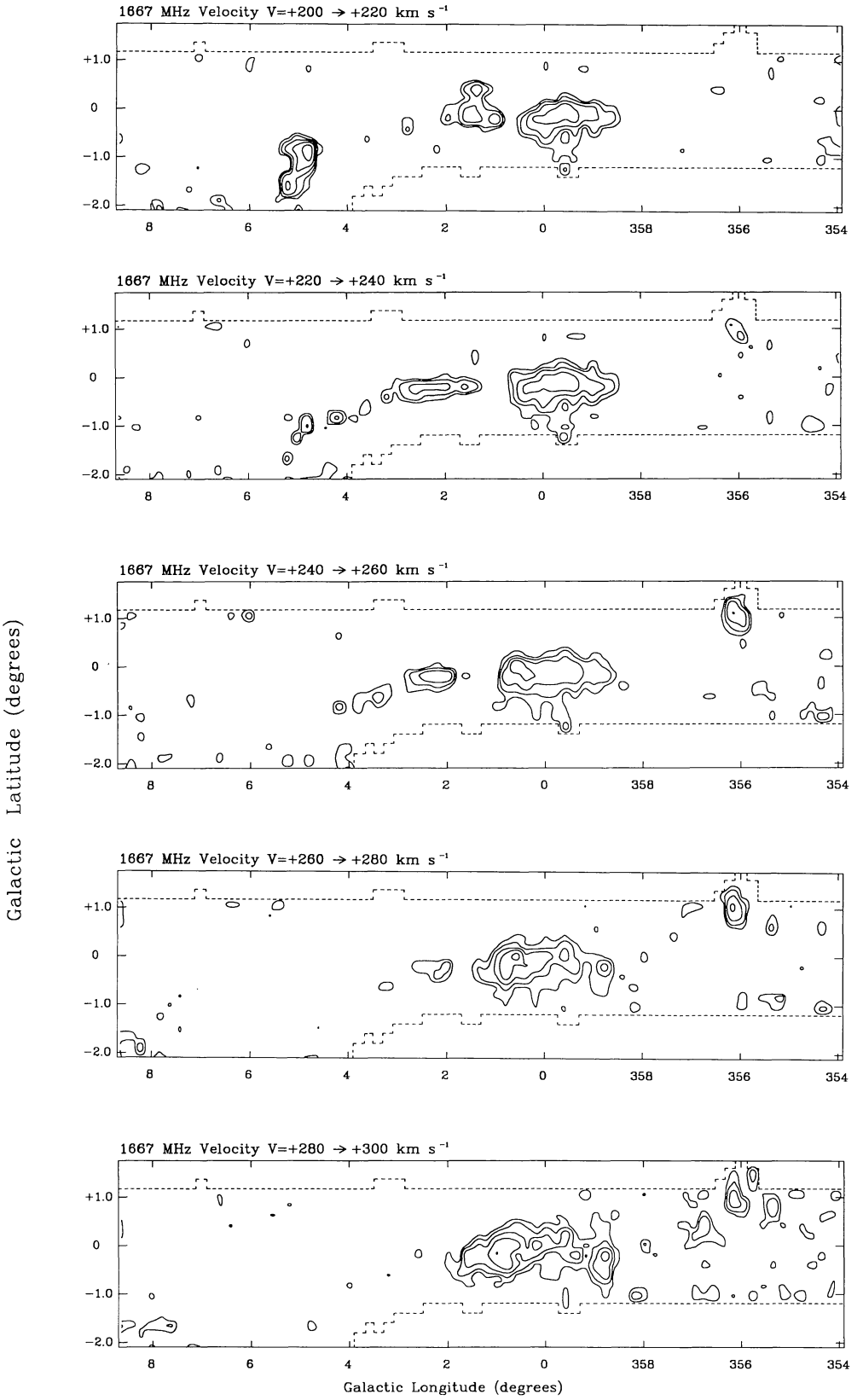

Fig. 8. continued

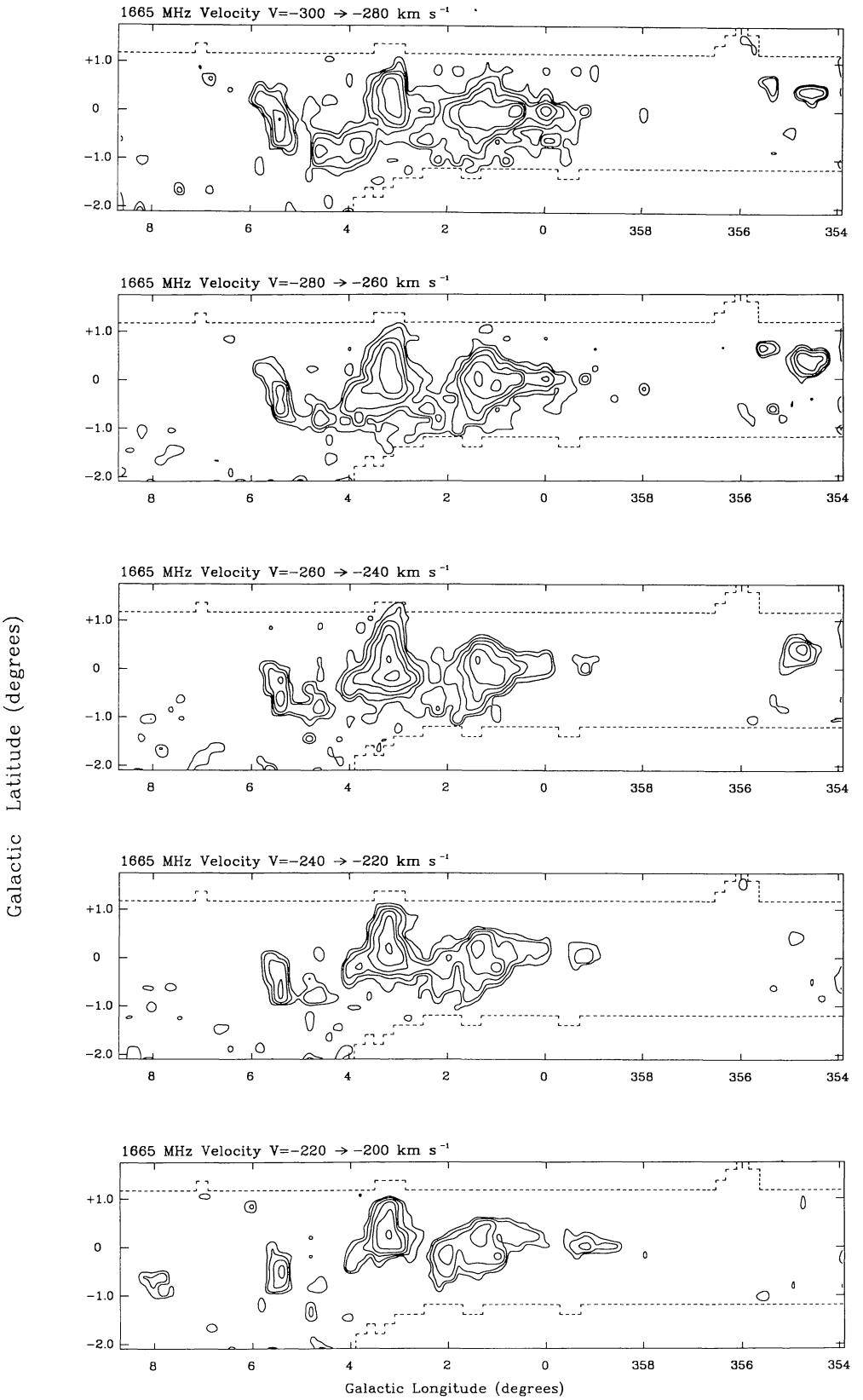

Fig. 9. Longitude–Latitude maps of OH apparent opacity from the 1665 MHz line averaged over 20 km s^{-1} intervals. Contour levels are set at 0.01, 0.02, 0.04, 0.08, 0.16, 0.32 and 0.64

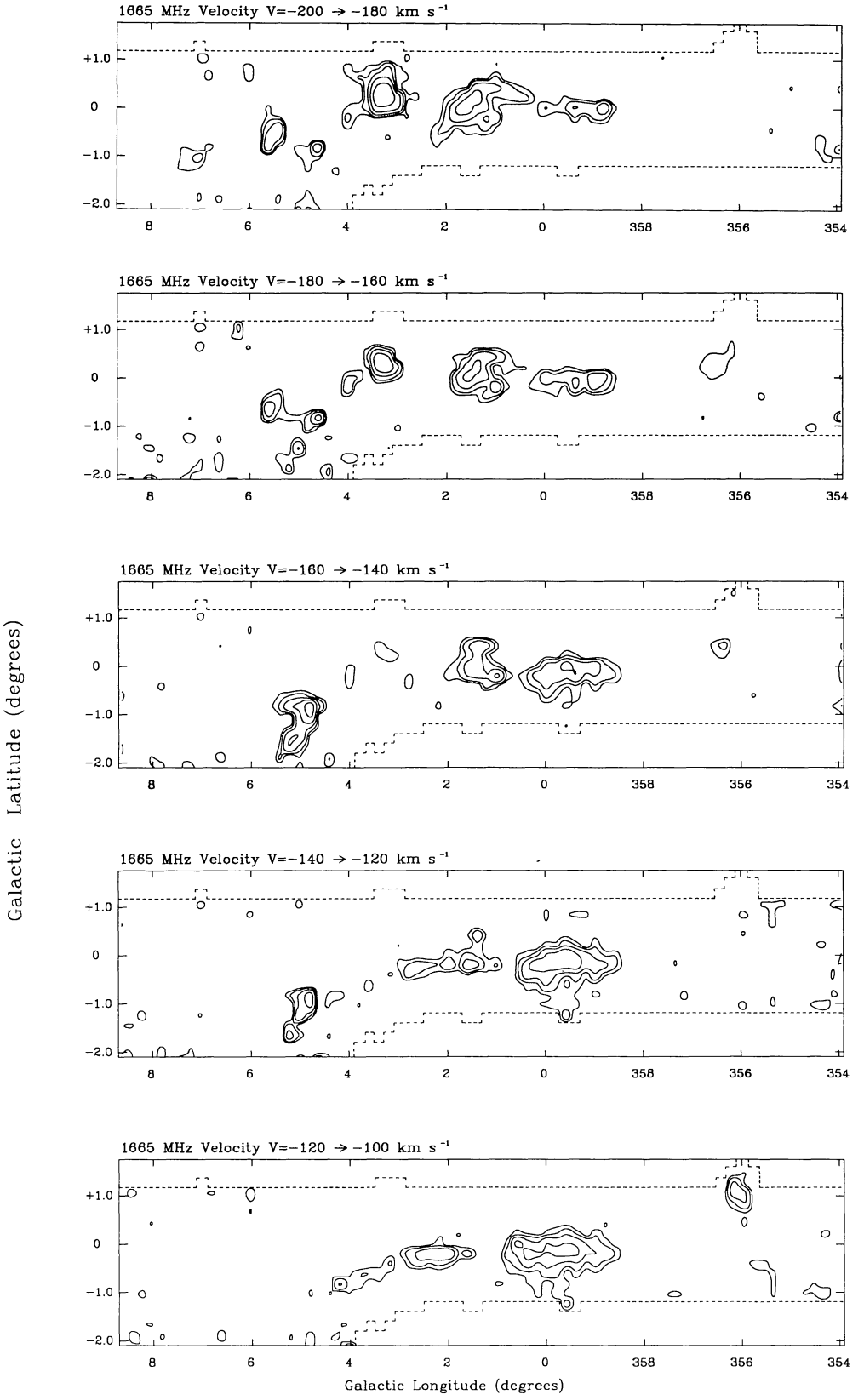

Fig. 9. continued

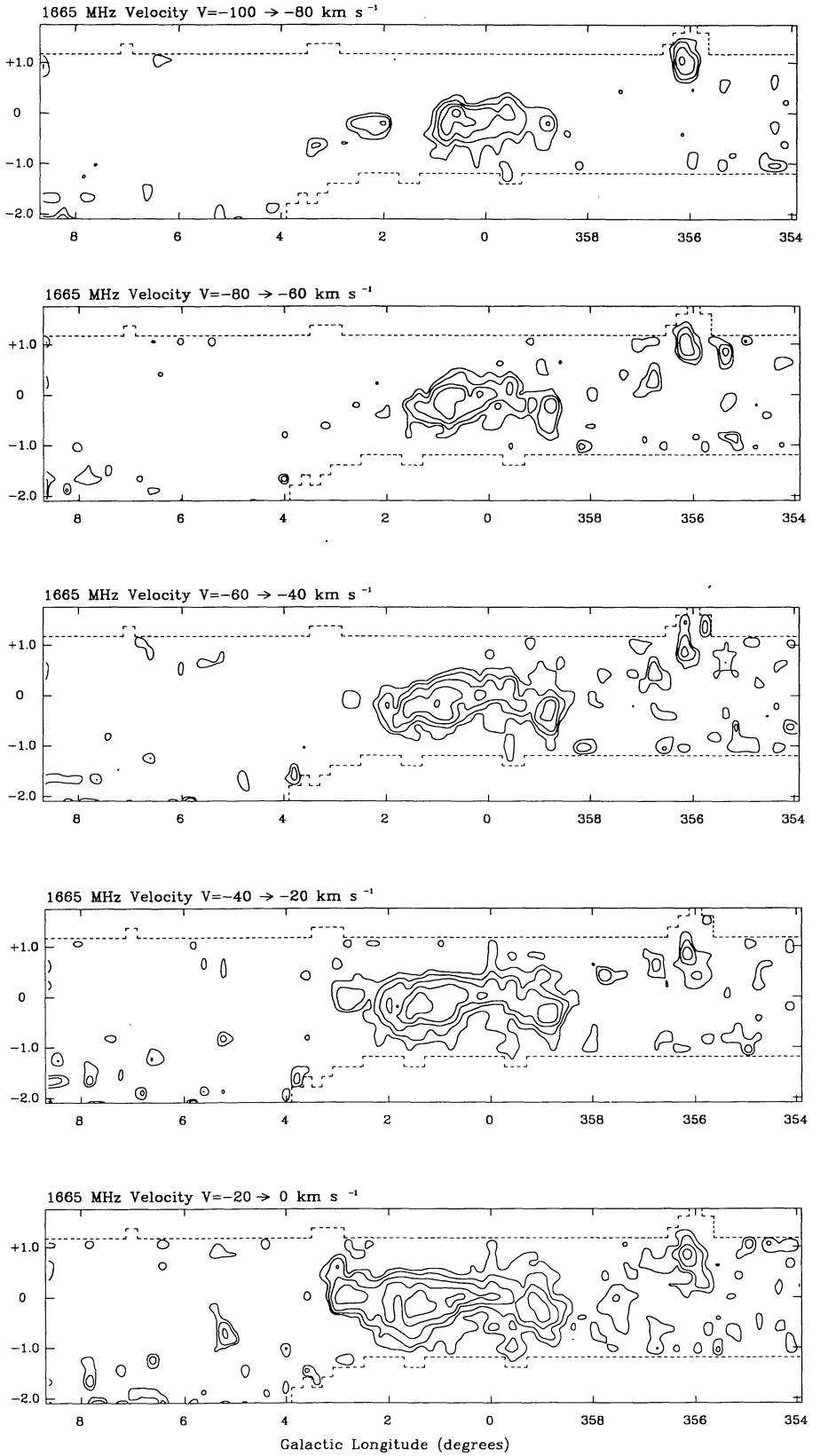

Fig. 9. continued

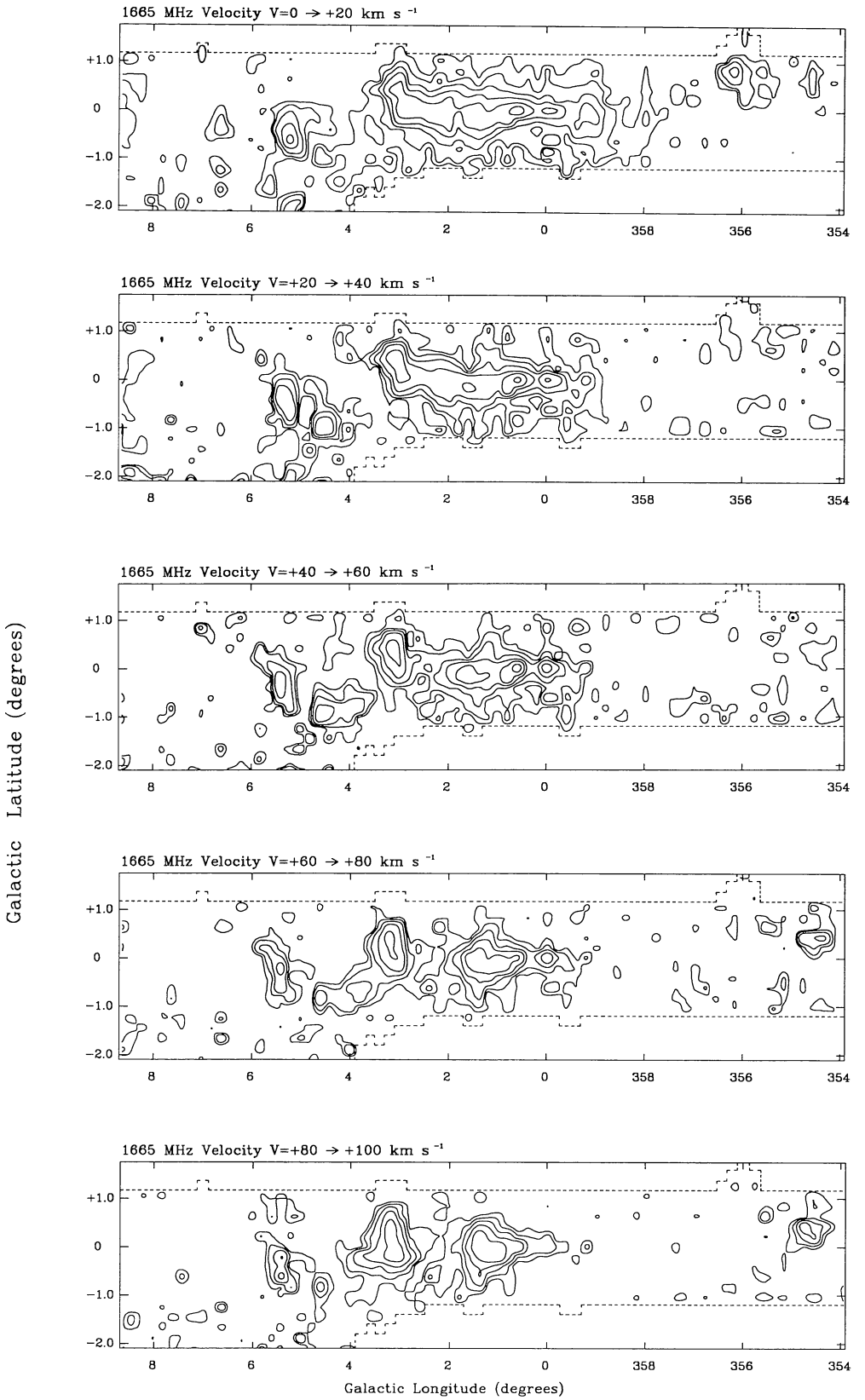

Fig. 9. continued

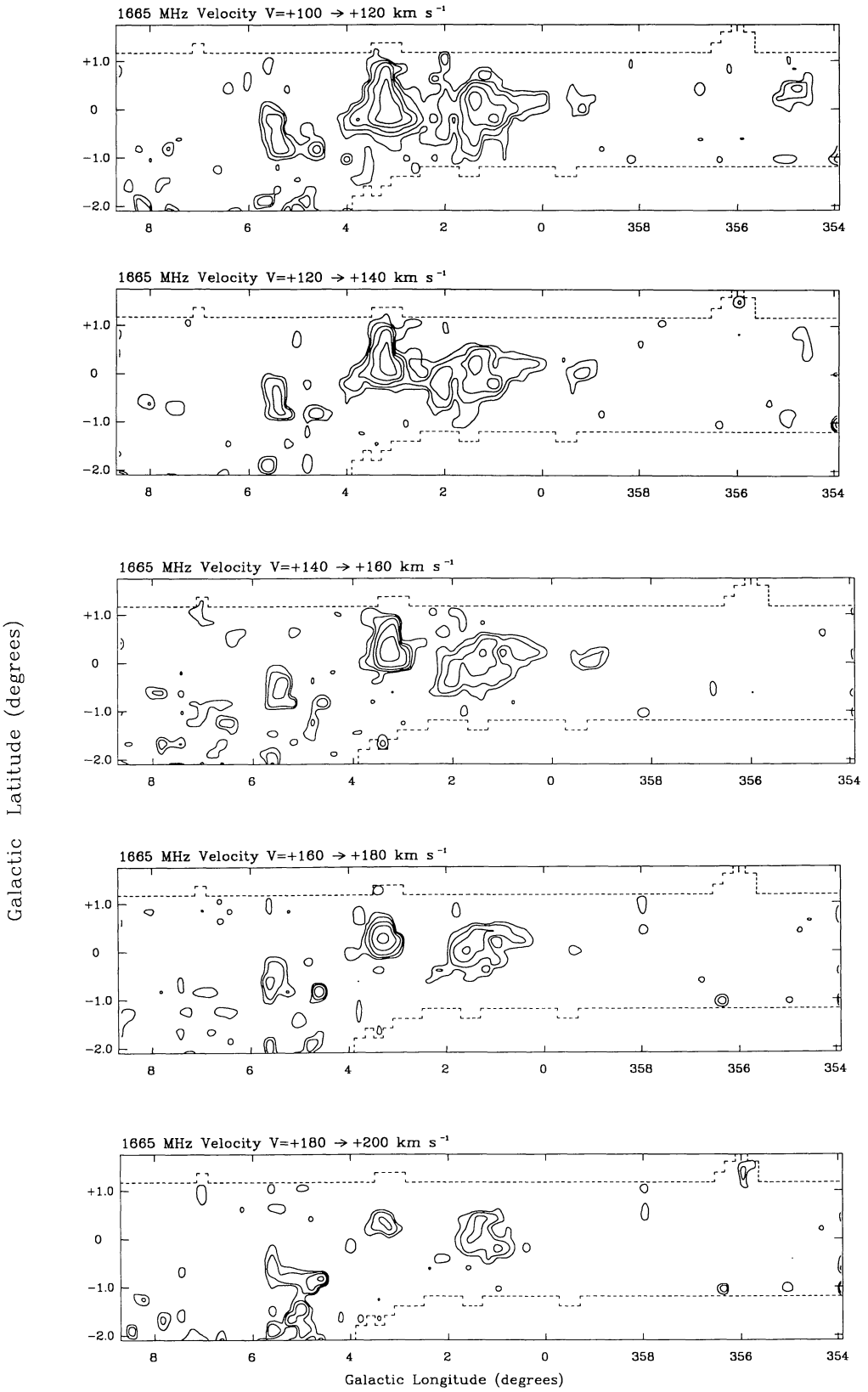

Fig. 9. continued

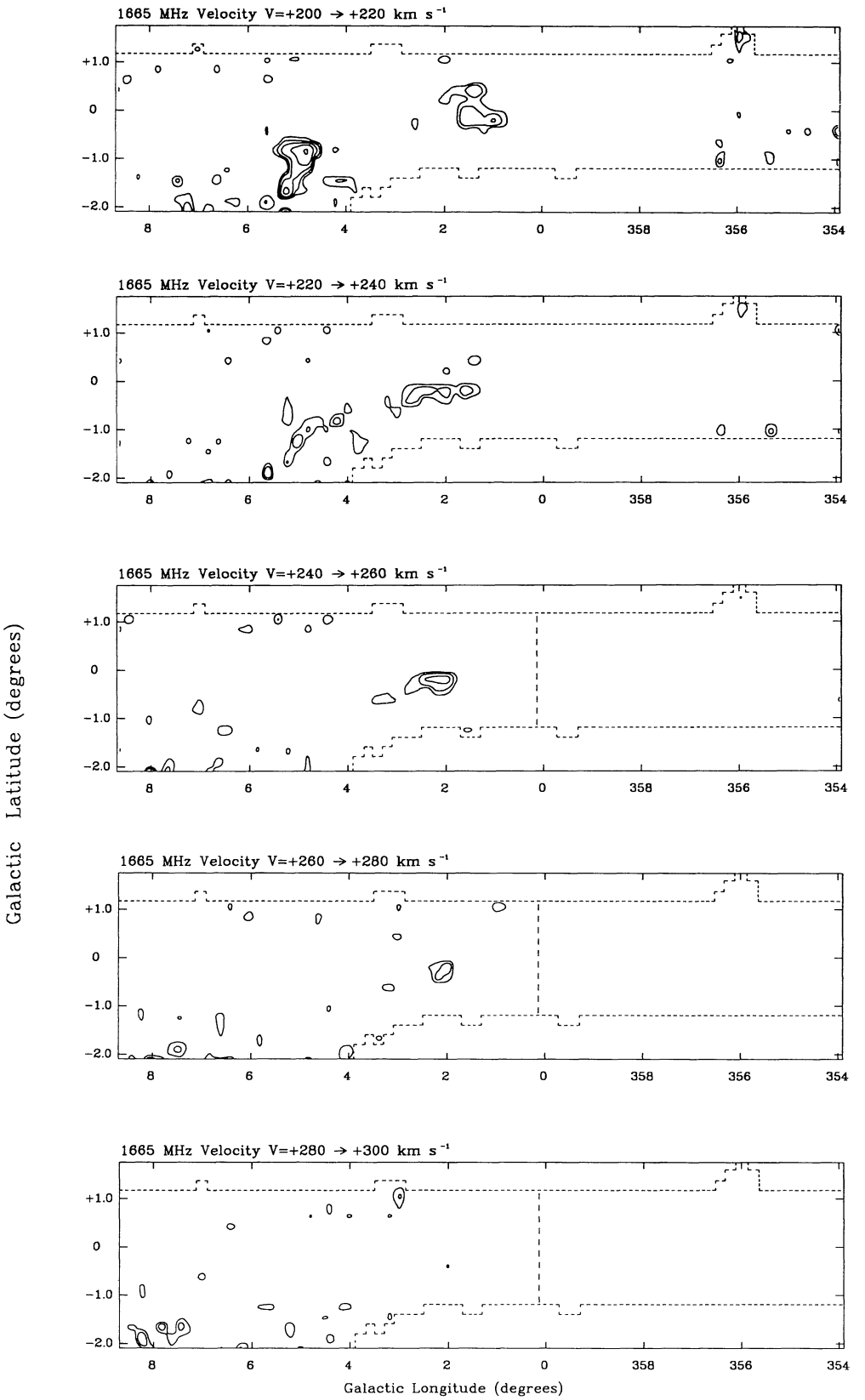

Fig. 9. continued

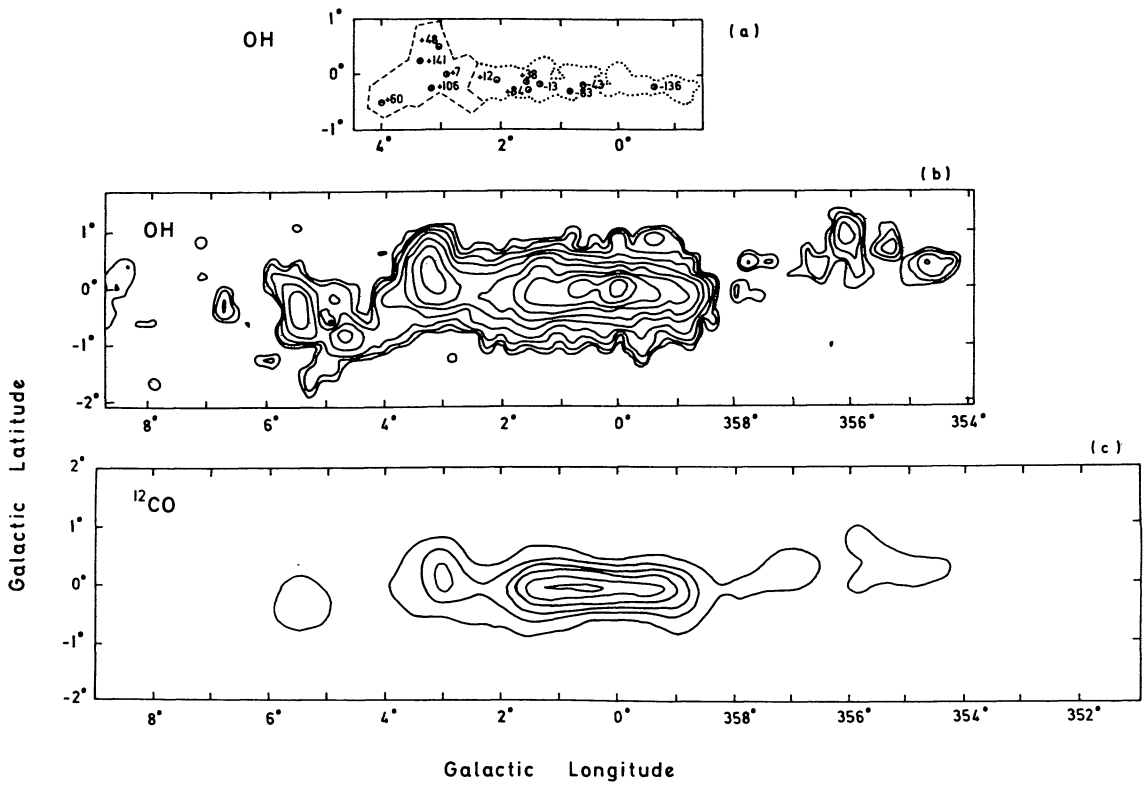

Fig. 10. a–c) The extent of the molecular nuclear disk as seen by, a) McGee et al. (1970), b) Dame et al. (1987) and, c) the present survey. The contour levels from the present survey are set at –8, –16, –32, –64, –128, –256, –512, –1024, –2048 and –4096 K km s^{-1}

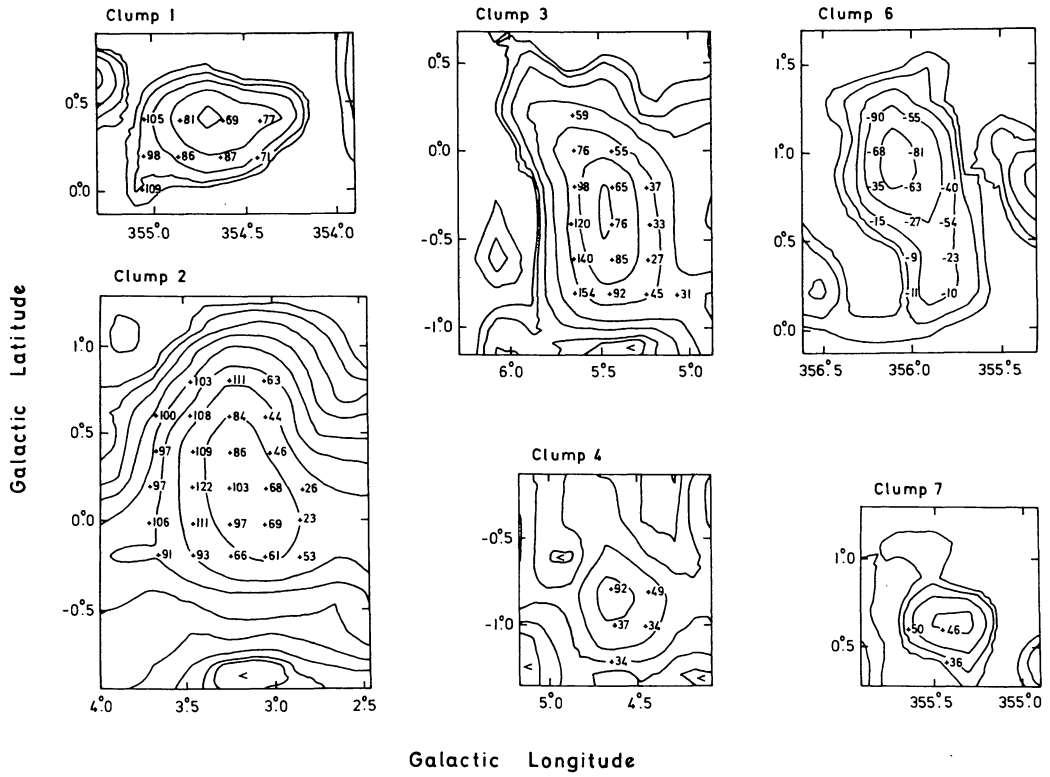

Fig. 11. Spatial maps of the clumps integrated over their total velocity extents in the 1667 MHz line with the central velocity of the profile at each observed position superimposed. Contour levels are at –2, –4, –8, –16, –32, –64, –128 and –256 K km s^{-1}

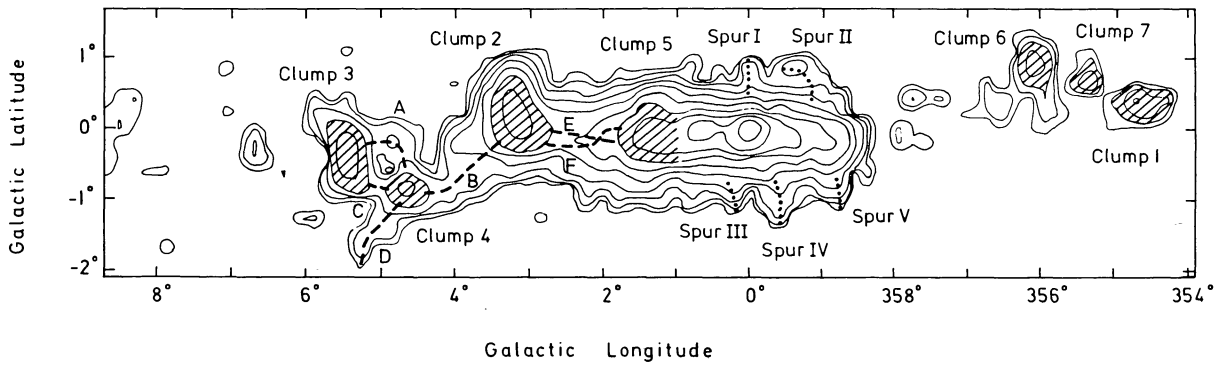

Fig. 12. An integrated OH line temperature map with positions of the broadline clumps, filaments and molecular spurs noted. Broadline clumps are illustrated by hatching. Filaments are shown by thick dashed lines. Molecular spurs are shown by dotted dashed lines

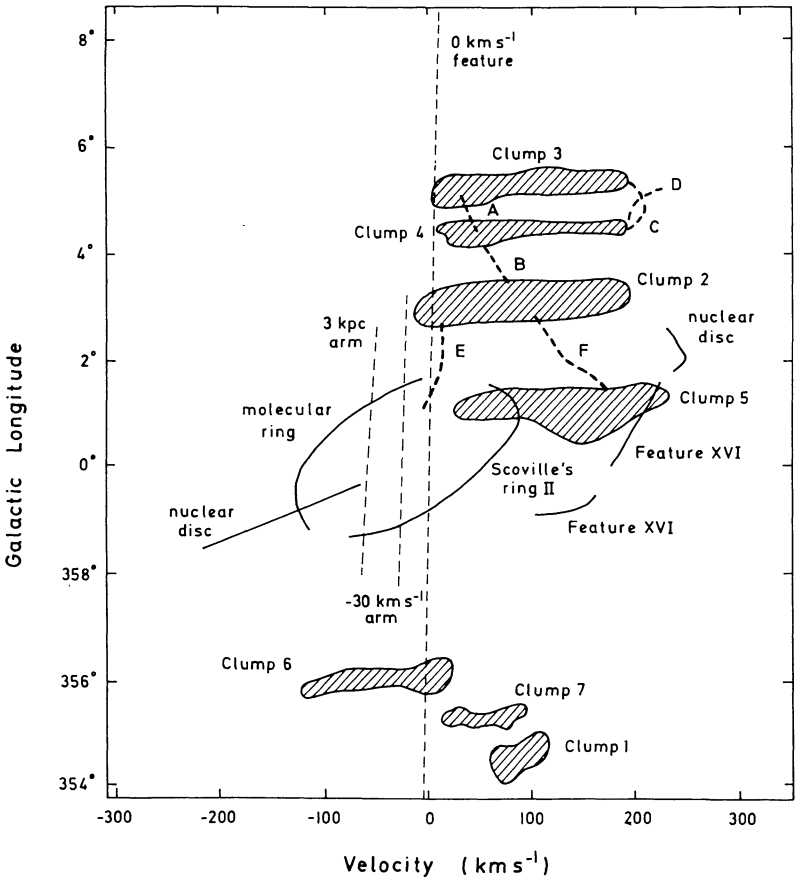

Fig. 13. *l–V* chart of the principal absorption features seen in the survey. Broadline clumps are illustrated by hatching. Filaments are shown by thick dashed lines. Features close to the nucleus are shown by solid lines. Features believed to originate outside the nucleus are shown by thin dashed lines

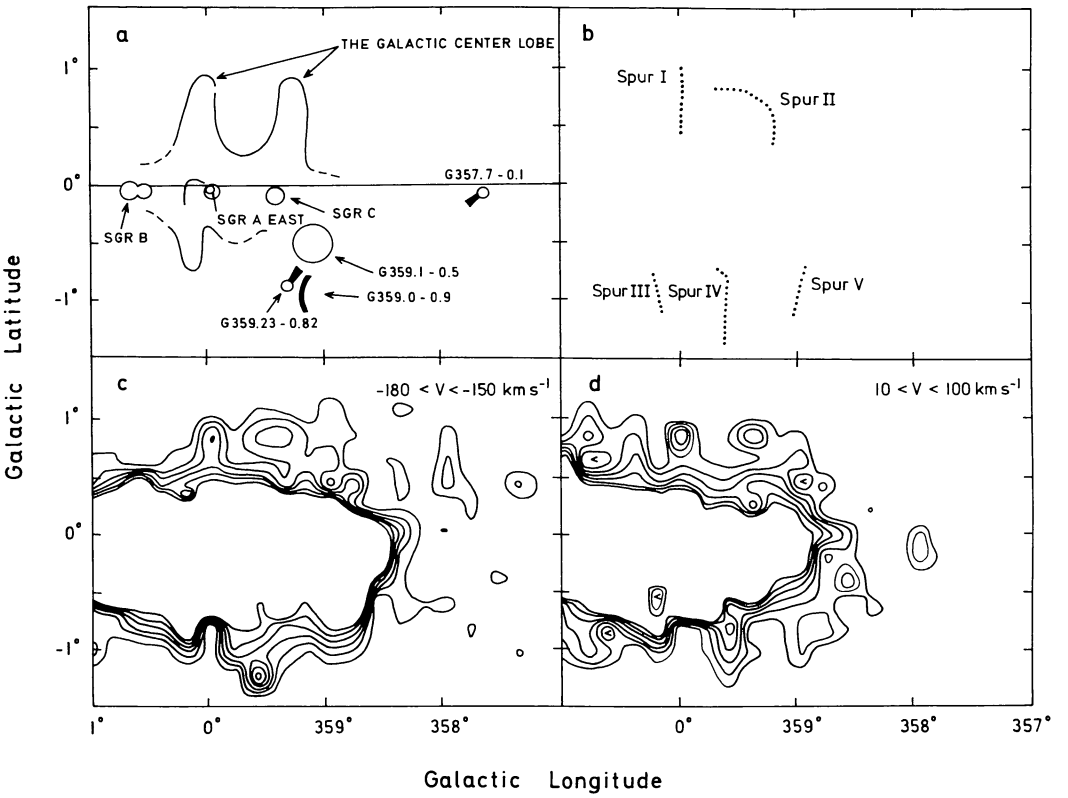

Fig. 14. a–d) A comparison of the molecular spurs with continuum features in the galactic nucleus, a) a schematic chart of continuum features close to the nucleus (from Uchida et al. 1990), b) a schematic chart of the locations of the molecular spurs, c) a map of the spurs obtained by integrating the 1667 MHz line temperature datacube over $V = -180 \rightarrow -150$ km s^{-1}. Contours are set at 2, 4, 6, 8, 10 and 12 K km s^{-1}, d) a map of the spurs obtained by integrating the 1667 MHz line temperature datacube over $V = +10 \rightarrow +100$ km s^{-1}. Contours are set at 2, 4, 6, 8, 10 and 12 K km s^{-1}